#177
4/11/80

DR. 1044

LBL-10022
UC-48

MASTER

annual report 1978-1979

Biology & Medicine Division

Lawrence Berkeley Laboratory
University of California, Berkeley

PREPARED FOR THE U.S. DEPARTMENT OF ENERGY UNDER CONTRACT NO. W-7405-ENG-48

DISTRIBUTION OF THIS DOCUMENT IS UNLIMITED

BIOLOGY AND MEDICINE DIVISION ANNUAL REPORT 1978–1979

Lawrence Berkeley Laboratory
University of California
Berkeley, California

DISCLAIMER

This work was supported by the Office of Environment of the U.S. Department of Energy under Contract W-7405-ENG-48.

CONTENTS

1. **INTRODUCTION** 1

Edward L. Alpen

2. **RESEARCH MEDICINE** 3

INSTRUMENTATION FOR THREE-DIMENSIONAL TOMOGRAPHY 3
Stephen E. Derenzo

MATHEMATICAL AND DIGITAL APPLICATIONS IN MEDICAL PHYSICS 4
Ronald H. Huesman

DEVELOPMENT OF RADIOPHARMACEUTICALS FOR RESEARCH MEDICINE 5
Yukio Yano and Jefferson W. Davis

STUDIES OF HEART MUSCLE BLOOD FLOW 7
Thomas F. Budinger

METHIONINE METABOLISM IN MENTAL DISORDERS 10
Thornton W. Sargent, III

KINETICS OF MEGAKARYOCYTE AND PLATELET TURNOVER 11
Shirley N. Ebbe, Elizabeth A. Phalen, and Gregory A. Threatte

TRANSFUSION OF ISOGENEIC MARROW IN THE STUDY OF STEM CELL FUNCTION 12
George Brecher

Donner Clinic

DONNER CLINIC PROGRAM 13
Shirley N. Ebbe, Thomas F. Budinger, Patricia A. Garbutt, Cathryne C. Allan, Carol S. Bohlen, Dorothy A. Carpenter, M. Jeanette Cornell, Myrtle L. Foster, and Dorothy B. Hedquist

3. **DONNER PAVILION** 15

PITUITARY IRRADIATION PROGRAM 15
John A. Linfoot, Eckehart Wiedemann, Jacob I. Fabrikant, and Jeanette S. Nakagawa

SERUM SOMATOMEDIN IN PATIENTS WITH PITUITARY TUMORS 17
Eckehart Wiedemann, John A. Linfoot, Robert G. Tang, Josephine A. Lundberg, Jeanette S. Nakagawa, Emanuela N. Catena, and Tamara B. Mihailovsky

INVESTIGATION OF HUMAN β-LIPOTROPIN 18
Eckehart Wiedemann, John A. Linfoot, and Tokuko Saito

DEVELOPMENT OF A SPECIFIC RADIOIMMUNOASSAY FOR HUMAN β-ENDORPHIN 19
Eckehart Wiedemann and Tokuko Saito

4. PERALTA CANCER RESEARCH INSTITUTE 21

CELL BIOLOGY PROGRAM 21
Adeline J. Hackett, Helene S. Smith, and Martha R. Stampfer

CANCER DIAGNOSIS PROGRAM 22
Adeline J. Hackett, Helene S. Smith, Otto W. Sartorius, and Martha R. Stampfer

CANCER TREATMENT PROGRAM 23
Adeline J. Hackett, Helene S. Smith, Tom K. Lee, and Martha R. Stampfer

5. ENVIRONMENTAL PHYSIOLOGY 25

EFFECTS OF ENVIRONMENTAL POLLUTANTS ON THE HEMATOPOIETIC SYSTEM 26
John C. Schooley

EFFECTS OF ENVIRONMENTAL POLLUTANTS ON STEROID HORMONE MECHANISMS 27
Gerald M. Connell

EFFECTS OF ENVIRONMENTAL POLLUTANTS ON PROTEIN METABOLISM 28
Jonathan S. Dixon

HORMONE STUDIES IN RATS EXPOSED TO ENVIRONMENTAL POLLUTANTS 30
Gisela K. Clemons and Joseph F. Garcia

EFFECTS OF ENVIRONMENTAL POLLUTANTS ON THE IMMUNE SYSTEM 31
Joan W. Goodman

STUDIES OF GROWTH AND DIFFERENTIATION OF LUNG IN FETAL, ADULT, AND REGENERATING LUNG TISSUE 31
John C. Schooley

PURIFICATION OF ERYTHROPOIETIN 33
Jonathan S. Dixon, Joseph F. Garcia, and John C. Schooley

ERYTHROPOIETIN RADIOIMMUNOASSAY 34
Joseph F. Garcia

^{90}Sr, ^{241}Am, ^{238}Pu IN MONKEY SKELETON 36
Patricia W. Durbin and Nylan M. Jeung

REMOVAL OF ^{238}Pu(IV) FROM MICE BY SULFONATED TETRAMERIC CATECHOYL AMIDES 37
Patricia W. Durbin and E. Sarah Jones, Frederick L. Weitl, and Kenneth N. Raymond

6. RADIATION BIOPHYSICS 41

Bevalac Studies

RADIOLOGICAL PHYSICS AND RADIATION CHEMISTRY 42
Aloke Chatterjee and John L. Magee

TRACER STUDIES WITH RADIOACTIVE BEAMS 44
Aloke Chatterjee, Edward L. Alpen, and Cornelius A. Tobias

PHYSICAL CHARACTERIZATION OF ENERGETIC HEAVY-ION BEAMS 46
Walter Schimmerling

RESPONSE OF A RAT RHABDOMYOSARCOMA TO HEAVY-ION BEAMS 48
Stanley B. Curtis, Tom S. Tenforde, Wolfgang A. Schilling, Susan J. Daniels, and Karen E. Crabtree

LATE EFFECTS OF HIGH LINEAR-ENERGY-TRANSFER (LET) RADIATIONS 52
E. John Ainsworth and Edward L. Alpen

CELL SURVIVAL STUDIES WITH HEAVY-ION BEAMS 53
Cornelius A. Tobias, Eleanor A. Blakely, Frank Q.H. Ngo, and Ruth J. Roots

RADIATION AND MAMMALIAN CELL TRANSFORMATION 59
Tracy C. Yang and Cornelius A. Tobias

CLINICAL PHYSICS FOR CHARGED PARTICLE RADIOTHERAPY 60
George T.Y. Chen and John T. Lyman

HEAVY-ION RADIOGRAPHY 63
Cornelius A. Tobias, Jacob I. Fabrikant, William R. Holley, and Eugene V. Benton

TREATMENT OF CANCER WITH HEAVY CHARGED PARTICLES 67
Joseph R. Castro

Magnetic Field Studies

BIOLOGICAL EFFECTS OF HIGH MAGNETIC FIELDS 69
Tom S. Tenforde

ANIMAL PHYSIOLOGY (Tom S. Tenforde, Cornelius T. Gaffey, Michael S. Raybourn, and Michael D. Edison) 69

DEVELOPMENTAL STUDIES WITH PLANTS AND INSECTS (Tracy C. Yang and Laurie M. Craise) 72

MOLECULAR STUDIES (Ruth J. Roots and Raymond S. Farinato) 72

Biophysical Studies

CNS NEUROTOXICITY STUDIES WITH ENVIRONMENTAL POLLUTANTS AND RADIOSENSITIZING AGENTS 73
Michael S. Raybourn, Walter Schimmerling, and Julia A. Twitchell

CELL-MEMBRANE BIOPHYSICS AND ENVIRONMENTAL AGENTS 75
Howard C. Mel

7. STRUCTURAL BIOPHYSICS 79

Electron Microscopic Studies

FLY ASH PARTICLE CHEMISTRY AND LUNG CELL EXPOSURE 80
Thomas L. Hayes, S. Jacob Bastacky, Clifford E. Lai, and Gerald L. Fisher

LOW TEMPERATURE SCANNING ELECTRON MICROSCOPY OF BIOLOGICAL MATERIALS HELD IN THE FROZEN-HYDRATED STATE 84
Thomas L. Hayes, James B. Pawley, Gregory R. Hook, and Clifford E. Lai

THE ELECTRON UTILIZATION EFFICIENCY IN SCANNING-TRANSMISSION ELECTRON MICROSCOPY (STEM) AND CONVENTIONAL-TRANSMISSION ELECTRON MICROSCOPY (CTEM) 87
Robert M. Glaeser

MORPHOLOGICAL MODEL OF THE SURFACE-LAYER ARRAY IN *SPIRRILLUM SERPENS* 87
Robert M. Glaeser

DNA and Genetic Studies

THE OPTICAL ACTIVITY OF DNA AGGREGATES 88
Marcos F. Maestre and Charles Reich

DNA REPAIR 90
Junko Hosoda

CRYSTALLIZATION OF DNA FOR ELECTRON DIFFRACTION STUDIES 91
Kenneth H. Downing

GENETIC STUDY ON YEAST *(SACCHAROMYCES CEREVISIAE)* 93
Robert K. Mortimer

Studies on Photosynthesis and Hydrocarbon Production

RESONANCE STUDIES IN PHOTOSYNTHESIS 95
Alan J. Bearden

HYDROCARBON BIOSYNTHESIS IN GUAYULE 96
Thomas E. Bauer

Lipoprotein Studies

LIPOPROTEIN METHODOLOGY AND BIOMEDICAL APPLICATIONS 99
Frank T. Lindgren, Mason M-S.Shen, and Ronald M. Krauss

INTERRELATIONSHIPS AMONG SUBGROUPS OF SERUM LIPOPROTEINS IN NORMAL SUBJECTS 100
Ronald M. Krauss

STRUCTURE AND FUNCTION OF HIGH DENSITY LIPOPROTEINS 100
Alex V. Nichols, Patricia J. Blanche, and Elaine L. Gong

LIPOPROTEIN TRANSPORT OF MUTAGENS 103
Helen M. Shu

CHARACTERIZATION OF FETAL CALF AND NEWBORN CALF SERUM LIPOPROTEINS 103
Trudy M. Forte and Julia Bell-Quint

SYNTHESIS AND METABOLISM OF LIPOPROTEINS BY MONOLAYER CULTURES OF RAT HEPATOCYTES 105
Julia Bell-Quint and Trudy M. Forte

Effect of Radiation and Pollutants on Mammalian Cells

SOLAR, NEAR ULTRAVIOLET, AND FLUORESCENT LIGHT DAMAGED MAMMALIAN CELLS 109
H. John Burki

TRITIUM DAMAGE IN SYNCHRONOUS CHINESE HAMSTER CELLS *IN VITRO* 109
H. John Burki

EFFECTS OF POLLUTANTS ON SOMATIC MAMMALIAN CELLS 110
Donald A. Glaser

APPENDICES

A. 1978–1979 PUBLICATIONS 113
B. BIOLOGY AND MEDICINE DIVISION STAFF 121

1. INTRODUCTION

Edward L. Alpen

In the introduction to our last annual report I remarked that the just preceding years had been a time of hectic growth and readjustment to new research goals and research initiatives. During 1978 and 1979 we have continued our consolidation of efforts and redirections to meet the new developing needs of our sponsors. We have accomplished this, I believe, while at the same time maintaining the central nature of the Donner Laboratory as a distinguished and creative center for biomedical research.

Moderate growth has continued during the past two years, but at a much more restrained pace. The facility and space problems that have been so worrisome for the last several years are starting to be resolved. The principal mechanisms for solving the problems, particularly that of space, are the completion of remodeling of the Research Medicine Building (Building 55) on the hill, and the new availability of about 10,000 square feet of wet-laboratory space in a leased off-site building. Donner scientific staff are now located in ten different physical sites, some of them several miles from the administrative center of operations. These diversified locations will cause some increased difficulty in maintaining a high level of scientific communication among our scientific and technical staff, but the added space more than compensates for this problem.

Some major scientific milestones have been passed during the last year. The 280-crystal positron emission tomograph designed by Professor Budinger has gone into full clinical operation during the past year, and a significant number of patient studies, mainly centered around myocardial infarct examinations, have been successfully completed. The heavy-ion radiotherapy program has now entered Phase III (controlled randomized trials); and clinical trials for the evaluation of the effectiveness of helium ion beams in the control of certain cancers have been fully launched. At the same time, the earlier stage Phase I and Phase II (exploratory and preliminary) trials of the carbon and neon beams at the Bevalac have also gotten under way.

In the structural biophysics area, Professor Hayes now has his scanning electron microscope cold-stage fully operational, and data are being collected on its operation. Another major breakthrough, which is at a stage of development that does not permit full evaluation of its impact, is the preparation of an electron diffraction pattern for small-crystal DNA. We believe this to be the earliest such study for crystalline DNA.

In our last report we mentioned the new addition to the Donner family of the Peralta Cancer Research Institute, operated by us at the Peralta Hospital as a joint project of the Hospital and the University of California. I am pleased to report that important progress is being made in the development and integration of this functional unit into our overall operations. Reports of scientific progress at the Institute are included in this progress report.

During 1978 and 1979 the scientific staff has participated in numerous meetings throughout the world. In addition, several conferences and workshops were sponsored by senior staff from the division:

- The Donner Pavilion Group, in conjunction with Alta Bates Hospital and the University of California Extension Division, sponsored a symposium "Recent Advances in the Diagnosis and Treatment of Pituitary Tumors," held in San Francisco May 31 to June 4, 1978. An internationally recognized faculty was brought together to review, update, and provide a comprehensive understanding of basic research in the biochemistry, histology, and physiology of the hypothalamo-pituitary axis.
- The Radiation Biophysics Group sponsored a workshop at Lawrence Berkeley Laboratory in September 1978 on "The Radiation Environment of the Solar-Powered Satellite."
- Members of the Structural Biophysics Group helped to organize and participated in a workshop held in San Franciscio March 5 to 7, 1979, on "High-Density Lipoprotein Methodology."

This report summarizes some of the highlights of the Division's scientific effort during 1978 and 1979.

2. RESEARCH MEDICINE

The Research Medicine Group, under the leadership of Dr. Thomas F. Budinger, continues its quest for knowledge about human biochemistry in health and in disease. In addition to the basic biochemistry and physiology inquiries, the special imaging and blood analysis tools being developed by this group are valuable for diagnostic nuclear medicine. The DOE program is served by inquiries, using methods developed by this team, into effects of magnetic fields on humans and the biological impact of pollutants from increased use of fossil fuels and other sources of energy production.

One of the highlights is the completion of the 280-crystal ring detector system in July 1978 and the use of this device for animal and human studies. The ability to visualize blood flow and metabolism of the heart is important in understanding heart disease. Our myocardial studies can help in four major areas of cardiology research: 1) early identification of the disease; 2) understanding whether diets and exercise for a person who has suffered a heart attack improve the blood supply to the myocardium; 3) determination of the extent of the heart attack and the effectiveness of therapy; 4) following people who have had bypass surgery to see if the improvement in blood supply to the heart muscle is sustained. Our major interest is in a fifth area which actually underlies all of the above—a basic understanding of the myocardium and its metabolism, and clues as to the causes of coronary artery disease.

This program is closely associated with the development of instrumentation. We are already moving toward a three-ring system which will provide multi-layer views for dynamic quantitative radionuclide imaging. New radiopharmaceuticals are also developed in this program to enable studies of *in vivo* biochemistry of amino acids, fatty acids, and glucose. During the past year carbon-11 labeled methionine was first used in studies of heart metabolism and brain metabolism in humans.

Research effort continues in the hematology area. Studies of the megakaryocytic cell system are helping us to understand platelet turnover and how the blood platelet level is regulated. This knowledge, important in understanding a broad spectrum of blood disorders, is also valuable for assessing effects of toxic environmental pollutants. Part of the hematology program includes the electron microscopy of white blood cells in the search for leukemia viruses.

The highlights of the research effort during the past year are summarized in the following reports.

Instrumentation for Three-Dimensional Tomography

Stephen E. Derenzo

The Donner 280-crystal positron tomograph (Fig. 1) was designed and built at LBL to image the three-dimensional distribution of positron-labeled compounds in the human body. The system consists of a continuous ring of 280 rectangular (8 mm × 30 mm × 50 mm) NaI(T1) detector crystals that completely encircle the patient. When a positron is emitted it travels a few millimeters and annihilates with an electron to produce two 511-keV photons that fly off in nearly opposite directions. Each crystal is coupled to a phototube and electronic circuits determine whenever any crystal has detected an annihilation photon in time coincidence (within 2 × 10^{-8} s) with any of the opposing 105 crystals.

Figure 1. Donner 280-crystal positron tomograph. The surrounding ring of crystals and phototubes makes 14,700 measurements of the internal distribution of a positron emitting compound. High-speed hard-wired circuits reconstruct three-dimensional images that tell how vital organs are functioning. CBB 795-6414

Events are accumulated in high-speed semiconductor memory. In a typical high resolution study [9-mm full width at half-maximum (FWHM)], 1 million events are collected in 2 minutes and the image is reconstructed in 10 seconds by a hard-wired arithmetic unit. Dynamic processes can be imaged with lower resolution (2 cm) by collecting a 50,000-event data set every 2 seconds.

The system became operational in July 1978, and has been used in studies of blood flow and amino acid metabolism in man and animals (see following report). Using the rubidium-82 generator (75-s half-life isotope) developed at Donner Laboratory (see Y. Yano report), it is possible to image the blood flow in human heart muscle with a low radiation dose. The size and location of sick heart muscle can be accurately determined in three dimensions.

In 1979 the imaging speed of this system will be doubled by replacing the NaI(Tl) crystals with bismuth germanate, a more efficient detector material that has recently become available in large, clear crystals.

Future work will center on a larger, multi-layer system able to image the entire heart or brain in nine transverse sections without mechanical motion. This system will have improved resolution and permit a significant reduction in patient dose and imaging time.

MATHEMATICAL AND DIGITAL APPLICATIONS IN MEDICAL PHYSICS

Ronald H. Huesman

AUTOMATIC DATA ACQUISITION, RECONSTRUCTION, AND DISPLAY SYSTEM

A special emphasis of the research medicine program is the development of methods for acquiring and manipulating data from positron-emission tomograph devices. A system has been developed to acquire data, calibrate and correct for attenuation, reconstruct transverse sections of radionuclide concentration, and display the resulting sections on a raster scan display monitor (see Fig. 1).

The data acquisition system, which was designed by J. Cahoon, is capable of taking 1 million events per second while simultaneously correcting for accidental events. Events are histogrammed into a 105 × 140 word 12-bit memory corresponding to the Donner 280-crystal positron tomograph. Seven additional memories, presently under construction, will allow the simultaneous acquisition of data for eight different time-slices of the cardiac cycle.

Data calibration and correction are handled by software (DEC PDP 11/10 computer). Transverse section reconstruction is performed by a hardwired reconstructor (Analogic Corp.) capable of reconstructing a 256 × 256 image from 140 projection angles in less than 3 seconds. A 256 × 256 display (DeAnza Systems, Inc.) allows interactive manipulation of the resulting images.

THE ULTRAFAST FOURIER TRANSFORM PARALLEL PROCESSOR (UFTPP)

The UFTPP, a peripheral device which increases the computational power of a host computer, has been designed by W. Greenberg and is now near completion. It will perform Fourier transforms at a rate of 1 million complex points per second, a rate ten times faster than commercially available devices. Its intended use is for post-processing of nuclear medicine images obtained from the Donner 280-crystal positron tomograph; however, its application is not limited to this area. It may be used for a broad spectrum of signal processing problems including image reconstruction, digital filtering, and NMR (nuclear magnetic resonance) analysis, to name a few.

The novelty of this project is embodied in its flexible architecture, which allows multiple arithmetic units to be used for parallel processing, and thereby increases speed. The simplicity of the architecture coupled with the use of LSI chips results in an extremely fast processor that is inexpensive in comparison with other currently available processors. In addition, this seems to be the first processor aimed specifically at the two-dimensional signal processing problem (image processing) with its inherent requirements for higher-precision arithmetic.

MATHEMATICAL PHYSICS

Continued effort by G. Gullberg in the field of mathematical physics includes analysis of noise propagation in emission-computed tomography (ECT). The errors in ECT are the result of noise propagated from statistical fluctuations in the emission photons, the incident transmission beam, and

the emerging transmission beam. Investigation is continuing into both the mathematical theory of the attenuated Radon transform and its application in medicine and biology. Analysis of back-projection operators appropriate for space-invariant filtering in fan-beam computed tomography has also been completed. Fan-beam techniques in computed tomography are especially useful in dynamic imaging because of their rapid data acquisition capabilities

Mathematical modeling techniques are being applied to kinetic studies which measure biochemical and hemodynamic parameters. The mathematical modeling involves developing computer codes that can estimate accurately and efficiently complicated interactions between physiological compartments.

Figure 1. Data acquisition, reconstruction, and display systems for the Donner 280-crystal positron tomograph. CBB 795-6416

DEVELOPMENT OF RADIOPHARMACEUTICALS FOR RESEARCH MEDICINE

Yukio Yano and Jefferson W. Davis

The purpose of this program is to provide positron-emitting radiopharmaceuticals for transverse-section imaging and quantitation of metabolic and flow processes by noninvasive methods. Radiopharmaceutical research is coordinated with the development of advanced instrumentation for positron transverse-section tomography.

The investigation of methods for production and labeling with radionuclides includes studies of irradiation parameters, targetry, radiolysis, rapid organic and enzymatic synthesis including shielding and automation, analytical characterization of the labeled compound, and studies of the *in vivo* distribution of the radiotracer in animals and humans. Other studies for radionuclide generators include the investigation of the ion exchange characteristics of organic and inorganic adsorbers and the elution yields with physiologically compatible eluant solutions.

Methods for the cyclotron production of ^{11}C, ^{13}N, ^{15}O, and ^{18}F for the organic synthesis of labeled amino acids, catecholamines, sugars, hemoglobin, water, and fatty acids to study the function of brain, heart, and the pancreas have been pursued.

Specifically, we are producing ^{11}C-methyl methionine, ^{11}C-valine, $^{13}NH_3$, ^{13}N-L-glutamic acid, ^{13}N-L-glutamine, ^{68}Ga-EDTA, ^{68}Ga-albumin, ^{68}Ga-platelets, ^{68}Ga red blood cells, and an ^{82}Rb generator of 60-mCi capacity.

Methionine-methyl-^{11}C may be useful for imaging and quantitating the demethylation process. The expired $^{11}CO_2$ in patients with psychic disorders would be measured, and the metabolic pathways of the methyl-^{11}C from methionine into neurotrans-

mitters would be followed. Another possible use of the labeled methionine is to study its uptake in the brain of patients with phenylketonuria.

^{11}C-methyl-methionine is prepared by a continuous flow process developed in our laboratories by J. Davis. The method consists of reduction of $^{11}CO_2$ to methanol and conversion of the latter to methyl iodide which is converted to methionine-methyl-^{11}C by condensation with the sodium salt of homocysteine in refluxing acetone. The preparation can be completed within 30 minutes after the end of the irradiation. Yields of up to 150 mCi of ^{11}C-methyl-methionine have been prepared.

Semi-micro glassware and teflon three-way solenoid valves were used to assemble the automated apparatus (Fig. 1) used in this reaction. The ^{11}C-carbon dioxide is absorbed in the reaction vessel as it is produced by the N_2 sweep of the cyclotron target. The sample is then decomposed with 0.1 to 0.2 ml of water and the sweep is continued for another 10 minutes under reflux. The acetone is then evaporated and the ^{11}C-methionine is brought into solution with sterile normal saline. ^{11}C-methionine activity is 50 to 100 mCi. An aliquot of the solution is analyzed by paper chromatography and HPLC (high pressure liquid chromatography).

Both animal and human studies were done with ^{11}C-methyl-methionine to determine blood clearance rates; levels of expired $^{11}CO_2$; and transaxial distribution images in the brain, heart, and pancreas.

Recent studies indicate that taurine is present in high concentrations in the brain and heart of primates. The intracellular concentration of this amino acid is much higher than its concentration in the extracellular fluids. This amino acid does not cross the blood-brain barrier. Taurine has a very high concentration in the brain and comprises more than 50% of the five-amino-acid pool in the heart. The concentration is constant (being different in different species), and is found altered only in the diseased state. The concentration doubles in the affected ventricle of persons dying of congestive heart failure and these changes are specific to the heart.

The high concentration of taurine in the brain and heart and the difficulty in determining its function and biosynthesis make it an interesting subject for study, which is evidenced by the increasing number of workers involved in this effort. Our interest in taurine in this project is based on the fact that the sulfur of this amino acid comes from methionine. The synthesis of ^{11}C-taurine for emission tomography in normal and diseased patients may help to explain some of the possible functions of this amino acid

This amino acid will be prepared by a modification of the procedure developed in our laboratories by the reduction of the sulfonitrile. The details of this synthesis have not been completely worked out, but we have shown that the hydroxyl group in cyanohydrins can be replaced by chloride.

We are pursuing the study of glucose metabolism with the labeled ^{18}F-2-fluoro-2-deoxyglucose which will be used for metabolic studies of the brain and heart. The development of the complex targetry and technology for handling $^{18}F\text{-}F_2$ as the precursor for organic synthesis of this compound is a joint research effort between Donner Laboratory and Cyclotron Corporation.

The alumina column ^{82}Rb generator was loaded with 70 mCi of ^{82}Sr. There was less than 10^{-4} breakthrough of Sr-82/85 over the 2- to 3-month useful life of the generator through several hundred elutions totaling more than 4 liters of 2% NaCl. Both normals and patients with heart disease were studied with ^{82}Rb. Dogs with induced myocardial infarction were also studied with ^{82}Rb. The results of these studies indicate that positron emission tomography with ^{82}Rb provides adequate information for diagnosis of myocardial infarction.

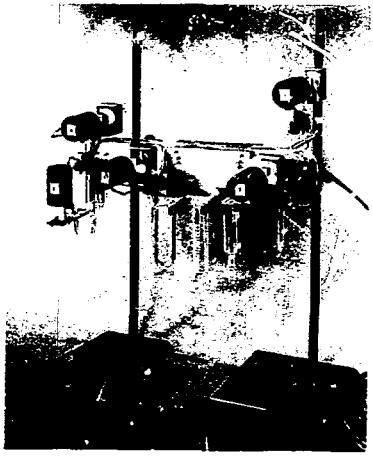

Figure 1. An automated remote-controlled system for the organic synthesis of ^{11}C-methyl-methionine by a continuous flow process; 1 to 5 are teflon solenoid valves.
CBB 7811-14881

STUDIES OF HEART MUSCLE BLOOD FLOW

Thomas F. Budinger

Upon completion of the Donner 280-crystal ring, the Research Medicine Group commenced studies of the ability to detect coronary artery disease and heart muscle infarction (heart attacks). First, dogs were tested using rubidium-82, which is a positron emitter of 75-seconds half-life. This isotope behaves like potassium in that the amount which accumulates in the heart muscle is proportional to flow. Rubidium-82 is so attractive because it can be obtained on demand from its parent strontium-82 using a table-top "generator" perfected by Y. Yano. The strontium-82 (25-day half-life) is obtained from Los Alamos. As much as 20 mCi of rubidium-82 can be safely injected, as the dose is less than that of one chest x-ray. Because rubidium-82 is a positron emitter, transverse sections or 3-D information regarding the isotope distribution can be obtained using coincidence detection of the annihilation photons.

After demonstration of the ability to detect heart attacks involving very small (2 cc) volumes of the heart muscle, clinical trials were started with patients who had sustained heart attacks in the recent past (Fig. 1). In addition, studies were made to evaluate the extent of increases in heart-muscle flow which can be affected by exercises or drugs (Fig. 2).

Researchers working on this project include T. Budinger, Y. Yano, S. Derenzo, R. Huesman, J. Cahoon, T. Vuletich, B. Moyer, P. Eisenbach, and G. Gullberg.

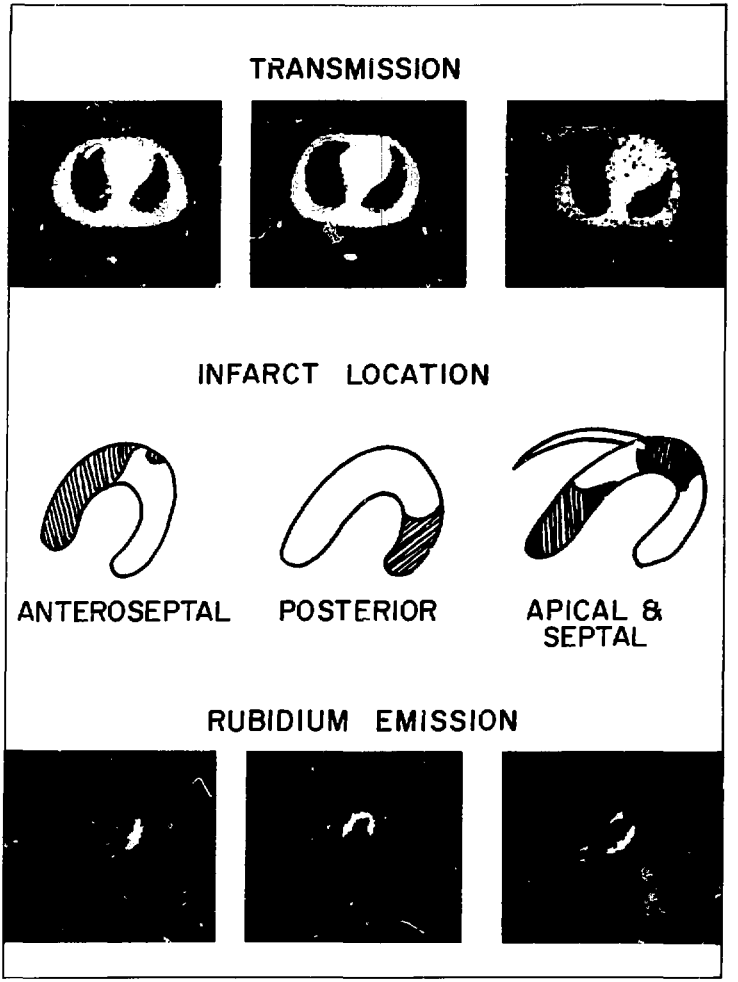

Figure 1. Rubidium-82 myocardial uptake studies in three patients who had suffered myocardial infarcts (anteroseptal defect; posterior wall defect; apical and septal defect). The filled-in areas of the center diagrams indicate the infarct locations. The pattern of heart blood flow is depicted in the rubidium-82 emission images at the bottom: note that the dark areas of those images correspond to the areas of heart damage indicated in the diagrams above.

XBB 794-4721

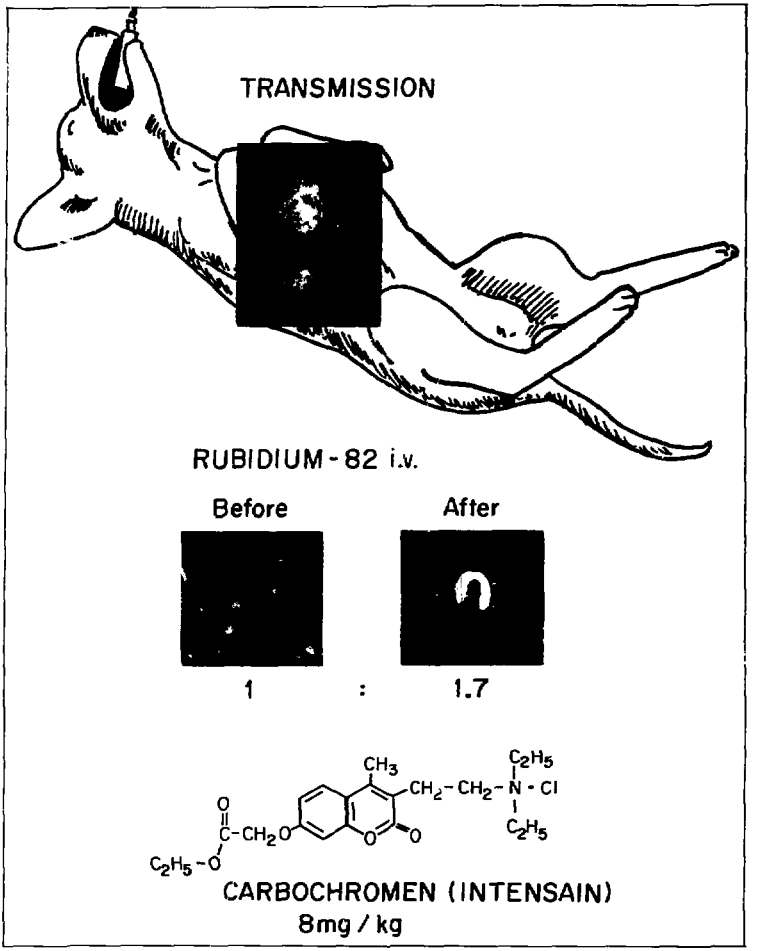

Figure 2. Relative uptake of rubidium-82 in dog heart before and 20 minutes after an intravenous injection of Intensain (8 mg/kg). This drug is known to increase heart blood flow, and the increased perfusion is shown by the increased isotope detected. XBB 794-4720

METHIONINE METABOLISM IN MENTAL DISORDERS

Thornton W. Sargent, III

Our program utilizes noninvasive *in vivo* radioisotope techniques to study metabolism in the brain. We use animal studies to develop the techniques, but our main purpose is to study human patients who have schizophrenia and manic-depressive illness. These diseases are now considered to have a biochemical basis, and we are using radioisotope-labeled metabolites to investigate several theories which have been proposed.

In the past year our emphasis has been on the production of methionine labeled in the S-methyl group with carbon-11, a 20-minute half-life, positron-emitting isotope. The transmethylation hypothesis of schizophrenia postulates that an abnormal methylation reaction involving this methyl group is the cause of the disease; a number of workers including ourselves have made observations supporting the hypothesis. We have produced ^{11}C-methionine and performed preliminary studies in a monkey using the Donner 280-crystal positron emission tomograph, and obtained the image of a section through the brain as shown in Figure 1 This has demonstrated the feasibility and patient studies are planned.

Using much smaller doses of ^{11}C-methionine we have studied two human subjects with the Radiocarbon Respiration Analyzer and measured the expiration pattern of the expired $^{11}CO_2$. We will now be able to repeat our earlier studies which used ^{14}C, showing abnormal methionine metabolism in schizophrenia, using the safer, short half-life ^{11}C. We have published a report describing abnormal methionine metabolism in the leukocytes of patients with schizophrenia, using an *in vivo* leukocyte culture technique to measure the $^{14}CO_2$ evolved; this adds another observation to the list of abnormalities of methionine-methyl metabolism in schizophrenia.

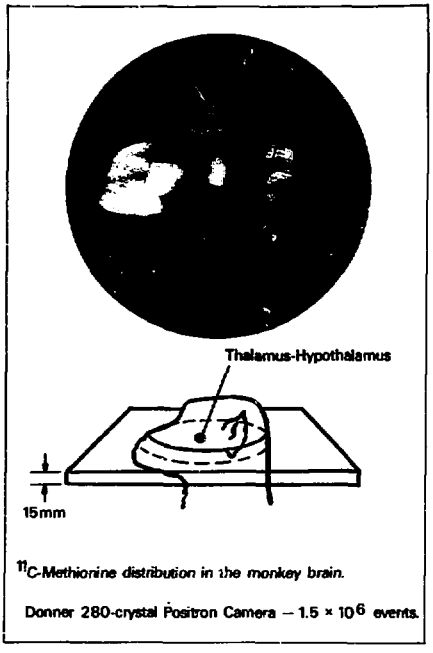

Figure 1. Tomographic section of S-methyl-^{11}C labeled methionine in monkey brain. The outline of the monkey's head is sketched in to indicate the location of the "slice." Note the accumulation in the hypothalamus.

XBB 789-10858

KINETICS OF MEGAKARYOCYTE AND PLATELET TURNOVER

Shirley N. Ebbe, Elizabeth A. Phalen, and Gregory A. Threatte

Platelets, the smallest formed elements of the blood, are essential because of their role in hemostasis, the processes by which blood coagulation is initiated and blood vessel injury is repaired. In the absence of platelets, excessive and spontaneous hemorrhages occur that are difficult to control. The number of blood platelets may be reduced (thrombocytopenia) or increased (thrombocytosis) by pathological alteration of the platelet-production rate; thrombocytopenia may also be produced by pathological acceleration of platelet destruction.

The process of platelet formation, megakaryocytopoiesis, takes place as follows. Platelets come from the bone marrow where they originate as cytoplasmic fragments from megakaryocytes, the largest of the hemopoietic cells. The story begins, however, with the pluripotential hemopoietic stem cells which produce blood granulocytes (white cells) and erythrocytes (red cells), as well as megakaryocytes. Young megakaryocytic cells undergo cell division, but the daughter cells eventually lose their capacity to divide further. However, these daughter cells continue to replicate their DNA, and thereby become polyploid.

At about the time when megakaryocytes are mature enough to be recognized morphologically by light microscopy, they cease synthesizing DNA. Subsequent development then consists of synthesis of cytoplasmic organelles and membranes, with the copious amount of cytoplasm being subdivided into platelets which are then shed into the blood. The amount of cytoplasm produced by each megakaryocyte, which determines the mass of the platelets it produces, may be regulated by the amount of nuclear DNA that it contains. Megakaryocytopoiesis is frequently abnormal in bone marrow disorders such as the leukemias, pre-leukemias, and aplastic anemia whether spontaneous or induced by cytotoxic agents. In fact, hemorrhage from thrombocytopenia is often the complication that produces morbidity and mortality in these disorders.

The processes of megakaryocyte production by stem cells and of platelet production by megakaryocytes are each subject to homeostatic regulatory mechanisms whose function appears to be the maintenance of normal numbers of platelets in the circulating blood. For example, it has been demonstrated that experimental perturbations of the number of circulating platelets will produce alterations in the rate of platelet production which will counter the perturbation and normalize the platelet count. In association with such changes, alterations of megakaryocyte turnover rate, number, size, and ploidy, and of platelet size, have been demonstrated. These events indicate that there is feedback regulation of megakaryocytes in the marrow by circulating platelets, possibly by a humoral agent whose production may be regulated by the number of platelets.

Such an agent has been found by other investigators and has been called thrombopoietin. It has proved difficult to demonstrate the presence of thrombopoietin by bioassay, and virtually nothing is known about its physiology. The tissue of origin of thrombopoietin has not been identified, the critical platelet functions that may be monitored to regulate production of this hormone have not been described, and the ways in which thrombopoietin may affect megakaryocytes and their stem cells have not been clarified.

We are trying to shed light on some of these problems by studying megakaryocytopoiesis in animals. Our approach is observing the effects of perturbations of the platelet count and of cytotoxic agents on this cell system, and also determining how the effects of cytotoxic agents may be modified by stimulation or suppression of megakaryocytopoiesis. The megakaryocytopoietic stimulation is achieved by depletion of circulating platelets by injection of heterologous antiplatelet antibodies; the suppression is produced by transfusions of homoiogous platelets.

Exposure of mice to gamma- or x-radiation regularly produces a reduction in megakaryocytes which is quickly followed by development of thrombocytopenia. The degree of thrombocytopenia is dependent on the dose of radiation, as is the capability for recovery. With sublethal doses of radiation (650 R gamma), maximal thrombocytopenia occurs 8 to 10 days after irradiation, and platelet counts recover to normal values about 2 weeks later. If, in addition, the animals are made acutely thrombocytopenic on the day of irradiation, the radiation-induced thrombocytopenia is less severe and of shorter duration than when they are exposed to radiation alone. This change is due to increased production of platelets, as confirmed by increased incorporation of ^{75}Se-selenomethionine or ^{35}S-sodium sulfate into platelets.

Therefore, it appears that a stimulus (? thrombopoietin) is generated as a result of thrombocytopenia, and that this stimulus affects a population of

megakaryocytic precursor cells that was not heavily damaged by the dose of radiation that was used. The action of the stimulus was on precursor cells rather than directly on differentiated megakaryocytes themselves, as shown by the failure of platelet production to be responsive during the first 4 days after irradiation.

Although a humoral mechanism for the stimulation of megakaryocytopoiesis in thrombocytopenic, sublethally irradiated mice seems likely, we have been unable to duplicate the effect with injections of plasma collected from thrombocytopenic donor mice. It has also become clear that the response of the megakaryocytic system to radiation may vary depending upon the length of time during which the system is stimulated prior to radiation exposure. This conclusion also applies to the way in which platelet production responds to other cytotoxic agents such as vincristine and hydroxyurea. Explanations for this phenomenon probably lie in a better understanding of changes in proliferative states of megakaryocytic precursor cells, and appropriate studies are underway to elucidate this area.

Even though blood platelet counts return to normal after appropriate sub-lethal doses of radiation, it has become apparent that the circulating platelet normality may be achieved in spite of residual reductions in numbers of megakaryocytes in the bone marrow. Under these conditions, the megakaryocytes themselves are macrocytic. A similar triad of findings (normal platelet counts, reduced megakaryocytes, and macrocytic megakaryocytes) is also found after administration of hydroxyurea and in genetically anemic mice of the W/W^v and Sl/Sl^d strains. All of these models are being investigated to evaluate the extent to which autoregulation of megakaryocytopoiesis may occur and to study associations among megakaryocyte size and ploidy and platelet size and number.

The role of the humoral factors in these conditions will be evaluated by observing the growth of megakaryocytes in cultures of marrow cells in diffusion chambers implanted intraperitoneally in mice. This technique has been successfully applied to other hemopoietic cells by other investigators, and preliminary experiments indicate that it will be useful for studying megakaryocytic stem cells and the humoral factors that affect megakaryocytopoiesis.

The over-all goal of these projects is to understand the ways in which platelet production is normally regulated. The consequence will be a better understanding of the ways in which platelet production and its regulation may be abnormal in a variety of human diseases, and this should lead to more successful management of these disorders.

TRANSFUSION OF ISOGENEIC MARROW IN THE STUDY OF STEM CELL FUNCTION

George Brecher

The behavior of hemopoietic stem cells, i.e., the precursors of all blood cells, is of interest because they constitute the effective elements of bone marrow transfusion, a still hazardous but potentially useful therapy of certain anemias and leukemias. In the past, marrow transfusions have been studied extensively in irradiated animals which can survive otherwise lethal doses of radiation if treated promptly with marrow transfusion. The transfused marrow contains stem cells which repopulate the irradiated marrow. However, transfused marrow cells do not proliferate in normal recipients, even when donor and recipients are identical and readily accept grafts of skin and other tissues.

We have conducted experiments to elucidate the failure of marrow to "take" in normal isogeneic recipients in order to acquire a better insight into the behavior of hemopoietic stem cells. In these experiments, we used male mice as donors and females as recipients. Special staining techniques (C-banding) allow the ready identification of the Y chromosome in dividing cells, and we could thus obtain an estimate of the proliferation of transfused donor cells in the recipients. Although mouse strains with marker chromosomes have been used for this purpose in the past, the new approach has the advantage of being applicable to any strain of mice.

We first tested the possibility that a "take" in normal recipients requires a stimulus for stem cells to divide. We postulated that the maintenance of a normal supply of blood cells by the marrow is ordinarily accomplished by replication of more mature cells without recourse to the early stem cells. In that case, division of stem cells would normally be a rare event.

We provided a stimulus for division by partial body irradiation *after* marrow transfusion. The dose

of radiation to the exposed part of the body was 770 rad, sufficient to deplete it of both endogenous and transfused stem cells. In the shielded part, both resident and transfused stem cells could survive and proliferate locally or seed into the irradiated portions of the bone marrow. When the trunk was shielded, approximately 60% of the hemopoietic cells in the irradiated femoral marrow were of donor origin, supporting our contention that stem cells require a special stimulus to divide.

When only one leg was shielded after transfusion, donor cells seeded and proliferated in the irradiated leg but not in the shielded leg, even though the shielded leg was the only possible source of donor cells. The results suggested that proliferation of normally quiescent stem cells requires not only a stimulus for division but also available proliferative sites which are normally occupied. Irradiation presumably empties these sites, without destroying the micro-environment necessary for proliferation of stem cells seeded from the shielded leg.

Cues provided by these experiments led us to study transplantability of isogeneic marrow under a variety of circumstances. The results indicate that donor cells can proliferate more readily in the recipient spleen than in the marrow. Temporary growth in the spleen may take place in entirely normal animals after transfusion of "stimulated" marrow, i.e., marrow of mice that had received neostigmine methyl sulfate. This drug has been shown to trigger stem cells into cycle. More recently, we found indications of similarly enhanced growth in the spleen after transfusion of marrow followed by injection of isoproterenol, another drug that stimulates stem cell division. We also found an increased tendency of marrow to "take" in previously irradiated mice, even after their peripheral blood values had returned to normal.

It thus appears that isogeneic marrow transfusions are indeed a useful tool in the study of stem cell kinetics. Experiments continue to seek drugs or procedures which will enhance the ability of transfused marrow to proliferate. Beyond further insights into stem cell behavior, an enhanced growth potential of hemopoietic stem cells may ultimately be useful for marrow transfusion in man.

Donner Clinic

DONNER CLINIC PROGRAM

Shirley N. Ebbe, Thomas F. Budinger, Patricia A. Garbutt, Cathryne C. Allan, Carol S. Bohlen, Dorothy A. Carpenter, M. Jeannette Cornell, Myrtle L. Foster, and Dorothy R. Hedquist. Attending Physicians: James L. Born, George Brecher, Hunter O. Cutting, Lester Hollander, Donald J. Rosenthal, and Henry H. Stauffer

The Donner Clinic developed from the first use of radionuclides in the treatment of human diseases over 40 years ago, under the leadership of Dr. John Lawrence. This institution was, in a large measure, responsible for demonstrating the effectiveness of such treatment and hence its adoption by the medical community as one of the standard options of treatment, especially for hematological and thyroid diseases. The major research and clinical interests in the clinic have continued to be in these two areas of medicine. Because of the clinic's pioneering role in the use of radionuclides in human beings, there continues to be a nucleus of patients who received radioactive isotopes before these drugs were in general use, and who provide a resource for determining if there are long-term consequences of the therapeutic use of radioactive drugs.

During calendar year 1978, 286 patients were seen 854 times by clinic physicians. Of these, 181 patients were seen in hematology clinic (742 visits) and 105 were seen in thyroid clinic (112 visits). In addition, there were 108 patient visits for special studies by the technological and nursing staff. Observation and treatment of many of these patients were relevant to the study of long-term effects of radioisotopes, clinical analysis of polycythemia or thrombocythemia, or participation in a collaborative international study of polycythemia vera. Weekly hematology rounds have been initiated to permit free exchange of ideas and review of clinic patients

in light of recent advances in diagnosis and treatment. In addition to clinic staff, the meetings are attended by research fellows from Donner, residents from collaborating hospitals, and guest researchers.

Long-standing plans and preparation resulted in DOE approval for establishment of a patient billing procedure for LBL's Donner Medical Group. This will permit reimbursement for those activities related to diagnosis and treatment of diseases. The clinic laboratory was licensed by the State of California and became a participant in the American Society of Internal Medicine laboratory evaluation program. Every 3 months we are tested by analyzing unknown samples from this program thus ensuring thoroughness, accuracy, and quality control in our laboratory procedures.

In the thyroid clinic, patients who were treated with ^{131}I for hyperthyroidism at Donner Clinic 5 or more years ago are being evaluated to determine the extent of long-term diminution of thyroid function. Patients are evaluated by blood tests for thyroid hormones and ^{123}I scintillation photograph of the neck region 4 weeks after discontinuance of their thyroid medication. Maximum residual thyroid function is also determined. This study will define the long-term effects of therapeutic dosage of radioactive iodine on thyroid function and determine if patients so treated are at risk to develop severe hypothyroidism if their thyroid medication is stopped.

In the hematology clinic, a comprehensive analysis of patients' records is underway to determine if the wealth of data on patients with polycythemia vera and chronic granulocytic leukemia will yield new insights into clinical course or pathogenic mechanisms of these disorders. Techniques for mathematical analysis of platelet size-distribution curves and for measurement of megakaryocytic nuclear content of DNA are being developed. These tests will be used to further analyze these disorders as well as other myelodysplastic states in which platelet production is abnormal.

The clinic has also collaborated actively with LBL researchers who are interested in erythropoietin. Clinic patients with hypoplastic anemia regularly collect their urine as a source of erythropoietin for research use. Plasma and serum samples were collected from 137 normal volunteers (mostly LBL employees) for assay for erythropoietin by a new technique, and plasmas were collected from all clinic patients for this test.

The clinic is in the process of undertaking a comprehensive analysis of the role of a humoral thrombopoietin in the regulation of platelet production. The goal of these studies is to elucidate the role of abnormalities in the regulation of thrombocytopoiesis, which may be important in a variety of human disorders. It is anticipated that a bioassay for thrombopoietin will be developed and that experiments will be done in animals to clarify the physiology of thrombopoietin. With these bases, human diseases will be studied.

As a facility to optimize research related to human beings, the Donner Clinic maintains physical facilities for dealing with human subjects, such as examining rooms, a phlebotomy room, a waiting room, and locked patient files. Physicians, licensed medical technologists, a nurse, and a medical secretary are among the staff of the clinic. During the past year, the clinic provided facilities, technical services, supplies, and/or personnel for 18 other LBL projects, as well as a 6-week concentrated course in hematology.

3. DONNER PAVILION

The Donner Pavilion Group continues to make significant contributions to the understanding of endocrinopathies associated with the pituitary gland, through investigations of hormonal interactions and the development of techniques for assessing alterations of molecular structures resulting from exposure to heavy-ion radiation or to environmental pollutants. For over 20 years, high-energy 910-MeV alpha particles have been used to suppress pituitary function in patients with disorders of the pituitary gland or those with diabetic retinopathy. Today, investigators are doing preliminary primate studies with carbon-12 ions. These higher-energy particle beams have additional radiobiological properties which will allow the physicians to extend the therapy program to include treatment of patients with hormonally dependent metastatic breast cancer, with advanced diabetic angiopathy, or with large destructive pituitary neoplasms which are not amenable to the lower-energy alpha-particle pituitary irradiation (APPI).

APPI continues to be recognized as an advantageous form of therapy for many pituitary tumors. An integral part of the program is the long-term follow-up of patients who received APPI, thus providing valuable data for investigations of the biological properties of the human pituitary. In studying effects of heavy ions on functioning tissues, investigators have a rather special opportunity to monitor both normal and pathological hormonal secretion. During the past year assays for two new hypothalamic peptides, beta-lipotropin and, more recently, beta-endorphin—the endogenous morphinomimetic peptide—were developed. Significant changes in circulating levels of these hormones were found in pituitary tumor patients, and the increased levels were lowered after APPI. Their role in the etiology of pituitary tumors as well as their physiological function are being explored.

A final area of great importance is the long-term follow-up of any side effects of localized heavy-ion exposure. All patients have incidentally had low-level, whole-body exposure to heavy ions at the time of treatment. Since this treatment is successful in controlling pituitary tumors, patients have been followed for substantial periods of time (up to 20 years at present) and provide a special population for studying these effects. The careful follow-up studies of these patients, with baseline and provocative tests performed before and periodically after treatment, provide a valuable source of information concerning the long-term effects of heavy-ion radiation. These data are of particular importance to the recent adaption of heavy-ion therapy for treatment of cancer of the brain, head and neck, and pancreas.

The highlights of the research effort over the past year are summarized in the following reports.

PITUITARY IRRADIATION PROGRAM

John A. Linfoot, Eckehart Wiedemann, Jacob I. Fabrikant, and Jeanette S. Nakagawa

The Donner Pavilion pituitary irradiation program brings together special skills from the fields of engineering, biophysics, and biochemistry, and expertise in medicine, radiology, and endocrinology to provide a unique long-term study of the radiobiological and pathophysiological effects of heavy ions in the control of functioning and non-functioning pituitary tumors. Protocols have been designed to investigate the acute and long-term effects of low-level, total-body and localized, high-intensity, heavy-ion exposure; to examine changes in physiological function of the endocrine, central nervous, cardiovascular, renal, and hematopoietic systems; and to study the histological effects on normal and abnormal pituitary tissues.

In 1978, our symposium "Recent Advances in the Diagnosis and Treatment of Pituitary Tumors," sponsored in conjunction with Alta Bates Hospital and the University of California Extension Division, focused on the diagnosis of pituitary tumors and the treatment of acromegaly, Cushing's disease, hyperprolactinemia, and other disorders of the hypothalamus and pituitary, and provided a comprehensive review and update of the basic anatomical and biochemical features of the hypothalamo-hypophyseal system.

An internationally recognized faculty reviewed and updated clinical features and techniques in the fields of neuroradiology, neurosurgery, and endocrinology, including the analyses of hypothalamic and pituitary hormones by radioimmunoassay and the new radioreceptor assays, and provided a comprehensive understanding of basic research in the biochemistry, histology, and physiology of the hypothalamo-pituitary axis. In addition to presenting the current status of the art and science required in the diagnosis and treatment of pituitary tumors, the participants elucidated a number of current problems in the management of pituitary tumors which serve as research goals in our effort today.

Patients treated with alpha-particle pituitary irradiation (APPI) are followed serially with baseline and provocative studies, and thereby provide valuable data concerning the long-term effects of heavy-ion radiation. These data have been instrumental in providing information for the heavy-ion treatment of cancer of the brain, head and neck, and the pancreas, and have contributed significantly to the investigation of other hormones such as somatomedin, β-lipotropin, and β-endorphin. The radioreceptor assay for somatomedin and radioimmunoassay for β-endorphin were developed this past year, and further information concerning these hormones and β-lipotropin is presented in the papers that follow this report.

A recent review of the long-term effects of APPI on patients treated for diabetic retinopathy continues to confirm the apparent improved survival in this patient group. Although a certain number of our diabetic population die of microangiopathic complications, specifically of nephropathy, this group may have a more favorable prognosis than is found in reports in the literature (see Fig. 1). The rate of deterioration of glomerular filtration rate was slower in APPI-treated patients. From these data we concluded that APPI may have had a positive effect on patients with diabetic renal disease, and this may be responsible for their improved survival. We continue our follow-up of these patients, who were treated from 10 to 18 years ago, and these findings will provide a basis for future studies in patients with diffuse diabetic angiography.

During the past year, with the cooperation of Laboratory workers in several heavy-ion disciplines, including heavy-ion radiography and radioactive beam scanning, and with the biophysical support team of the pituitary group, we have identified several approaches by which we can improve pituitary tumor localization. This effort will increase our success in treating pituitary tumors by allowing better control of tumor growth and hormone secretion, and reducing the incidence of side effects such as hypopituitarism.

Although APPI is successful in the treatment of many functioning and non-functioning pituitary tumors, techniques for precise localization and delivery of higher energy (Bragg peak) radiation to the pituitary are required before we will have optimal therapy to treat patients with hormonally dependent metastatic breast cancer; diabetic angiopathy; and large, invasive, pituitary tumors.

We have initiated a study using heavier ions available at the Bevalac with the following objectives: 1) to develop precise localization and physical dosimetry using carbon-12 particles for the destruction of pituitary gland in primates; 2) to develop improved techniques for imaging the primate skull, particularly the pituitary (sella turcica) using computerized tomographic (CT) scans and heavy-ion radiography; 3) to use this noninvasive methodology to treat animal models such as canine Cushing's disease; and 4) to eventually be able to use the higher-energy radiation for performing total hypophysectomies in patients with hormonally dependent breast cancer or advanced diabetic retinopathy. Both these conditions require rapid pituitary ablation not possible with the lower energy APPI.

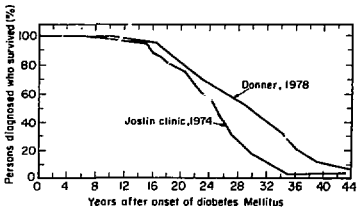

Figure 1. Survival of patients with diabetic renal disease (nephropathy) who were treated for proliferative diabetic retinopathy with alpha particle (910 MeV helium ions) pituitary irradiation (APPI). There is an apparent improvement in survival of patients following APPI when compared to patients with comparable degree of renal function followed at the Joslin Clinic for the same period of time. (Kussman, M.J., Goldstein, H.H., and Gleason, R.E. JAMA 236: 1861–1863, 1976.) XBL 7812-12388

We are using the monkey as an animal model for studying the effect of carbon-12 Bragg-peak pituitary irradiation. Baseline pituitary function studies were performed prior to the irradiation procedure. The responses of pituitary hormones to stimulation of the hypothalamic pituitary axis during several provocative tests were determined. These tests included stimulation with thyroid releasing hormone (TRH), with gonadotropin releasing hormone (GnRH), with insulin-induced hypoglycemia, and with arginine infusion.

The appropriate rises in thyroid stimulating hormone (TSH) and prolactin were seen in response to TRH; luteinizing hormone (LH) rose in response to GnRH; and growth hormone (GH) responses to insulin and arginine were demonstrated. This endocrine protocol will serve as the *in vivo* monitor of the progressive change in pituitary function following carbon-12 Bragg peak therapy. In addition to following the pituitary peptide hormone levels, we will also follow serially the changes in basal thyroxine, cortisol, and testosterone levels. These studies will provide further information concerning the sensitivity of various pituitary cell types to heavy-ion exposure, the rate of development of pituitary ablation, and, finally, the sensitivity of the surrounding neural structures to carbon-12 therapy.

SERUM SOMATOMEDIN IN PATIENTS WITH PITUITARY TUMORS

Eckehart Wiedemann, John A. Linfoot, Robert G. Tang, Josephine A. Lundberg, Jeanette S. Nakagawa, Emanuela N. Catena, and Tamara B. Mihailovsky

During the past year we have continued and nearly completed the first phase of our investigation of somatomedin (SM) in pituitary tumor patients. Our findings, although in part still preliminary, promise to affect the diagnostic approach to acromegaly in medical practice and to shed new light on our understanding of the nature of pituitary tumors and of somatomedin and growth hormone (GH) physiology.

The somatomedins are a family of hormone-like peptides generated in the liver under the influence of pituitary GH and believed to mediate the most prominent physiological action of GH, namely the stimulation of body growth. It is still uncertain whether somatomedins also mediate other GH actions including those produced by GH excess in acromegalic patients.

We have now assayed serum SM in more than 150 acromegalics and found that although radioreceptor-assayable SM is increased in virtually all cases, bioassayable (or biologically active) SM is elevated in only about 70%. Thus, the development of classical acromegalic symptomatology apparently does not depend on an increased concentration of bioactive SM in serum. Nevertheless, there is evidence for at least a contributory role of SM in the pathogenesis of acromegalic symptoms and signs.

We have identified a small subgroup of less than 5% of the total Donner acromegalic population in whom GH levels are consistently within the commonly accepted normal range of less than 5ng/ml either in the basal state or 1 hour after oral glucose administration (rising blood glucose normally inhibits GH secretion). In these patients the diagnosis was made and treatment initiated on the basis of typical clinical findings in spite of the low GH results. As shown in Table 1, their serum SM was elevated, often strikingly so. Very probably in many more acromegalics with similarly low GH levels and less conspicuous physical stigmata, the diagnosis is not made and patient not treated. Our results suggest that in questionable cases the somatomedin assay may be very useful to establish the diagnosis. Future experience will have to show if the SM assay will also be useful in the detection of early acromegaly, when GH concentration is only mildly or inconsistently elevated, symptoms are mild, and the tumor is still small and hence more responsive to therapy.

Table 1. Serum bioassayable somatomedin activity in acromegalics with low plasma GH.

Subject	Basal GH ng/ml	GH Nadir ng/ml	SM* U/ml
1	2.3	2.7	2.44
2	3.0	1.9	2.08
3	3.4	2.8	4.45
4	3.8	3.8	5.26
5	5.6	3.9	3.56
6	6.5	4.3	3.90
7	6.9	4.9	5.17

**Normal range (82 adult subjects) = 0.45 – 1.70 U/ml.*

The determination of bioassayable SM in serum of patients with Cushing's disease and prolactin-secreting pituitary adenomas also yielded some surprising results. In both conditions GH secretion is commonly severely impaired because of either GH inhibitory action of cortisol or disruption of the anatomical connection between hypothalamus and pituitary. Yet, in neither condition was serum SM as low as would be expected in GH-deficient subjects, and as was actually the case in diabetic subjects made GH-deficient by heavy-particle pituitary irradiation in an attempt to halt the progression of their severe diabetic retinopathy (Table 2). Among the many possible explanations for the normal SM levels in GH-deficient pituitary tumor patients, one is particularly intriguing: the possible production by these tumors of a substance other than GH which stimulates SM production or which is a somatomedin itself. This, as well as other possibilities, remains to be investigated.

Table 2. Bioassayable serum somatomedin activity.

	N	SM* U/ml
Normal adults	82	1.03 ± 0.33
Patients with Cushing's disease, untreated	26	0.96 ± 0.49
Patients with prolactinoma, GH-deficient	14	0.83 ± 0.41
Patients with diabetes mellitus, GH-deficient post heavy-particle pituitary irradiation	13	0.40 ± 0.32

*Mean ± SD.

INVESTIGATION OF HUMAN β-LIPOTROPIN

Eckehart Wiedemann, John A. Linfoot, and Tokuko Saito

This project is an NIH-supported investigation of the normal and pathological physiology of the pituitary hormone β-LPH (beta-lipotropin), made possible by our development of a sensitive and specific radioimmunoassay which permits measurement of this hormone in a fraction of a milliliter of raw plasma.

β-LPH is derived from a 31,000 dalton precursor which also gives rise to another important pituitary hormone, ACTH (adrenocorticotropic hormone). Not surprisingly, therefore, we have previously demonstrated that plasma levels of both hormones tend to rise and fall together. We did, however, discover divergent behavior of the two peptides in patients with pituitary tumors. The β-LPH/ACTH ratio was increased in all cases of Cushing's disease with unequivocal evidence of a pituitary tumor in contrast to a minority of cases with radiologically completely normal pituitary fossa, some of which may have pituitary hyperplasia rather than adenoma. Thus, β-LPH may be a tumor marker in pituitary Cushing's disease and we proposed that a normal β-LPH/ACTH ratio may identify those cases of Cushing's disease caused by hyperplasia and hence not curable by pituitary surgery. Studies are continuing to test this hypothesis.

During the past year we have measured β-LPH in cerebro-spinal fluid (CSF) obtained during diagnostic pneumoencephalography in patients without and with pituitary tumors (Fig. 1). This investigation produced several important results. The most important and surprising finding was a striking elevation of CSF β-LPH in acromegaly, but not in Cushing's disease in which it was not different from patients without pituitary tumors. This is in contrast to our earlier findings concerning plasma β-LPH which is markedly increased in Cushing's disease and on the average twice as high as in acromegaly, although mild to moderate β-LPH elevations were seen in many acromegalics.

Another remarkable result was that CSF β-LPH was several times higher than plasma β-LPH both in patients without pituitary tumors and in patients with acromegaly. Some of the conclusions to be drawn from this study include: 1) the high CSF levels of β-LPH suggest that, in addition to its hormonal function, β-LPH plays a role in the central nervous system; 2) in Cushing's disease there is an abnormal distribution of β-LPH between plasma and CSF; and 3) acromegaly is a disorder not only of CH metabolism, but also of β-LPH metabolism.

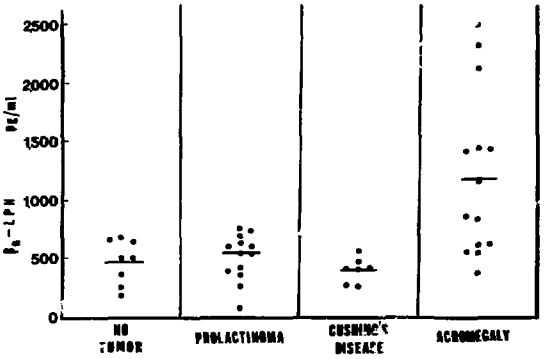

Figure 1. β-LPH in cerebrospinal fluid of patients with and without pituitary tumors.
XBL 795-9724

DEVELOPMENT OF A SPECIFIC RADIOIMMUNOASSAY FOR HUMAN β-ENDORPHIN

Eckehart Wiedemann and Tokuko Saito

β-endorphin (β-EP) is the most potent of several recently recognized endogenous morphine-like peptides. It occurs both in the pituitary and in the brain where it acts as a neurotransmitter and is thought to be involved in pain perception, mood, narcotic addiction, and mental disease. Its amino acid sequence is identical with the carboxy-terminal 31-residue segment of the pituitary hormone β-LPH (beta-lipotropin), from which it is derived by enzymatic cleavage either before or after separation of β-LPH from a larger precursor molecule common to ACTH (adrenocorticotropic hormone) and β-LPH.

This common origin of β-EP with two pituitary hormones suggests the possibility that β-EP itself, besides functioning as a neurotransmitter in the brain, may also serve as a hormone in blood. We have, therefore, in collaboration with C. H. Li of San Francisco, developed a radioimmunoassay for human β-EP which, in contrast to some other recently developed assays, is highly specific for β-EP and sensitive enough to detect 1 pg in 200 microliters of raw plasma. With this assay we have measured β-EP under basal condition in normal subjects and in patients with disorders of ACTH-β-LPH secretion (Fig. 1).

β-EP is clearly present in plasma of healthy subjects under basal conditions, although the concentration is frequently below the detection limit of the assay. Concentrations were much higher in Cushing's disease and enormously elevated in patients with Nelson's syndrome. Like ACTH and β-LPH, β-EP was found to decrease after dexamethasone administration and to increase after metyrapone administration and after insulin-induced hypoglycemia.

These results suggest that β-EP functions as a hormone, although no target organ has yet been identified. With this assay we plan to investigate the regulation of plasma β-EP under physiological conditions as well as in various disease states including mental disease and narcotic addiction. In addition, since the assay also detects rat β-EP and can be applied to other biological fluids and tissue extracts, it may serve as a valuable tool to investigate, in an animal model, the effects of drugs, toxic agents, and environmental pollutants upon brain β-EP levels and distribution, and to correlate possible alterations thereof with behavioral, biochemical, and anatomical changes.

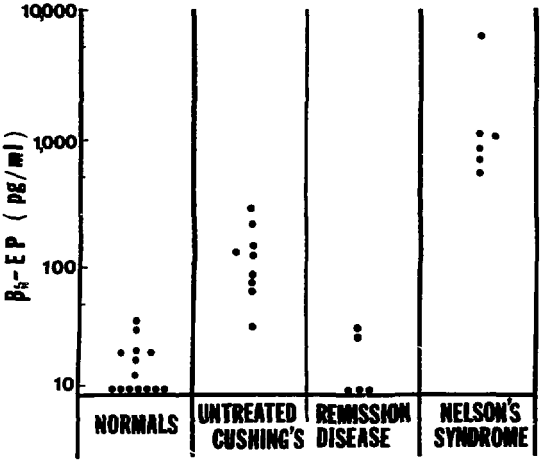

Figure 1. Plasma β-endorphin concentration in human subjects. XBL 795-9529

4. PERALTA CANCER RESEARCH INSTITUTE

The Peralta Cancer Research Institute (PCRI), directed by Dr. Adeline J. Hackett, was formed in May 1974 as an association of Peralta Hospital, Oakland, with the University of California, Berkeley. The Institute's goal is to encourage mutually beneficial interactions between basic researchers and clinicians practicing oncology. Thus, the tumor biologist gains clinical information needed to design new and perhaps more relevant model systems, and the clinician can be provided with important new and effective tools for the early diagnosis of disease and improved patient care. Since July 1977, PCRI has been affiliated with the Biology and Medicine Division of Lawrence Berkeley Laboratory.

The investigators in the cell biology program at PCRI have pioneered in the development of techniques for culturing human epithelial cells. This achievement is particularly important, since approximately 90% of human cancers are malignancies of this cell type and, until recently, no one had successfully grown most human epithelial cells in culture. The cancer diagnosis program has been concerned with researching new techniques for early diagnosis of breast cancer in women.

Studies have concentrated on developing and evaluating a simple test on breast-fluid samples that would be similar to the "pap" smear which has been so successful for early detection of cervical cancers. Further plans include working with oiologists and physicists to evaluate heavy ion radiation technology as a potential modality for early diagnosis of breast cancer. The cancer treatment program has been concerned with applying cell biology and biochemistry advances to improve cancer management. This group has begun to apply the expertise in culturing human cells developed at PCRI to test cancer cells for sensitivity to chemotherapy drugs. Hopefully, this approach will optimize chemotherapy effectiveness by determining the most effective drug combinations and by ruling out ineffective agents thus eliminating unnecessary patient toxicity.

These programs demonstrate how effectively the Lawrence Berkeley Laboratory can work together with the local medical community to apply basic research advances for improved patient care.

CELL BIOLOGY PROGRAM

Adeline J. Hackett, Helene S. Smith, and Martha R. Stampfer

Many relevant assays have been developed to evaluate the carcinogenicity of various compounds, including *in vivo* studies with rodents, and *in vitro* studies assaying mutagenicity using various eukaryotic and prokaryotic systems or transformation of rodent tissue culture cells. However, one of the major sources of concern regarding chemical carcinogens is evaluating the applicability of these various tests to humans.

Since many differences have been observed between human and murine cells which may be relevant to carcinogenesis assays (i.e., variability in enzyme populations, metabolic pathways, and growth properties, as well as differences in the incidence of cancer among various species), it is extremely important to study the effects of carcinogens on human cell substrates to directly validate results obtained with other transformation systems.

Furthermore, most murine tissue-culture transformation systems have utilized fibroblastic rather than epithelial substrates. Since approximately 90% of human cancers are carcinomas, that is, tumors derived from epithelial cells, it is also important to test for chemical carcinogenesis on epithelial cell substrates, as there may be significant differences in the effect of chemicals depending on the cell type utilized.

One of the major difficulties with developing an assay to test carcinogens on human cells has been the inability to grow the cells in culture. During the past few years the cell biology group at the institute has had a major breakthrough in this difficult area. M. Stampfer has developed a medium using various hormones and growth factors which readily supports the short-term culture of human mammary epithelial cells derived from reduction mammoplasties. The cooperation of local surgeons in providing tissue specimens necessary for this work further illustrates the way in which PCRI has become a catalyst for promoting cooperation between LBL staff and the medical community.

Figure 1 illustrates a confluent culture of normal

Figure 1. Human mammary epithelial cells in culture forming secretory domes. XBB 788-9644

mammary epithelial cells showing the differentiated property of secretory dome formation. The function of mammary epithelial cells *in vivo* is to secrete fluid; the cultured cells maintain this function and secrete a fluid "bubble" underneath the cell monolayer thus forming the secretory dome.

We have begun to use this newly developed culture technology to study the effect of the combustion-produced carcinogen, benzo(a)pyrene (BaP), on human mammary cells. Figure 2 illustrates the toxicity of BaP for the mammary epithelial cells. In contrast, mammary fibroblasts from the same donor showed little or no effect of the chemical. To our knowledge, this is the first report of BaP toxicity for human mammary epithelial cells. The figure also graphically illustrates the importance of studying the effect of carcinogens on epithelial cells (the cell type which most commonly becomes cancerous) rather than fibroblasts (the cell type most easily studied in culture).

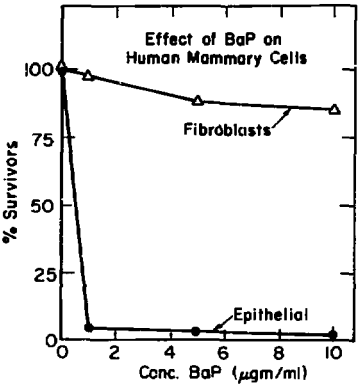

Figure 2. Effect of carcinogen, (benzo (a) pyrene) on cultured fibroblasts and epithelial cells derived from normal human breast tissue. XBL 795-3478

CANCER DIAGNOSIS PROGRAM

Adeline J. Hackett, Helene S. Smith, Otto W. Sartorius, and Martha R. Stampfer

A technique has been developed at PCRI for diagnosis of breast cancers or benign breast lesions which are too small to be palpated or diagnosed by mammography. By means of a nipple aspiration device invented by O. Sartorius, intraductal fluid can often be obtained from nonlactating women. The fluid which contains ductal epithelial cells is then processed, stained by the Papanicolaou method, and examined cytologically by a cytotechnologist under the direction of a qualified pathologist.

When abnormal cells are discovered, a new x-ray technique developed by Dr. Sartorius termed "contrast ductal mammography" is used to locate the lesions. With the aid of a dissecting microscope, a very fine nylon catheter is inserted into the appropriate duct, and a water soluble contrast material is injected. X-rays are then taken, the fluid withdrawn from the ductal system, and cytological studies performed for corroboration of the previously obtained abnormal cytology. Use of the contrast fluid allows x-rays to be taken using approximately 20-fold less radiation than a standard mammogram.

CANCER TREATMENT PROGRAM

Adeline J. Hackett, Helene S. Smith, Tom K. Lee, and Martha R. Stampfer

The cancer treatment program at PCRI offers to East Bay oncologists a clinical test that assays breast cancers for hormone receptors. This test helps the clinicians to evaluate when a patient's breast cancer will respond to hormonal manipulation. Basic research at PCRI on the hormone receptor proteins is concerned with determining the relationship between the quantity and molecular size of these proteins and the patient's response to hormonal manipulation. These studies are being done in cooperation with the Northern California Cancer Program in an attempt to standardize assays and coordinate patient follow-up in order to optimize usefulness of this new test.

The cancer treatment program has also begun some basic research studies to determine whether it will be possible to evaluate a patient's response to chemotherapy drugs using cultured tumor cells. One of the problems with applying such studies to breast cancer is that the tumors elicit an extreme proliferation of stromal cells, so that pure epithelial cultures are difficult to obtain. The group is therefore attempting to evaluate toxicity using a histological approach which would permit the observer to distinguish the drug's effect on the tumor cells from its effect on any contaminating fibroblasts. Figure 1 illustrates the effect of various drug concentrations on a culture of normal mammary epithelial cells. Current experiments are directed toward calibrating such a histological approach with more quantitative cell measurements developed with model systems.

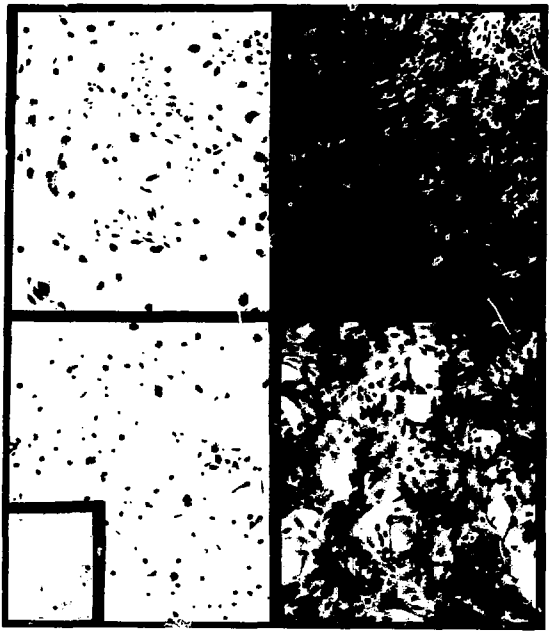

Figure 1. Effect of drugs on growth of normal mammary epithelial cells. XBB 792-2900

5. ENVIRONMENTAL PHYSIOLOGY

The Environmental Physiology Group, led by Dr. Joseph F. Garcia, continues to investigate changes that occur in physiological activity when the living organism attempts to maintain homeostasis—the constant internal environment required for good health. Investigators are using knowledge and expertise gained from studies of how disease mechanisms alter homeostasis to shed light on how environmental pollutants exert their effects on the body's internal environment. These findings would provide a scientific basis for successfully treating such effects should they occur. Furthermore, methods could then be developed for the early detection of adverse effects from exposure to environmental pollutants, thereby allowing the establishment of appropriate exposure standards for the general population.

The internal metabolic processes in several body systems of rodents are being studied to assess quantitatively the effects of representative types of environmental pollutants. Homeostasis in the hematopoietic (blood-forming) system is delicately regulated by a variety of feedback mechanisms mediated in some instances by circulating hormones, and in others by cell-cell interactions. Investigators are looking at the progenitors of mature red cells and platelets to find out how the regulatory process might be altered as a result of exposure to environmental pollutants. For example, there is some inhibition of these hematopoietic cell progenitors in the blood plasma of animals exposed to ozone, and investigators are trying to characterize that effect.

Others are studying the effects of pollutant exposure on the steroid hormone mechanism. There is a well defined male-female difference in the sensitivity of rodents to ozone exposure: female mice have demonstrated a significantly greater tolerance to the deleterious effects of ozone. Investigators are carrying out various endocrine manipulations in mice to study the possible role of male and/or female sex hormones in this effect.

The biological interface to the atmospheric environment is the lung, and some studies are directed at understanding environmental pollutant effects on the growth and differentiation of lung tissue. Pulmonary macrophages, the large cells in the lung that engulf foreign material and thereby comprise the chief line of defense against inhaled bacteria, viruses, and inert particulates, come into contact with environmental agents at the lung interface. Investigators are studying subsequent changes in these cells, looking for agents that cause a decrease in the number of macrophages present and/or a change in their biological activities which would have grave consequences for health.

Other investigators concentrate their attention on the effects of gaseous-pollutant exposure on the biochemical integrity of lung tissue. Lung cells are rapidly damaged at very low levels of toxic gases. During the repair process following such damage, there is the possibility that proteins ordinarily not present in the blood stream may enter and subsequently initiate an immune response. In addition, these proteins may have been altered by the action of proteases, or pollutant gases such as ozone may react directly with the lung tissue proteins, leading to the presence of unrecognized foreign proteins.

The immune response to the native or foreign proteins could provide a means of assessing the magnitude of the initial lung damage. Furthermore, the proteolytic enzymes released from damaged lung cells are capable of digesting lung proteins and of producing anatomical changes in the lung, leading to the development of lung disease. Work is in progress to develop immunological methods for assessing lung damage at the cellular level and to understand the role of enzymes released from damaged tissue on the pathophysiological development of lung disease.

With the purification of erythropoietin, the primary hormonal material controlling the production of red blood cells, the sensitive radioimmunological assay for detecting its presence has become available. This valuable technique is presently being used in a broad spectrum of clinical and physiological investigations to find out how the erythropoietin concentration responds to various physiological situations and to study the relationship of these changes to the development of anemia.

The continuing study of actinide (strontium-90, americium-241, lead-234) metabolism in monkey skeletons is providing models for understanding the behavior of these heavy elements in man. Investigators are also looking for biological effects of low plutonium exposures to obtain information required to establish appropriate protection standards for persons employed in the nuclear energy industry and for the general population.

The highlights of achievements during the past year in these and other areas of investigational interest are presented in the papers that follow.

EFFECTS OF ENVIRONMENTAL POLLUTANTS ON THE HEMATOPOIETIC SYSTEM

John C. Schooley

Cells of the circulating blood differentiate from several continuously renewing populations in the bone marrow. Distinct blood-cell types have specific functions, but ultimately all are derived from primitive stem cells. Homeostasis in the hematopoietic system is delicately regulated by a variety of feedback mechanisms mediated in some instances by circulating hormones, and in other instances by cell-cell interactions. Proliferation of stem cells and their subsequent differentiation into the recognizable cells of the circulating blood involve complex interactions between mature circulating cells, the humoral regulators, and the various pools of precursors. Thus, damage resulting from disease, radiation, or exposure to pollutants can affect this diffuse system at many levels. Our specific aim is to quantify the effects of pollutants on the blood-forming tissues at different stages of development and maturation, using animal models.

It has become quite clear from our studies of two representative pollutants—the heavy metal, lead, and the gaseous pollutant, ozone—that stimulation of the most primitive precursor that can be measured by available experimental methods is triggered to rapidly proliferate in acute lead poisoning, but is markedly inhibited in animals breathing ozone. Our major concern has been to investigate the physiological mechanisms for these observed changes.

During acute lead poisoning, the primitive precursors of the hematopoietic system, termed CFU-S (colony-forming unit—in the spleen), are dramatically increased in the circulating blood and in the spleen, and less of an increase occurs in the bone marrow. In the absence of the spleen, a significant increase is observed in the bone marrow and blood, indicating the possibility that the marked increase observed in the spleen, and particularly in the blood, is a bone marrow phenomenon rather than a splenic phenomenon. Measurements utilizing *in vitro* systems of a progenitor of the granulocytic and macrophage system, the CFU-C (colony-forming unit—in culture) indicate a marked increase in the bone marrow and spleen. In addition, in the serum of lead-poisoned animals, we have observed a marked increase in the concentration of the humoral agent termed CSA, which is believed to be involved in the regulation of the growth of CFU-C.

The circulating platelets are also derived from the primitive progenitor cell through an intermediate population, and can be measured utilizing *in vitro* techniques or a bone marrow repopulation technique. We have found that following acute lead poisoning the platelet concentration in the circulating blood is reduced for about 4 days, and then dramatically increases above the normal level. Other studies have indicated that this increase is the result of extensive proliferation of platelet precursors in the hematopoietic tissue. The latter is probably related to a marked increase in a humoral agent regulating platelet formation, which occurs during the second and third day following lead poisoning. Considerable effort has been devoted to understanding the mechanism of this platelet increase following lead poisoning. After lead is injected, it appears to have a direct effect upon a small number of platelets; but the surviving platelets appear to survive in the circulating blood to the same extent as normal platelets.

Our specific aim is to determine the nature of the stimulators involved in increasing the concentrations of CFU-S, CFU-C, and platelet precursors following lead poisoning. Particular emphasis has been given to the nature of the humoral agents involved and to the kinetic changes in the proliferation of the various precursor cell populations.

In contrast to the reaction of animals with acute lead poisoning, mice breathing ozone at 1 ppm display a marked inhibition of CFU-S development in the spleen, bone marrow, and peripheral blood. Using *in vitro* systems, we have observed an inhibitor of the development of CFU-C. Our major effort has been to determine the nature of the inhibitor, and whether it plays an important role *in vivo*.

Another aspect of this proposal has been to determine the sensitivity of femoral CFU-S to heavy charged particles produced by the Bevalac. The objective of these studies is to define critical radiobiological parameters. Our current estimates of the extrapolation number and rate of cell killing (Do)

are 1.8 and 115 rad for ^{60}Co radiation, 1.1 and 82 rad for carbon, and 1.4 and 78 rad for neon, utilizing the spread out Bragg peak. Thus, as linear energy transfer (LET_∞) or mass/charge of the heavy charged particles increases, the principal effect is on the extrapolation number, rather than the slope of the survival curve.

Studies of the cellular proliferation of hematopoietic tissue, particularly studies concerned with the effects of pollutants, will be extended in the future to other heavy-metal pollutants and to gaseous pollutants such as carbon monoxide, carbon dioxide, the oxides of nitrogen and sulfur, as well as to aromatic hydrocarbons.

EFFECTS OF ENVIRONMENTAL POLLUTANTS ON STEROID HORMONE MECHANISMS

Gerald M. Connell

Within the past few years our experiments in the field of environmental pollutants have focused upon the sex-dependent differences for ozone toxicity exhibited by male and female mice. Female mice demonstrate significantly greater tolerance to the deleterious effects of ozone, a common component of photochemical smog. Our studies have sought a possible endocrine or hormonal explanation for these observations.

Presently, experiments involving ozone exposure in conjunction with a variety of endocrine manipulations are in progress. These manipulations include orchidectomy and oophorectomy to eliminate the major endogenous sources of male and female sex steroid hormones. In addition some of these castrated males are treated with estrogen hormones and some of the castrated females are treated with androgen hormones. From these studies, we may be able to determine to what extent the female sex steroids provide a protective mechanism against—or perhaps to what extent the male sex steroids predispose the organism to—the toxic effects of ozone.

Recent results from ozone exposure experiments have identified subpopulations of both male and female mice which demonstrate increased sensitivity to ozone toxicity when compared to littermate control mice. This intriguing observation is one that is similar to responses noted in other laboratories involving human subjects and gives us added support in our choice of the mouse-model for the laboratory examination of the harmful biological effects of ozone. A variety of endocrine parameters in these "sensitive" and "resistant" mice are being quantitated and these results will be contrasted to our endocrine replacement studies.

It is possible that in some species, including man, some individuals may be more susceptible to environmental pollutants than are other individuals. To examine the possibility that these differences are genetically determined, we have completed preliminary breeding experiments with various combinations of ozone-"sensitive" and ozone-"resistant" mice. It appears that some inherited traits may predispose these rodents to the toxic effects of the photochemical agent. Lungs of unaffected mice are normal in their gross characteristics; those of affected mice are edematous, and two to three times normal size. A significant number of the sensitive mice were sired by resistant parents. We are continuing our studies in this area.

Examination of the biochemistry of the testis of animals exposed to various metal pollutants continues. In the past, we have demonstrated that the metals cadmium and mercury can severely interfere with the production of the male hormone, testosterone. More recent experiments suggest that the testes of rodents chronically exposed to either 3 ppm or 10 ppm cobalt may produce somewhat more androgen than normal. The explanation for this unusual response is presently being sought.

In addition to various pollutants which might affect the organism (especially its steroid hormone mechanisms), we have examined the effects of conventional ^{60}Cobalt (^{60}Co) and heavy-ion irradiation on testicular function. Although it is well known that radiation affects spermatogenesis, little is known about its affect on steroidogenesis. The results shown in Figure 1 illustrate several important testicular responses which occur after ^{60}Co irradiation. When radiation damage occurs, the testis weight (●- - - ●) declines because of destruction of the very sensitive developing spermatogonia within the tubular compartment.

As the radiation dose is increased, greater damage occurs within the tubular compartment and, consequently, a greater testis weight loss is observed. The Leydig cells, the sites for testosterone

production, are located between the seminiferous tubules in the interstitial tissue, and this tissue compartment appears to be resistant to the effects of radiation. *In vitro*, the Leydig cells of ^{60}Co-irradiated testis appear able to produce much more testosterone (○——○) than normal, and this production is related to radiation dose and testis size. Our results with ^{60}Co and the heavy-ion beams of carbon, helium, neon, and argon show similar response. The reasons for these unusual responses are presently being investigated.

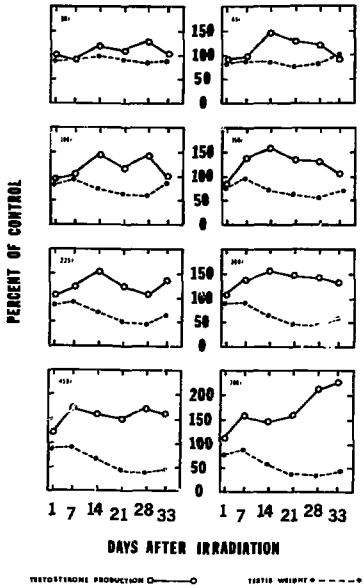

Figure 1. In vivo testis weight change and in vitro testicular testosterone production after whole body cobalt irradiation. Ten-week-old $B_6D_2F_1$ male mice were irradiated with various doses of ^{60}Cobalt (30 rad to 700 rad). Animals were sacrificed at 1, 7, 14, 21, 28, and 33 days after irradiation. The testes were weighed and their ability to produce testosterone in vitro after luteinizing hormone stimulation was quantitated. The testis weight (● - - - ●) declines as radiation dose increases and as the time after irradiation lengthens. The capacity of the testis to produce testosterone (○—○) appears to be increased and is related to radiation dose and the time post-irradiation. Animals receiving the maximal dose (700 rad) produced the greatest quantities of testosterone in this in vitro assay system.

XBL 781-6907

EFFECTS OF ENVIRONMENTAL POLLUTANTS ON PROTEIN METABOLISM

Jonathan S. Dixon

This project is based upon the premise that detailed biochemical or morphological investigations carried out on the primary target organs of pollutant-exposed small animals will reveal changes that are also manifested in quantifiable changes in peripheral blood or in urine. Possibly these results may be used by direct extrapolation to set allowable exposure limits in hormones, or at least they will point the way to analytical procedures that can be adapted by others to the screening of a large segment of the population.

For inhaled pollutants, the lung must be considered the primary target organ. Along with others in the laboratory, we have developed and installed facilities that are suitable for exposing small animals to controlled atmospheres contaminated with known amounts of ozone, one of the representative oxidative air pollutants. Among the primary defen-

ses in the lung against the effects of breathing ozone-polluted air are the pulmonary macrophages. These cells may be eluted intact from the lung (along with surfactant and other non-cellular products) by suitable lavage procedures, and grown in culture on agar plates.

We have attempted to compare the plating efficiency of pulmonary macrophages of exposed test animals (female mice, exposed to 1 ppm of ozone for 1 day) to that of non-exposed animals. Despite considerable difficulty in getting good yields of cells by the lavage procedure, and in plating on agar (because of the presence of red blood cells), viable cells from ozone- and non-exposed lungs were recovered, plated on agar, and counted after 20 days of growth. Morphologically, the colonies were rather small, ranging from 8 to 16 cells per colony. There was no difference in plating efficiency—4.6% for the control and 4.3 ± 0.5% for the ozone exposed cells; these are below values (40%) found in the literature.

In other work accepted for publication in *Environmental Research,* we examined the iron- and copper-containing proteins in whole blood by low-temperature elution paramagnetic resonance spectroscopy, looking at the effects of *in vitro* and *in vivo* exposure of animals to atmospheres containing NO, NO_2, and O_3.

In vivo exposure of animals (or humans, Fig. 1) to air containing a few ppm NO or NO_2 gives rise to significant accumulations of both Hb-NO and methemoglobin. This effect can be seen under typical ambient conditions. Exposure to moderate levels of O_3 fails to alter the state of hemoglobin in whole blood, nor does it generate a measurable change in organic free-radicals. However, all three gases significantly increase the signal due to high-spin ferric catalase, while NO, NO_2, and O_3 all depress the level of iron transferrin.

Besides adding to the fundamental knowledge of the effects of exposure of both animals and humans, this paper provides a method for simply and noninvasively gathering information about the level of contamination in humans by the oxides of nitrogen. All that is required is that a small sample of blood, withdrawn by vein puncture, be placed in a quartz tube, frozen, stored, and transported to the laboratory for analysis at some future date. Samples could be readily collected by trained personnel at nearly any location, including the workplace or home. Further work is indicated by the finding in this investigation that all three of the oxidant gases measured depress the level of iron transferrin.

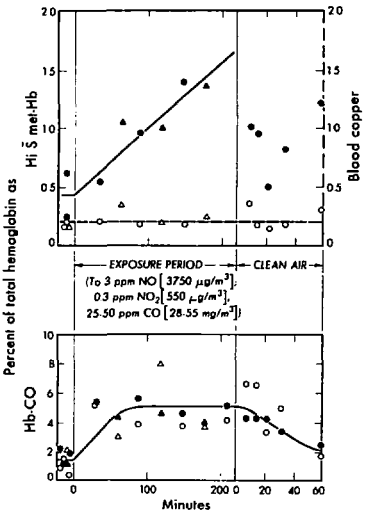

Figure 1. In vivo experiment involves blood samples drawn at various times during exposure of humans to air containing combustion effluents in the concentrations shown, and then during the immediate subsequent exposure to clean air; drawn samples were immediately frozen for later analysis. Circles represent results from one experiment; triangles are from a second experiment.

Above: high-spin methemoglobin (solid symbols) and g=2.04 copper (II) (open symbols) as detected in blood by EPR spectroscopy. Concentrations are expressed as percent of heme.

Below: carboxyhemoglobin (Hb-CO) in the blood samples is measured optically at two (open and solid symbols) wavelengths in the visible region. No nitroxyhemoglobin detected. XBL 7512-9595

HORMONE STUDIES IN RATS EXPOSED TO ENVIRONMENTAL POLLUTANTS

Gisela K. Clemons and Joseph F. Garcia

The main objective of our proposal is to study the effect of non-nuclear energy pollutants on the production, secretion, and metabolism of protein and polypeptide hormones in laboratory animals. A variety of gaseous and metal pollutants, presented both acutely and chronically, are being studied. The radioimmunoassay technique has been extensively employed for hormone measurements. Initial studies concerned with the effects of ozone on hormonal systems have led us to an extensive study of the hypothalamo-pituitary-thyroid axis of rats perturbed with this pollutant.

Exposure of rats to ozone concentrations of 1 ppm for 24 hours resulted in the hormonal changes seen in Table 1. A highly significant ($p < 0.001$) decrease of circulating thyrotropin and thyroxine levels was observed. Triiodothyronine levels were also reduced ($p < 0.05$). Plasma prolactin levels were significantly elevated ($p < 0.005$). The thyroid weight was always significantly increased in ozone-exposed rats (41.92 ± 2.9 mg) when compared to control animals (25.92 ± 2.99; $p < 0.01$).

In an attempt to dissect the primary effect of ozone on this hormonal system, a variety of *in vivo* and *in vitro* studies were initiated. *In vivo* and *in vitro* studies with the hypothalamic-thyrotropin releasing hormone (TRH) indicated that the anterior pituitary was capable of normal function. The thyroid gland itself appears to respond normally to its stimulatory hormone, and exposure of rats to a cold stimulus immediately following ozone exposure indicated that the hypothalamus was capable of normal function.

Whether the observed disturbance of the hypothalamo-pituitary-thyroid axis is attributable to peripheral changes of thyroid hormone metabolism or possibly to a lowered hypothalamic setpoint of TRH release is currently being investigated. Indications are that lowered thyroid hormones are beneficial for the protection of the animals during ozone exposure and, therefore, that changes in peripheral hormone metabolism or a reduced hypothalamic setpoint are an adaptive mechanism or induced homeostasis.

The occurrence of edema in the lung and the thyroid after ozone exposure indicates that there are significant fluid shifts occurring within the animals. Because prolactin has been implicated as an osmoregulatory factor in mammals, the elevated prolactin levels observed after ozone exposure may play a functional role and will be further investigated. The nature of the edema of the thyroid gland will also be further studied using standard morphological approaches of light and electron microscopy.

Endocrine disturbances following chronic and acute administration of metal pollutants, especially mercury, cobalt, cadmium, nickel, and arsenic, are currently being investigated. Most metals tested so far alter either pituitary hormone synthesis or release into the circulation. Cobalt is of particular interest because we have indications that at low physiological levels cobalt may play an endocrine role as a possible cofactor in the release of prolactin. Chronic administration of cadmium in drinking water will also be pursued at 0.5, 5, and 25 ppm for 12 months, because our previous study at 5 ppm—the maximum limit established by the WHO, already led to endocrine disturbances.

Table 1. Circulating hormone levels in male rats after 24-hour ozone exposure at 1 ppm.

	Control	Ozone	n	p
TSH (uU/ml)	338.8 ± 45*	174.2 ± 12	25	.001
PRL (ng/ml)	63.3 ± 3.1	93.8 ± 9.5	23	.005
T4 (ug/100 ml)	57.5 ± 3.0	39.3 ± 2.6	28	.001
T3 (ng/100 ml)	56.0 ± 4.1	44.0 ± 1.1	16	.05
PBI (ug/100 ml)	4.93 ± 0.2	3.9 ± 0.22	18	.001
T3 uptake (%)	60.89 ± 0.82	62.26 ± 0.71	24	NS

*Values are expressed as MEAN ± SE.

EFFECTS OF ENVIRONMENTAL POLLUTANTS ON THE IMMUNE SYSTEM

Joan W. Goodman

Because bone marrow is a continuously renewing cell population, it is extremely vulnerable to damage from a variety of agents that affect dividing cells, such as energy-related pollutants. It is important to know as much as possible about the normal physiology of this organ and about its reaction to insults, for the body's functional integrity depends on its products: the formed elements of blood and of the immune system. All of these peripheral cells have been shown to come from a single multipotential marrow stem-cell, but for each differentiation pathway there are probably sequential intermediate progenitors. The regulation of the many differentiative steps in this highly integrated system is necessarily complex. It is thought to involve direct cellular interactions as well as the mediation of hormones such as erythropoietin and thymosin.

Energy-related pollutants such as lead and ozone have been shown to alter hemopoietic stem-cell kinetics and to depress immune functions in experimental animals. The possible consequences of such changes, although not yet explored in detail, could be life threatening. For example, there is a suppressive factor in serum of ozone-exposed animals that significantly inhibits *in vitro* growth of monocyte-macrophage colonies. If this factor is similarly active *in vivo*, all functions dependent on macrophages (and this includes most of the body's defense mechanisms) can be expected to be depressed.

In the past year we have initiated studies of effects of the environmental pollutant lead (Pb) on immune function in a genetically defined hybrid mouse. Proliferative responses to T lymphocyte (phytohemagglutinin and Concanavalin A or ConA) and B lymphocyte (lipopolysaccharide or LPS) mitogens were studied after intravenous injection of 1% lead acetate (0.2 ml per mouse) in 5% dextrose in water. After 3 or 4 days, at which time spleen and blood CFU-S (colony-forming unit—in the spleen) are elevated, spleens were removed aseptically and prepared for *in vitro* culture with the mitogens.

Three experiments to date have confirmed in $B6D2F_1$ mice that, insofar as response to mitogens reflects cell populations in the spleen, acute lead exposure causes no decrease in T and B lumphocytes. Culture results are not so easily interpreted, however. The actual CPM (counts per minute) values (from incorporation of ^3H thymidine into DNA) of Pb-spleen cells exposed to mitogen do not differ much from those of Na-acetate control spleen cells exposed to the same mitogen, but because the values for unstimulated (NIL) cultures of Pb cells are so high, relative to controls, "delta" CPMs (mitogen-NIL) and SIs (stimulation index: $CPM_{mitogen}/CPM_{NIL}$) are much lower. Clearly low deltas and SIs in this case do not reflect loss of reactive cells but rather increased "baseline" DNA synthesis.

These studies are continuing with respect to the time course of the lead effect. It is not known to what extent non-lymphoid cells are contributing to the greatly elevated NIL values. This question can be addressed by specifically eliminating either T- or B-lymphocytes, or both, with antiserum and complement. Additional parameters of immune function are also being explored, and particular attention is being given to bone marrow progenitors of the immune system.

STUDIES OF GROWTH AND DIFFERENTIATION OF LUNG IN FETAL, ADULT, AND REGENERATING LUNG TISSUE

John C. Schooley

The lung is one of the first major organ systems exposed to toxic gaseous pollutants. Our specific aim is to develop immunologic methods for assessing lung damage at the cellular level and to understand the role of enzymes released from damaged tissue on the pathophysiological development of lung disease.

The lung is a complex organ comprised of a large number of cell types. It is only during the last decade that it has become clear that the lung has a complex metabolic function in addition to its respiratory function. The cells of the lung are severely damaged, particularly those of the alveoli, following exposure to airborne gaseous pollutants. The alveolar capillary is composed of a continuous layer of squamous, alveolar Type I cells, interspersed with alveolar Type II cells separated from the underlying capillaries by a basement membrane. Macrophages

are found within the alveoli. The endothelial cells of the capillaries also rest on a basement membrane. The capillary endothelium is continuous, and in the interstitial space between the basement membrane of the endothelial and epithelial cells are found fibroblasts, macrophages, polymorphonuclear leukocytes, and collagenous and elastic fibers.

A "protease pathogenesis" hypothesis of lung disease has been advanced by some investigators. The view is that proteolytic proteases, released from damaged lung cells such as polymorphonuclear leukocytes and pulmonary macrophages, are capable of digesting lung proteins and of producing anatomical changes in the lung, leading to the development of lung disease. It has been demonstrated that the instillation of such proteases into the lung do produce lesions characteristic of lung disease. The activity of these released proteases is inhibited by a number of compounds termed antiproteases.

In the blood plasma, about 10% of the total proteins are antiproteases, and at least six specific antiproteases have been described. But the two major antiproteases found here are the Alpha-1 antitrypsin, having a molecular weight of about 54,000, and the Alpha-2 macroglobulin, with a molecular weight of about 725,000. The development of respiratory lesions as a result of protease released following cell damage is thus minimized if sufficient amounts of antiproteases are present at the site where the proteases are released. It is known that human beings with a decreased level of Alpha-1 antitrypsin are prone to the development of pulmonary emphysema. Because of these findings, we have initiated studies to determine the behavior of antiproteases in mice exposed to 1 ppm ozone for various periods of time.

Elastase is a protease found in a number of lung cells but particularly in the polymorphonuclear leukocytes, where it comprises about 5% of the total soluble proteins. We have found, following the injection of I^{125}-labeled elastase into normal mice, a multiphasic pattern of elimination of the protease. Analysis of this multiphasic curve of disappearance of I^{125} has demonstrated that the enzyme is almost immediately bound to Alpha-1 antitrypsin and Alpha-2 macroglobulin. The enzyme inhibitor complex formed with Alpha-2 macroglobulin disappears rapidly from the blood plasma with a half-life of about 6 to 8 minutes, whereas the combination of the protease with Alpha-1 trypsin disappears much more slowly with a half-life of about 1½ hours.

A particularly interesting finding is that a significant transfer of protease from the slowly disappearing antitrypsin molecule to the rapidly disappearing Alpha-2 macroglobulin normally occurs following injection of the enzyme. Transfer of the enzyme in the opposite direction also occurs in some instances. Most interesting is the fact that the disappearance of the enzyme inhibitor complex from the plasma is decreased when the amount of injected enzyme is increased. We have also found in rodents exposed continuously to ozone that a 5 to 10% drop of the inhibitor concentration in the general circulation occurs. We are now attempting to determine those processes involved in regulating the synthesis of the two major antiproteases in our experimental animals and to clarify whether this synthetic rate is altered in pollutant-exposed animals.

The large-molecular-weight Alpha-2 macroglobulin is not normally found outside the vascular system, so that its role in neutralizing the proteolytic action of proteases released in tissues is unclear. When the integrity of the vascular system is compromised in an injured tissue, such as the lung exposed to pollutants, it is likely that these plasma protease inhibitors move outside of the vascular system. One phase of our experiments is to determine the magnitude of this movement.

Another aspect of our study is concerned with the hypothesis that the damaged lung releases proteins which enter the bloodstream and subsequently initiate an immune response. Membrane proteins characteristic of the alveolar lining cells of the lung are not normally exposed to the immune mechanisms of an animal, so it is possible that, following lung damage, these native proteins when absorbed into the bloodstream initiate an immune response. But, in addition, the possibilities exist that these proteins have been altered by the action of proteases, leading to unrecognized foreign protein, or that pollutant gases such as ozone directly react with the lung tissue proteins, leading to a foreign protein.

A number of clinical observations, including studies of emphysema and Goodpastures Disease, have indicated that humans may have rather high titers of antibody against some lung proteins. In general, these proteins have been derived from the basement membrane; in most cases, antibodies are against collagen or denatured varieties of collagen or elastin. Further subcharacterization of the type of lung protein and whether this specific protein is associated with a particular lung cell type has not been undertaken. We consider the possibility that at least two proteins found only in the lung might initiate an immune response which then would characterize specifically lung damage. These are (1)

the apoprotein believed to be produced by the alveolar Type II cell which leads to the formation of surfactant, and (2) a specific antiprotease protease produced by lung cells. Specific investigations in this area to date have been to utilize polyacrylamide-gel electrophoretic separations to determine whether changes in the lung protein of ozone animals occurs, and we have observed distinct changes in some protein classes. We are now attempting to identify these proteins and determine to which of the various cell types of the lung these proteins are related. In order to accomplish this objective, experiments have been initiated to separate and purify the major cellular types of the lung and characterize their membrane proteins.

PURIFICATION OF ERYTHROPOIETIN

Jonathan S. Dixon, Joseph F. Garcia, and John C. Schooley

We have been engaged in the purification of erythropoietin. The starting material has been either a crude, somewhat hydroscopic powder supplied by the National Institutes of Health, or raw urine from two anemic patients that is made available to us through the efforts of S. Ebbe at this laboratory.

Many years ago a process for concentrating the erythropoietin in the urine of anemic patients was developed in this laboratory. In this procedure, the urine was subjected to pressure filtration through freshly prepared membranes. The product retained by the membrane contained the erythropoietin and was recovered by dissolving away the membrane. We have re-investigated this method of isolation as well as some others, and have concluded that hollow-fiber diafiltration together with lyophylization is a more efficient method for processing the raw urine, since it results in an easily dissolved dry powder (about 100 mg per liter of raw urine) which contains all the erythropoietic activity as assayed in the plethoric mouse assay.

Using the powder, we have processed about 100 liters of urine, from which we have recovered about 100,000 units of erythropoietin. Such material constitutes the crude starting point from which we hope to recover the highly purified erythropoietin, the glycoprotein hormone which regulates red-blood-cell formation in animals and humans. Since calculations show that 10 grams of this material contains less than 2 mg of pure erythropoietin, it is evident that fractionation procedures to recover the pure material presents a large task.

Several steps of purification are under investigation. These include extraction into phenol (see chart), followed by extraction and partial ethanol precipitation in aqueous ammonium acetate-ethanol solution, gel chromatography on Sephadex G-150, and chromatography in Bio Gel A. We have already succeeded in obtaining a small amount of material enriched about 100-fold in erythropoietic activity. Much more purification is still needed, and the rate of progress is restricted by the small amount of glycoprotein hormone present, but the good yields and high recovery of active materials in our isolation procedures augur well for the eventual success of this project.

In addition to bioassay in the plethoric mouse, we have been able to rely heavily on radioimmunoassay results for evaluation of our various purification techniques.

TYPICAL PHENOL EXTRACTION

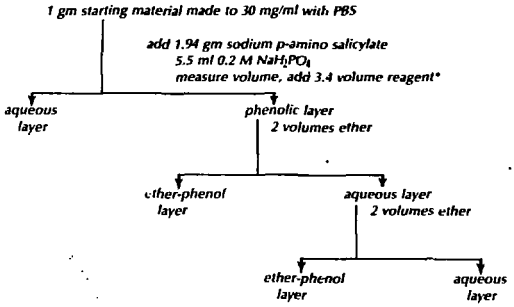

*Lower phase of 1 volume PBS, 1 volume 0.2 M NaH_2PO_4, 3 volumes 0.475 M sodium p-aminosalicylate, 5.67 volumes liquefied phenol.

ERYTHROPOIETIN RADIOIMMUNOASSAY

Joseph F. Garcia

It is now generally accepted that the control of the production of red blood cells is humorally mediated by the hormone erythropoietin. Erythropoietin can be extracted from the plasma and urine of a variety of animal species, including man. Until recently, the accepted method for measurement of this hormone has depended, almost exclusively, on *in vivo* bioassays which involve elaborate animal preparations, and yet are relatively insensitive, requiring the injection of at least 50 mU (milliunits) of erythropoietin as a minimal level of detectability. Since erythropoietin has been shown to be antigenic, several immunological approaches for its measurement have been attempted.

Erythropoietin has been characterized as a glycoprotein hormone with a molecular weight of about 40,000, approximately 50% of which is carbohydrate. It has recently been purified to a specific activity of 70,400 units per mg protein, and it is the use of such material that has made the immunological assay for this hormone feasible.

We have developed a radioimmunoassay for erythropoietin using ^{125}iodine-labeled purified human erythropoietin and an antierythropoietin antiserum prepared in rabbits immunized with human erythropoietin. The erythropoietin was labeled using the lactoperoxidase method, and a double antibody scheme was used for the separation of the free and antibody-bound labeled hormone. The second International Reference Preparation of human erythropoietin was used as a standard. A typical erythropoietic radioimmunoassay curve is presented in Figure 1. This curve shows that an appreciable competition exists with an erythropoietin concentration of 4 mU/ml. Since only 100 microliters of sample is used in this assay, this is equivalent to an absolute amount of erythropoietin, equivalent to 0.4 mU. Bioassays for erythropoietin require approximately 100 times this amount.

The use of purified erythropoietin as the labeled reactant has removed certain discrepancies seen in our previous attempt to develop an immunological assay for this hormone, i.e., plasmas from patients without kidneys do not give the high values previously seen. Plasma from anemic individuals not only result in high radioimmunoassay values, but also show a parallel relationship with the erythropoietin standard when halving dilutions are analyzed. As shown in Figure 2, bleeding of a normal individual increases the plasma erythropoietin level and transfusion decreases it. Such changes are undetectable by bioassay techniques. Erythropoietin from a variety of laboratory animals is also reactive in this radioimmunoassay, with very high values

being observed in hypoxic animals. This radioimmunoassay for erythropoietin is presently being used in a broad spectrum of clinical and physiological studies.

Supplementary to this program, a large amount of urine from severely anemic humans is being collected, in collaboration with J. Dixon and S. Ebbe, as a continued source of human erythropoietin.

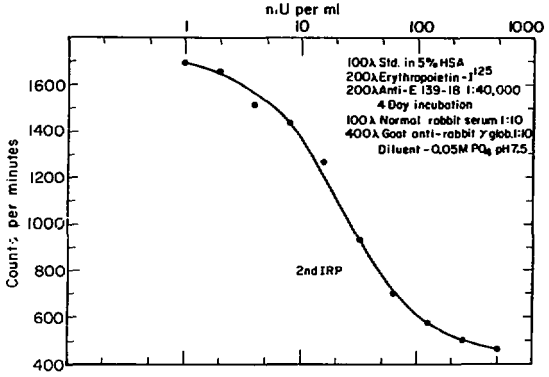

Figure 1. A typical standard curve for erythropoietin radioimmunoassay. XBL 786–3247

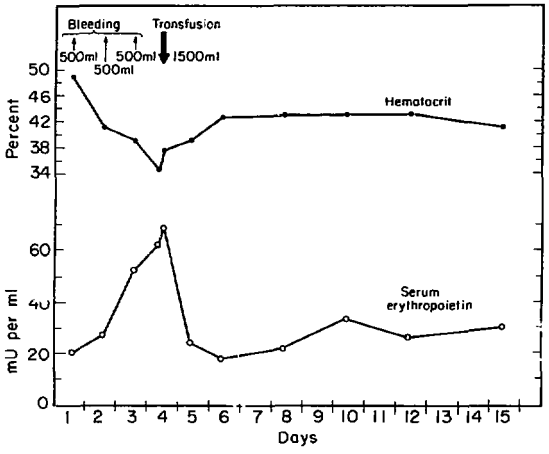

Figure 2. Radioimmunoassay serum values in a normal individual during bleeding and transfusion. XBL 786–3246

^{90}Sr, ^{241}Am AND ^{238}Pu IN MONKEY SKELETON

Patricia W. Durbin and Nylan M. Jeung

Bone is a major site of deposition of the actinide elements, whether they enter the body by ingestion or inhalation[1] and malignant tumors of the skeleton are the major late consequence of that deposition.[2] Radiation protection standards for the actinides seek to prevent deposition of hazardous amounts of those elements in the human body by limiting intakes. Metabolic models for the actinides (that describe their distribution in and elimination from the body) are essential components in the calculation of intake limits. The models available for actinide metabolism in man are primitive,[1,3] and none take account of what is now known about the intra-skeletal distribution of the actinides.[4,5]

Because they are so close to man phylogenetically, non-human primates should provide the best animal model of the differential behavior of the actinides in the adult human skeleton. Adult macaques *(M. mulatta, M. fascicularis)* were injected with a radionuclide in citrate buffer. Injected amounts and study intervals were as follows: ^{90}Sr, 5 to 15 μCi/kg, 1 to 7120 days; ^{241}Am, 0.3 to 0.9 μCi/kg, 1 to 2199 days; ^{238}Pu 0.3 μCi/kg, 1 to 1099 days. At autopsy all tissues and bones were sampled and analyzed radiochemically.

Representative examples of the basic features of skeletal depositions of the test nuclides in individual monkeys at early and late times after administration are shown in Table 1. Data for ^{90}Sr are included because a large body of information has been accumulated on the matabolism of ^{90}Sr and its chemical analogue, ^{226}Ra, in man,[6] and the behavior of ^{90}Sr (also a bone-seeking element) can now be compared directly in primate and human skeletons.

The fraction of the administered dose of the nuclides initially deposited in bone was similar for all three radionuclides, at least for the three monkeys shown in Table 1. Results from additional monkeys killed shortly after injection suggest that the average initial skeletal deposition of ^{241}Am is greater than, and the depositions of ^{90}Sr and ^{238}Pu are the same as or less than, shown here. Deposition of all three nuclides was higher in those parts of the skeleton that contain significant amounts of trabecular bone (spine, thorax, pelvis, long bone ends) than in the compact bone (long bone shafts). The tendency to be deposited preferentially in trabecular bone was much greater for ^{238}Pu than for ^{90}Sr or ^{241}Am.

By 15 years after injection, the total amount of ^{90}Sr remaining was roughly 10% of the initial deposit, and retention of ^{90}Sr in the compact bone was greater than for trabecular bone (for example, the ratio of ^{90}Sr concentration in the bones of the thorax to the average concentration in the skeleton declined from 1.5 to 0.82, while the concentration ratio of long bone shafts increased from 0.51 to 0.89). The study intervals for ^{241}Am (6 year) and for ^{238}Pu (3 year) were not long enough to provide definite proof of loss from the skeleton (at least not based on comparisons of individual monkeys).

However, (a) continued excretion of the two actinides after the liver and soft tissues were essentially cleaned of their initial actinide contents, and (b) shifts in the skeletal concentration ratios (declines of ^{238}Pu in trabecular bones and increases in compact bone) suggest both some real loss of actinides from primate bone over the 3- to 6-year period, and some redistribution caused by normal bone remodeling. More refined data on local actinide deposition (in vertebral bodies and sternum which are almost exclusively composed of trabecular bone) are being compiled and will be used along with estimates[6] of the gross composition of the human skeleton to predict the total amounts of tetravalent (e.g., Pu^{+4}) and trivalent (e.g., Am^{+3}) actinides that may be deposited in the adult human skeleton.

REFERENCES

1. International Commission on Radiological Protection. 1972. *The metabolism of compounds of plutonium and other actinides.* Report of a Task Group of Committee 2, ICRP Pub. 19. Oxford: Pergamon Press.
2. Stover, B.J. and Jee, W.S.S. 1972. *Radiobiology of plutonium.* Dept. of Anatomy, University of Utah, Salt Lake City: The JW Press.
3. International Commission on Radiological Protection. 1959. Report of Committee II on Permissible Dose for Internal Radiation. *Health Phys.* 3:1-380.
4. Vaughan, J., Bleaney, B., and Taylor, D.M. 1973. Distribution, excretion and effects of plutonium as a bone-seeker. In *Handbook of experimental pharmacology, vol. 36, uranium, plutonium, transplutonic elements*, H.C. Hodge, J.N. Stannard, and J.B. Hursh, eds, pp. 349–502. Berlin: Springer-Verlag.
5. Durbin, P.W. 1973. Metabolism and biological effects of the transplutonium elements. In *Handbook* (see ref. 4), pp. 739–896.
6. International Commission on Radiological Protection. 1973. *Alkaline earth metabolism in adult man.* report of a Task Group of Committee 2. ICRP Pub. 20. *Health Phys.* 24:129–221.

Table 1. Intra-skeletal distribution of ^{90}Sr, ^{241}Am, and ^{238}Pu in adult monkeys at early (2 to 8 days) and late time (3 to 15 yr) after injection.

	% dose	Fraction* of skel. burden	Ratio of concs.†	% dose	Fraction* of skel. burden	Ratio of concs.†
^{90}Sr in bone		(R8M, 2 days)			(R61M, 5372 days)	
Spine	6.2	0.25	1.55	0.55	0.20	1.24
Thorax	3.8	0.15	1.50	0.20	0.074	0.82
Pelvis	2.2	0.088	1.08	0.20	0.074	0.86
Head‡	4.9	0.20	1.10	0.77	0.28	1.42
Long bone ends§	3.2	0.13	1.10	0.28	0.10	0.62
Long bone shafts‖	4.7	0.19	0.51	0.71	0.26	0.89
Total skeleton	24.9	1.0	—	2.71	1.00	—
^{241}Am in bone		(C8F, 8 days)			(C75F, 2199 days)	
Spine	8.7	0.33	1.48	10.6	0.36	1.61
Thorax	3.0	0.12	1.25	3.3	0.11	1.12
Pelvis	2.4	0.092	1.16	2.8	0.093	0.97
Head	5.0	0.19	0.19	5.7	0.19	0.83
Long bone ends§	3.1	0.12	0.91	3.4	0.11	1.02
Long bone shafts‖	3.9	0.15	0.56	4.0	0.13	0.54
Total skeleton	26.0	1.0	—	29.8	1.00	—
^{238}Pu in bone		(C109F, 7 days)			(C80F, 1100 days)	
Spine	11.4	0.40	2.05	2.9	0.33	1.64
Thorax	4.2	0.14	1.77	1.3	0.15	1.42
Pelvis	2.0	0.071	1.04	0.72	0.083	1.05
Head‡	5.6	0.19	0.77	1.8	0.20	0.87
Long bone ends§	3.2	0.11	1.13	0.77	0.089	0.77
Long bone shafts‖	2.4	0.082	0.27	1.0	0.12	0.44
Total skeleton	20.0	1.0	—	8.7	1.0	—

*Fraction of skeletal burden = (% dose in bone)/(% dose in total skeleton).
†Ratio of concentrations = (% dose/g ash in bone)/(% dose/g ash in total skeleton).
‡Does not include teeth.
§Includes patellae and fabellae.
‖Includes paw bones.

REMOVAL OF $^{238}Pu(IV)$ FROM MICE BY SULFONATED TETRAMERIC CATECHOYL AMIDES

Patricia W. Durbin (Biology and Medicine Division) and E. Sarah Jones, Frederick L. Weitl, and Kenneth N. Raymond (Materials and Molecular Research Division)

Enteric bacteria (*e.g., E. coli*) synthesize the most potent known Fe(III)-binding agent, enterobactin (EB); it consists of three catechoyl (2,3-dihydroxybenzoic acid) functional groups attached by amide linkages to a cyclic 1-serine triester backbone.[1] The three pairs of o-hydroxyls satisfy the 6-coordinate geometry favored by Fe(III). The catechoyl functional group reacts strongly with metal ions of high charge, small ionic radius, and high acidity; and it reacts weakly, if at all, with other metal ions. Actinides in the (IV) state are chemically similar to Fe(III), and in animals Pu(IV) is associated with Fe-transport and Fe-storage proteins.

Tetrameric catechoyl amide (CAM) molecules were synthesized to accommodate 8-coordinate Pu(IV).[2,3] The 1-serine ester backbone of EB is unstable to hydrolysis, so hydrocarbon chains, $(CH_2)_n$, were used to join the functional groups, providing structural stability and the appropriate intergroup spacings to form a metal-coordination cavity that can accommodate Pu(IV). Sulfonation of the ligands (CAMS) made them water soluble and stable to air oxidation. The structures of cyclic (CY) and linear (LI) CAMS ligands are shown in Figures 1 and 2. Because of the great stability of Th(IV) and U(IV) complexes with catechol[4] ($K_i \sim 10^{52}$) and the low reac-

tivity of catechol with other metals, the CAM ligands should be ideal for *in vivo* binding of Pu(IV).

Mice were injected intravenously (i.v.) or intraperitoneally (i.p.) with ~1.5μCi/kg of ^{238}Pu(IV) citrate, and 1 hour later ~25μmole/kg of a CAMS or other test ligand was injected i.p. The mice were killed 24 hours after the ^{238}Pu injection, and ^{238}Pu in tissues and excreta was measured using the L x-rays. Nine CAMS ligands and $CaNa_3$ diethylenetriaminepentaacetic acid (DTPA) and desferrioxamine (DFOM) were tested. Saline-injected ^{238}Pu controls were killed at 24 hours (13 groups of five mice) to provide data on ^{238}Pu in tissues at the time of sacrifice of the treated mice, and 4 groups of five mice were killed 1 hour after the ^{238}Pu injection to provide a baseline of ^{238}Pu distribution at the time the test ligands were administered. The distribution of ^{238}Pu in treated and control mice is shown in Table 1.

The prototype compound, 3,3,3,3-CYCAM, is sparingly soluble in water. It complexed a significant amount of ^{238}Pu, but the complex could not be excreted. The nitrated molecule, 3,2,3,2-CYCAM-NO_2, also complexed ^{238}Pu *in vivo*, but the complex was not excreted. Sulfonation of the benzene rings, as in 3,3,3,3-CYCAMS, improved the *in vivo* binding of ^{238}Pu, and 37% of the injected dose of ^{238}Pu was

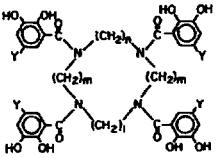

Figure 1. Structure of cyclic (CY) tetrameric catechoyl amide (CAM) ligand. Abbreviation (Y) (1,m,n): 3,3,3,3-CYCAM(H) (3,3,3); 2,3,3,3-CYCAM(SO_3Na) (2,3,3); 3,3,3,3-CYCAM(SO_3Na) (3,3,3); 2,3,2,3-CYCAM(NO_2) (2,3,2).

XBL 794-3344

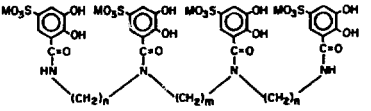

Figure 2. Structure of linear (LI) tetrameric catechoyl amide (CAM) ligand. Abbreviation (N,n,m): 2,3,2-LICAMS (K 2 3); 3,3,3-LICAMS (Na 3 3); 4,4,4-LICAMS (Na 4 4); 4,3,4-LICAMS (K 4 3); 3,4,3-LICAMS (Na 3 4).

XBL 794-3345

*Table 1. Effect of tetrameric catechoylamides in the distribution of ^{238}Pu(IV) in the mouse. Ligands were administered at 1 hour, and mice were killed 24 hours after injection of ^{238}Pu(IV) citrate.**

	Percent of absorbed dose ± S.D. at 24 hr after ^{238}Pu injection					
CAM compounds, (mode of ^{238}Pu injection)	Liver	Skeleton	Soft tissue	GI tract (full)	Kidneys	Whole body
3,4,3-LICAMS (i.v.)	22.3 ± 8.9	6.6 ± 1.2	1.8 ± 0.3	3.3	1.2	35.4
4,4,4-LICAMS (i.v.)	25.0 ± 5.7	8.0 ± 1.2	3.0 ± 0.8	3.0	1.5	40.7
4,4,4-LICAMS (i.p.)	17.2 ± 3.9	4.8 ± 0.4	5.6 ± 0.5	6.7	2.4	36.6
3,3,3-LICAMS (i.v.)	41.2 ± 6.3	9.1 ± 0.4	2.8 ± 0.2	3.3	1.0	55.9
4,3,4-LICAMS (i.v.)	29.8 ± 6.1	11.2 ± 1.6	3.7 ± 0.6	4.3	7.5	56.6
2,3,3,3-CYCAMS (i.v.)	27.6 ± 6.6	18.0 ± 2.1	7.0 ± 1.4	4.7	4.0	61.4
2,3,2-LICAMS (i.p.)	26.3 ± 2.9	12.6 ± 1.0	12.0 ± 1.3	8.1	3.9	63.0
3,3,3,3-CYCAMS (i.v.)	31.6 ± 4.4	14.0 ± 1.4	9.8 ± 2.3	4.7	4.7	64.7
3,3,3,3-CYCAMS (i.p.)	23.7 ± 3.5	17.3 ± 3.4	10.2 ± 2.4	8.0	3.7	62.9
3,3,3,3-CYCAM (i.m.)	23.0 ± 7.0	18.1 ± 4.3	3.3 ± 0.8	3.6	40.9	88.9
3,2,3,2-CYCAM-NO_2 (i.p.)	36.6 ± 8.2	7.9 ± 0.8	26.0 ± 4.0	16.3	6.0	92.8
Other ligands						
$CaNa_3$DTPA (i.p.)	17.3 ± 4.4	10.5 ± 1.4	3.3 ± 1.4	5.2	0.5	36.7
DFOM (i.p.)	22.5 ± 5.9	19.7 ± 2.4	4.1 ± 1.0	4.2	1.6	52.2
^{238}Pu controls						
1 hr (i.v.)	30.0 ± 5.2	22.6 ± 2.2	31.8 ± 2.3	12.3	3.4	~100
24 hr (i.v.)	50.6 ± 7.0	31.1 ± 6.3	5.1 ± 0.8	4.6	2.6	93.9

**Five mice per group except for 4,4,4-LICAMS (10 mice); 1-hr controls (7 mice); 24-hr controls (34 mice).*

excreted. The linear analogue, 3,3,3-LICAMS, promoted excretion of 44% of the ^{238}Pu. Studies of the pH titration of the Th(IV) complex with 3,3,3,3-CYCAM indicated that only 6 of the 8 available donor groups were participating in complex formation. Two new CAMS ligands were synthesized, 4,4,4-LICAMS and 3,4,3-LICAMS, with longer carbon chains separating the functional groups and, therefore, larger metal coordination cavities. Both of those longer-chain LICAMS ligands were more efficient in promoting ^{238}Pu excretion (up to 60% of the injected dose) and the skeletal burdens of ^{238}Pu were reduced to about 0.3 of the amount present at 1 hour (the time the ligands were administered).

The CAMS ligands were subjected to a preliminary test of acute toxicity; five mice were injected daily for 5 days with ~25μmole/kg of the ligand, and at 7 days they were weighed and their tissues were examined for gross changes. None of the CYCAMS or LICAMS with methylene or propylene bridges were acutely toxic. The 3,2,3,2-CYCAM-NO_2 was lethal. Gross changes (mainly shriveling and some hemorrhage) were observed in liver and kidneys of some mice given 4,4,4-LICAMS, and they showed variable weight loss; but the 3,4,3-LICAMS appeared to be well tolerated.

Dose-response curves are in progress for 4,4,4-LICAMS and 3,4,3-LICAMS, and both agents are effective at much lower dosages than those reported here.

REFERENCES

1. Raymond, K.N. 1977. Kinetically inert complexes of the siderophores in studies of microbial iron transport. *Adv. Chem. Sci. No. 162, Bioinorganic Chem.-II*, pp. 33–54. Am. Chem. Soc.
2. Weitl, F.L., Raymond, K.N., Smith, W.L., and Howard, T.R. 1978. Specific sequestering agents for the actinides. 1. N, N^{I}, N^{II}, N^{III}-tetra (2,3-dihydroxybenzoyl) tetracyclo-tetra- and-hexadecanes. *J. Am. Chem. Soc.* 100:1170–1172.
3. Weitl, F.L. and Raymond, K.N. In press. Specific sequestering agents for the actinides. 3. Polycatecholate ligands derived from 2,3-dihydroxy-5-sulfobenzene conjugates of diaza- and tetraazaalkanes *J. Am. Chem. Soc.*
4. Sofen, S.R., Abu-Dari, K., Freyberg, D.P., and Raymond, K.N. 1978. Specific sequestering agents for the actinides. 2. The crystal and molecular structures of tetrakis (catecholato) uranate (IV) and -thorate(IV). *J. Am. Chem. Soc.* 100:7882–7887.

6. RADIATION BIOPHYSICS

The Radiation Biophysics Group, led by Dr. Cornelius A. Tobias, carries out extensive radiobiological investigations using high-energy beams composed of carbon, neon, or argon nuclei accelerated up to 90% of the speed of light at the Bevalac. By systematically studying the physical, chemical, and biological characteristics of these heavy-particle beams, the investigators continue to make significant contributions to our understanding of the nuclear physics of high-energy heavy ions. This knowledge has important applications in biology, medicine, and health protection. For example, in one program, "Treatment of Cancer with Heavy Charged Particles," such information is used for selecting the most appropriate heavy-particle beam to achieve maximum benefit in a specific therapeutic situation.

When radiation energy is absorbed in a living cell, chemical changes take place initially which are responsible for the biological effects that follow. Radiation interacts primarily with water, a major (80%) component of the cellular medium, and the radiolytic products of water can exert damaging effects on DNA molecules. Investigators are studying these underlying chemical processes in detail to help us understand how radiation exerts its effect on organisms. Such knowledge could be used to estimate the biological damage which occurs in human cells when subjected to various types and amounts of ionizing radiation, and these findings may have important applications in radiation safety programs and in achieving optimal use of ionizing radiation in cancer therapy.

When heavy-particle beams pass through tissue, nuclear interactions occur along the path which result in the production of lighter fragments and a consequent modification of the beam's biological effect. Investigators are studying these nuclear interactions and developing calculational methods to predict their effect on dosimetry, so that heavy-ion dosimetry can be precisely determined for therapeutic situations.

Other investigators are continuing tracer studies with radioactive fragments of heavy-ion beams. These resultant energetic radioactive beams can be used for localization of the Bragg peak and accurate positioning of the treatment beam. Studies with phantoms will soon be extended to preliminary animal studies, so that eventually Bragg peak radiation can be used to treat precise tumor volumes, such as the pituitary gland, with great confidence. Energetic radioactive beams will also provide an important biomedical tool for tracer studies. The radioactivity deposited by the beam in tissue will be followed in a manner similar to that used in current diagnostic studies employing administered radioactive pharmaceuticals.

Studies continue which are designed to examine the effects of heavy-ion exposure on human kidney T1 cells and Chinese hamster cells in culture. By analyzing the radiobiological properties of cells in culture, and the effect of high-LET (linear energy transfer) particles administered under varying conditions, these investigators are gaining a better understanding of the basic mechanism involved in cell killing by ionizing radiation. This knowledge provides an important contribution toward achieving the ultimate goal of optimal therapeutic use of ionizing radiation.

Other studies are directed at the response of a solid rhabdomyosarcoma tumor system in rats to high-energy, heavy-charged-particle beams from the Bevalac. Investigators are studying tumor response following irradiation *in vivo* and *in vitro* using various charged-particle beams in single and in fractionated exposures. They have observed differences between radiobiological responses of the R1 tumor cells to peak carbon ions and peak neon ions; they found narrow peaks to be more useful than broad peaks; and they noted an indication that when the depth of tissue penetration is large, as required for treating deep-seated tumors, then carbon ions might be more advantageous than neon ions. The investigators hope to provide a comprehensive model of tumor response to high-energy, charged-particle radiation under various situations to help radiotherapists determine the optimal beam (or beams) to use for specific clinical applications.

The clinical trial to evaluate the use of heavy charged particles in radiotherapy of human cancer continues. Randomized clinical trials are now under way at LBL in cooperation with the Northern California Oncology Group (NCOG) for treatment of cancers of the pancreas and uterine cervix. Additional non-randomized studies are carried out with NCOG for treatment of esophageal cancer and ocular melanoma. Patients have been treated with helium, carbon, and neon ions. In March 1979, following extensive investigations to characterize suitable configurations of the argon beam from the Bevalac, argon ions were first used to treat a cancer patient.

Clinical physics investigators work with the radiotherapy program to assure precise dose localization to the specified target volume. These members of the team seek to maximize the tumor dose while minimizing the dose to surrounding normal structures for each therapeutic situation. They calculate the dose distribution involved in multiport radiotherapy with charged-particle beams, and then quantitatively assess the processes which affect the calculated dose distributions. Using this information, they design ridge filters for use in each specific therapeutic procedure to insure a satisfactory dose distribution throughout the entire tumor volume.

Heavy-ion radiography is being further explored by another group of investigators. The sharpness of the range of high-energy, heavy-ion beams led to their use in radiography. Investigators have shown that this noninvasive imaging procedure can be used to resolve minute density differences found in soft tissues of the body with a low radiation dose to the patient.

The rapid development of technologies for energy production and storage that utilize high magnetic fields, including steady-state and pulsed-mode fusion reactors, magnetohydrodynamic systems, and magnetic energy-storage rings, has resulted in a need for information concerning the biological effects of high magnetic fields. The magnetic fields program is directing its attention to three major areas: 1) a broad-spectrum evaluation of physiological functions in small mammals exposed to high magnetic fields; 2) the in-depth analysis of selected macromolecular systems and tissues with a high degree of sensitivity to magnetic fields, including the visual and cardiovascular systems; and 3) the study of developmental patterns in plants and insects exposed to magnetic fields. Results of these studies will provide quantitative baseline data for the establishment of human exposure guidelines.

Some investigators are studying central nervous system (CNS) neurotoxicity. They are using neural cultures of certain neurons (cerebellar Purkinje cells) to monitor the spontaneous bioelectric activity of test systems. Their *in vitro* bioassay technique, utilizing electrophysiological recordings, is being used to determine effects of various known toxins as well as potentially harmful environmental agents. This neurophysiological model system may prove valuable in ascertaining the potentially deleterious effects of environmental pollutants and of low-level radiation on the CNS. These investigators are also looking into the effects on CNS tissues of various radiosensitizing agents which are used to potentiate radiotherapeutic effect in cancer treatment. Such information would be helpful in understanding and possibly eliminating the side effects which sometimes accompany the use of these agents.

Another group continues their biophysical studies on cell membranes, looking especially at populations of red blood cells. Using "resistive pulse spectroscopy" (RPS), a rapid, automated method developed in their laboratory, these investigators are characterizing cell-membrane systems according to size, form, deformability, fragility, and membrane kinetic responses. The variations in patterns of RPS response have been used to study normal and abnormal cellular development, and the response of the cell-membrane biophysical properties to various physical and chemical agents. The ability to rapidly monitor many cell-membrane characteristics and their changes (chemical, mechanical, osmotic, and electrical) will help clarify the intrinsic differences between normal and altered cells.

The highlights of achievements during the past year in these diverse areas of radiation biophysical research are presented in the papers that follow.

BEVALAC STUDIES

RADIOLOGICAL PHYSICS AND RADIATION CHEMISTRY

Aloke Chatterjee and John L. Magee

The effects of radiation on living cells have been of interest for a long time. Much progress has been made over the last 20 years in understanding these effects, but many aspects still remain obscure. For safety, as well as for optimal use of ionizing radiation in cancer therapy, one has to understand in detail the underlying processes that occur after energy from radiation is absorbed. The purpose of this program is to increase our fundamental understanding through systematic evaluation, and thus build a theoretical model for general use.

It is generally believed that energy from ionizing radiation is deposited in a given medium, such as human cells, in about 10^{-16} seconds. There is a lapse of about 5 orders of magnitude in time before the chemical changes in and around the biological molecules start to occur. These chemical changes then lead to biological changes, such as cell killing and carcinogenesis. It is the chemical stage which is least understood.

At LBL, various types of radiation (x-rays, γ-rays, protons, helium particles, and other heavy charged particles) are available, which can be used as a probe to create different amounts of damaging radicals within biological targets. In a cellular medium, where water is a major component (80% by weight), radiation interacts primarily with water. The effects of radiolytic products of water can be damaging to DNA molecules (which constitute the most sensitive target). Radiation, especially heavier charged particles, can also interact directly with DNA molecules and bring about damaging changes. The various decomposition products of water which include both radicals and molecular products, are given by the following equation:

$$H_2O \xrightarrow{\text{radiation}} \text{-OH};\ \text{-H};\ H_2O;\ H_2O_2;\ \text{-}H_2O;\ O_2.$$

We are investigating the production and distribution in the medium of the hydroxyl radical (-OH), the most damaging radical to DNA.

We have calculated the yield of various chemical species from our evaluation of the geometrical pattern of energy distribution (track structure). Figure 1 presents some results of our calculations for electrons of different initial energies. Yields are given in terms of numbers of species per 100-eV energy absorption (G-value). This is a very fundamental curve for application in radiobiology. We have obtained similar curves for heavy particles after evaluating their track structure. This structure is depicted schematically in Figure 2.

In the central region (the "core") of heavy-particle tracks, where deposition of energy is the most dense, we expect enormous biological change. Streaking out of the core region are energetic electrons which are created by heavy particles in the medium.

From results similar to those shown in Figure 1, we are in the process of estimating biological damage to human cells subjected to various types and amounts of ionizing radiation. We have proposed a promising [illegible] ion model for biological damage.

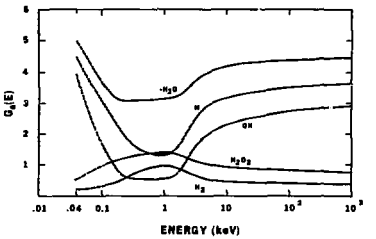

Figure 1. Yields of various radiolytic decomposition products of water for electrons at different initial energies. These results can be used for understanding radiobiology.
XBL 782-7147

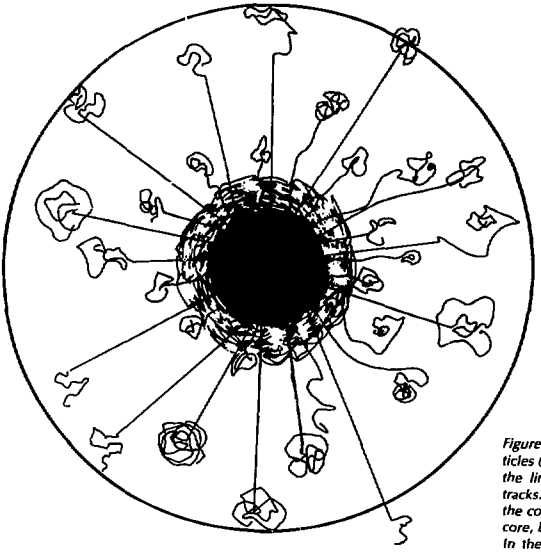

Figure 2. Schematic model of track structure of heavy particles (cross-sectional view). The radii r_c and r_p are shown; the lines in the penumbra indicate individual electron tracks. The energy deposition at the boundary separating the core and the penumbra is not as dense as it is in the core, but in this region the tracks of electrons do overlap. In the present model, this region has not been treated explicitly. XBL 778-3712

TRACER STUDIES WITH RADIOACTIVE BEAMS

Aloke Chatterjee, Edward L. Alpen, and Cornelius A. Tobias

High-energy, heavy charged particles have many special advantages over the conventional mode of radiation therapy of cancer patients. The LBL Bevalac is the only available source for laboratory production of high-energy heavy particles, and currently some selected patients are being treated with these beams.

One of the many advantages of heavy-particle therapy lies in the possibility of concentrating the dose to the localized tumor volume and depositing a very little dose to the surrounding normal cells. This possibility is attributed to the Bragg ionization phenomenon, and the region where the peak dose appears is called the "Bragg-peak phenomenon."

The purpose of this project is to demonstrate a technique which will enable a therapist to treat tumor volumes, using Bragg-peak radiation with great confidence. The technique involves the use of energetic radioactive beams (possible only at the Bevalac) and a good detector system (see Fig. 1). The present goal is to localize the Bragg peak within ±1 mm of the location of the tumor volume. It is a very direct approach to the solution of an important problem which has been a hindrance to the use of Bragg-peak therapy for a long time.

Bragg-peak localization is not the only usefulness of radioactive beams. Many new diagnostic techniques will be possible which may be of great benefit in nuclear medicine. For definitive clinical applications, some preliminary but systematic studies have been designed, and the proof of principle can be demonstrated for human use in about 5 to 7 years.

Figure 1. A photograph of the positron emitting beam analyzer (PEBA). The analyzer has 24 Na(Tl) crystals in each bank. Each crystal is connected to a photomultiplier tube (not shown). The existing PEBA has good position accuracy (1 mm) only in one dimension (the direction of the beam). For volume reconstruction PEBA will be modified to perform in a three-dimensional mode. CBB 792-2547

The average linear energy transfer (LET) of a heavy charged particle is given by the stopping power formula:

$$-dE/dx = \frac{4\pi z^2 e^4}{mc^2\beta^2} NZ \left[\ln \frac{2mc^2\beta^2}{I(1-\beta^2)} - \beta^2 + \text{correction terms} \right] \quad (1)$$

where z is the charge on the incident particle,
NZ is the number of electrons/volume in the medium,
β is the incident velocity of the particle in units of the velocity of light, c,
I is the mean excitation potential of a medium,
e is the electronic charge,
m is the mass of an electron.

Correspondingly, the range R of a particle of incident energy is given by

$$R = A \int_0^E \frac{dE'}{|dE'/dx|} \quad (2)$$

where A is the particle mass number.

Thus, in a homogeneous medium, the range of a particle can be calculated quite accurately, and placing the Bragg peak in a predetermined position is not a great problem. But if the medium is nonhomogeneous, such as a human patient, and if we do not know how much tissue, fat, bone, or blood, etc., have to be penetrated before the particle comes to a stop at a given depth, then Eq. (2) cannot be applied adequately. A knowledge of electron density and composition of each volume element that a beam penetrates is essential for calculating the depth of penetration of a charged particle for a given energy.

In vivo target activation has been suggested as a method to overcome the above mentioned problem: a few experiments have been conducted with 200-MeV proton beams, but there have been difficulties. The yield of the activity *in vivo* can be about a factor 50 less than can be achieved by radioactive beams. Also, for proton beams—whose threshold energy for target activation is 20 MeV—the range in tissue-equivalent material is 5 mm. Thus, the last 5 mm of proton penetration will show no activity, and may cause a considerable error in placing the Bragg peak. Another problem is that neutron background may cause a great amount of uncertainty. The radioactive-beam technique is free from all of these problems, and may prove to be the most direct and reliable method.

Using relatively pure (90%) ^{19}Ne and quite pure (99%) ^{11}C beams, we have made several measurements of the stopping region of these beams in various simple but heterogeneous targets. Figure 2 shows the Bragg ionization curve measured for the ^{19}Ne beam. Beyond the sharp and enhanced ^{19}Ne Bragg peak, there are small peaks of ^{17}F and ^{15}O which could not be filtered out. But their presence does not create any problem. The targets were a single lucite rod, a mixture of lucite plate (tissue-like), a $CaSO_4$ plate (bone-like), an air gap (for lung simulation), and a paraffin wax plate (fat-like). All the measurements were made in one dimension, and a comparison with calculations showed agree-

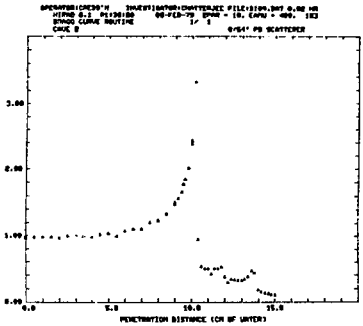

Figure 2. Measured Bragg ionization curve of relatively pure ^{19}Ne beam. The ^{19}Ne beam has been obtained from 425 MeV/n ^{20}Ne beam fragmenting in a 3-cm-long beryllium block placed at F1. The range and the depth of Bragg peak are 10.2 cm and 10.0 cm, respectively. There are very small amounts of impurities, such as ^{15}O, ^{17}F, and their individual Bragg peaks are also shown. XBL 792-8442

ments within ± 1 mm. Figure 3 shows a picture of the ^{19}Ne beam-stopping region as viewed in a video monitor (Ramtek) when the heterogeneous targets were used.

Experiments with phantoms are in progress before we make measurements in animals, which will prepare the way for eventual use in human patients.

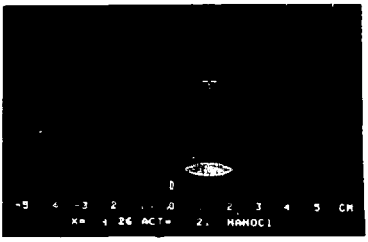

Figure 3. Stopping region of ^{19}Ne beam in a lucite rod. Before entering the lucite rod, the ^{19}Ne beam was reduced in energy by a 3-mm $CaSO_4$ plate, 1 mm of lucite plate, and 9 mm of paraffin, which were placed in that order between the beam and the stopping lucite rod. The picture from the video display monitor shows the region where most of the beam is deposited. XBB 792-2137

PHYSICAL CHARACTERIZATION OF ENERGETIC HEAVY-ION BEAMS

Walter Schimmerling

Beams of carbon, neon, and argon nuclei, accelerated up to 90% of the speed of light, are available from the Bevalac. These high-energy, heavy-ion beams are important in biological and medical fields because they have advantageous radiobiological properties. Our fundamental studies of the various beams will advance understanding of the nuclear physics of high-energy heavy ions, will provide the information required to work out heavy-ion dosimetry for therapeutic applications, and will lead to their use in valuable diagnostic procedures.

PROTONS AND NEUTRONS

Although the dose contributions of secondary protons and neutrons are small (in most beams less than 3%), these particles are an important source of background radiation in and around the medical cave, and quantitative information concerning these particles is essential. Such information is especially important when sensitive tissues are close to the treatment area, as is the situation in a heavy-ion protocol in which Drs. J. Castro, J. Quivey, and associates are treating eye tumors with a narrow, pencil beam of helium ions from the 184-Inch Synchrocyclotron.

The beam line elements used to shape, collimate, and flatten the beam are sources of neutrons and protons. A set of experiments was performed at the 184-Inch Synchrocyclotron to measure the lateral- and exit-dose distributions of these helium beams. This phase of the work was undertaken in collaboration with members of the Health Physics Group and the Accelerator Division.

The distribution of neutrons produced in the various elements of the 184-Inch Synchrocyclotron medical beam was measured using activation detectors along the beam line and perpendicular to it, in a plane containing the patient isocenter. The radioactive yield of different activation detectors was unfolded from known energy dependence of the cross sections to yield a neutron energy spectrum. The unfolded spectrum is not unique, but constitutes a "best" spectrum in the least-squares sense. How-

ever, the total dose calculated from such a neutron spectrum is not very sensitive to small changes in the detailed shape of the spectrum. In addition, part of the radioactivity is induced by the charged particles produced together with the neutrons, and the unfolded spectra must be corrected for this effect.

A computer program was written to calculate the neutron dose due to the helium beam, and it is available for calculations in modified geometries. The calculations were made using the sparse neutron-production data available before the experimental work reported in the previous section. Doses calculated in this manner were approximately 50% higher than those obtained from the unfolded neutron spectra. Use of the data from the current Bevalac experimants should improve these calculations significantly.

The results of this investigation allowed us to identify the most significant sources of neutrons in the beam line. These were, not surprisingly, the water column and the collimators used for beam shaping close to the patient. The relative contribution of these sources, as well as the neutron-dose perpendicular to the beam axis in a plane containing the patient isocenter, were also obtained. The measurements give an upper limit of absorbed dose in soft tissue due to neutrons and protons that decreases from about 5 x 10^{-1} rad on the beam axis to about 1 x 10-3 rad at 20 cm from the beam axis, per plateau rad of incident beam. The dose increases somewhat when a phantom is inserted in the beam to simulate the patient, as shown in Figure 1, where the perpendicular dose distribution has been plotted for both cases. A gaussian distribution has been fitted to the rising portion of the curves for ease in the use of these data. The full width at half-maximum (FWHM) is 22 cm with a phantom in the beam, and 27 cm without a phantom.

The measurements give an upper limit of the absorbed dose in soft tissue that will typically result in a dose of <10 rad to the eye, well below the threshold for cataract incidence determined for fission neutrons.

In a separate series of experiments performed at the Bevalac with J. Kast (LBL) and R. Madey, B. Anderson, and R. Cecil (Kent State University), we have measured the probability (double-differential cross section) of producing neutrons at a given energy and a given angle with respect to an incident heavy-ion beam, when nuclei in the beam interact with the nuclei in targets of carbon, aluminum, copper, lead, and uranium. The energy of the neutrons is obtained from the time of flight between the target and each of the neutron detectors, placed at different angles around the target. The neutron detectors are rectangles of plastic scintillator, 1 cm wide, 12.5 or 25 cm high, and 10 cm thick. In addition to the time of flight, we record the light output and the position at which each neutron generated the recoil charged particles that give rise to the detected signal. This results in a more accurate assignment of the detector efficiency and angular distribution.

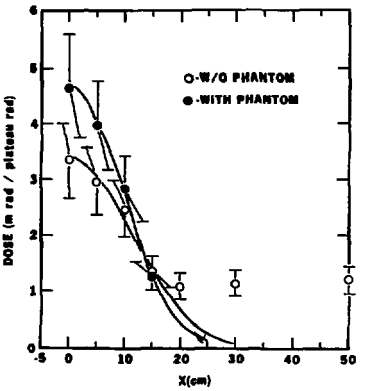

Figure 1. Dose due to neutrons in and near the 900-MeV therapy helium beam of the 184-Inch Cyclotron. X is radial distance from the center of the beam. The presence of a tissue-equivalent phantom increases the central portion of the neutron dose. XBL 791–7886

Data were taken in December 1977 with neon beams of 250 and 400 MeV per nucleon, and for angles of 30, 45, 60, 90, and 150 degrees. Results, limited in quantity by accelerator malfunctions, were obtained in October 1978 for helium and carbon beams of 400 MeV per nucleon and angles of 0, 10, 20, 30, 60, and 150 degrees. It was our hope to study the forward-angle production in more detail, since this region is not easily accessible in charged-particle experiments. Finally, data were taken with neon beams of 400 MeV per nucleon, at 30, 45, 60, and 90 degrees in March 1979.

The detection of neutrons is generally more difficult than that of charged particles. Several detectors can be used to verify the detection of a charged particle, by measuring the ionization produced along its path; i.e., the same charged particle can be sensed several times. This is not, in general, the case for neutrons, which are uncharged and

produce no direct ionization. Detection of a neutron proceeds by recording the ionizing particles produced when the neutron has suffered a generally destructive, nuclear interaction. Thus, a neutron can only be detected once, rendering neutron measurements especially susceptible to background effects, such as room-scattered neutrons. The experimental runs of October 1978 and March 1979 were designed to study such effects on our apparatus, using "shadow bars" to block neutrons originating in the target to estimate the effect of those neutrons originating in extraneous structures (beam stop, floor, ceiling, etc.).

The data are still being analyzed and final results are not expected for several months. However, preliminary results continue to show an excess of neutrons over protons, for neon incident on uranium, and at neutron energies below approximately 100 MeV. This difference is somewhat smaller than was seen in the December 1977 data, after correcting for the backgrounds studied with the "shadow bar" measurements, but it continues to be significant.

FRAGMENTATION

We have continued the analysis of data taken earlier in collaboration with the group headed by V. Perez-Mendez (LBL). A Bragg curve obtained for the separately identified primary argon from a 525-MeV-per-nucleon argon beam incident on a variable-thickness Lucite absorber is shown in Figure 2. The sharpness of the peak, which is limited by the mass of the detector, and the peak-to-plateau ratio are much greater than that of a conventional Bragg curve, which includes all fragments entering the ionization chamber.

Analysis of these data has proceeded at a reduced rate due to the need to maintain an adequate level of effort for the neutron experiments. Work has also been intensified on the design of future fragmentation experiments, involving W. Schimmerling, S.B. Curtis, D. Ortendahl, J. Kast, S. Kaplan, and C.A. Tobias. An arrangement has been worked out to share the use of a solid-state detector telescope with researchers from the Nuclear Science Division, and experiments planned for Fall 1979 should enable us to obtain data such as are shown in Figures 2 for all isotopes of importance.

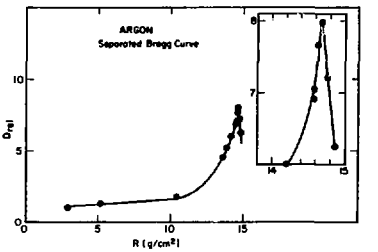

Figure 2. Bragg curve obtained from the separately identified primary argon from a 525-MeV-per-nucleon argon beam incident on a variable-thickness Lucite absorber. Inset: expanded view of peak area. XBL 795-3465

RESPONSE OF A RAT RHABDOMYOSARCOMA TO HEAVY-ION BEAMS

Stanley B. Curtis, Tom S. Tenforde, Wolfgang A. Schilling, Susan J. Daniels, and Karen E. Crabtree

An extensive series of experiments is underway to study the response of a solid rhabdomyosarcoma tumor system in rats to the high-energy, heavy-charged-particle beams available at the Bevalac. The objectives are: (a) to compare tumor response from irradiation *in vivo* and *in vitro* by various charged-particle beams in both single and fractionated exposures in order to aid in the selection of the most promising beam (or beams) for clinical application; and (b) to study in depth the heavy-ion radiation response of this tumor via several end points, including tumor control dose (TCD_{50}), radiation-induced growth delay, cell survival (*in vitro* assay) after irradiation *in vivo*, cell survival of both oxygenated and hypoxic cells after irradiation *in vitro* and, in addition, several cell-kinetic end points. Over the past year considerable progress has been made in several of these areas. The major results are discussed briefly below.

IN VIVO TUMOR CELL SURVIVAL ASSAYED *IN VITRO*

Cellular survival in R1 tumors exposed to 225-kV x-rays and to 4-cm extended-peak carbon and neon ion radiation was determined by an *in vitro*

:say for clonogenic cell survival. The resulting survival curves for tumors irradiated *in situ* in air-breathing and nitrogen-gas-asphyxiated rats are shown in Figure 1. In the x-ray survival curve, an hypoxic break is apparent at a dose of approxiapproximately 8 Gy (800 rad), and the ratio of survivals in the air-breathing and hypoxic curves a. high radiation doses yields a value of 35% for the chronically hypoxic cell fraction. Relative biological effectiveness (RBE) values at the 10% survival level, for animals under air-breathing conditions, were 2.0 and 3.1 for the peak carbon and neon ion beams, respectively. Because of the different radiosensitivity of the R1 subline used in these experiments from that of the original subline that we received from the Barendsen group in Holland, tumor volume-response studies were also carried out with this subline to obtain RBEs for tumor growth delay. The values of RBE obtained for 50-day growth delay were 2.3 and 2.9 for carbon and neon ions, respectively.

IN VITRO RBE AND OXYGEN ENHANCEMENT RATIO (OER) MEASUREMENTS

A cell suspension technique has been used to characterize the radiation response and the oxygen effect for R1 cells exposed to accelerated carbon, neon, and argon beams with ranges in tissue of ~11 to 14 cm and ~22 to 24 cm. Cell survival curves have been measured under both oxic and hypoxic conditions in the plateau and the 4-cm and 10-cm extended peak regions of these beams. For example, Figure 2 demonstrates the variation in RBE and OER throughout the Bragg curve for carbon, neon, and argon beams with a 10-cm extended peak and 14-cm range.

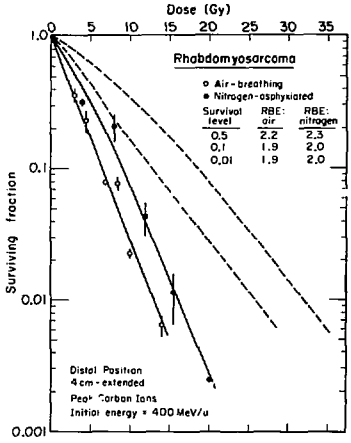

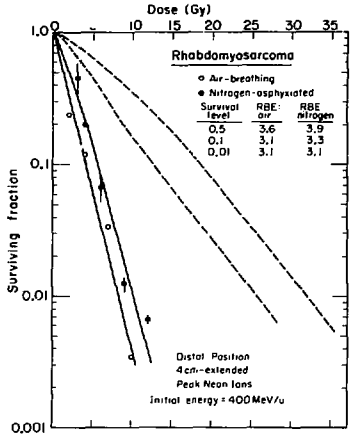

RBE's FOR CELL KILLING AND GROWTH DELAY

Radiation modality	$RBE_{0.1}$	$RBE_{50\ days}$
Peak carbon ions	1.9 ± 0.3	2.3 ± 0.2
Peak neon ions	3.1 ± 0.6	2.9 ± 0.2

Figure 1. Cell survival curves are plotted as a function of absorbed dose for R-1 tumors irradiated in situ with 225-kV x-rays (dashed lines) and carbon-ion and neon-ion beams in the distal position of a 4-cm extended peak. Tumors were excised immediately following irradiation, and subsequently dissociated enzymatically and plated in vitro for determination of the surviving cell fraction. Control plating efficiencies under air-breathing and hypoxic conditions were 18.2 ± 1.7% (N=38) and 17.0 ± 1.9% (N=27). A comparison of RBEs at 10% survival and for a 50-day radiation-induced growth delay is shown in Table 1. XBL 7810-3647

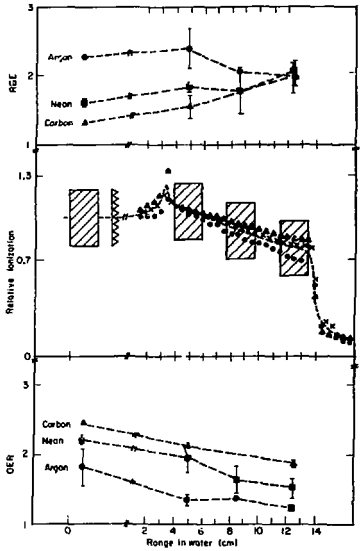

Figure 2. Physical depth-dose distributions and RBEs and OERs at the 10% survival level are shown for carbon, neon, and argon beams with 10-cm extended peak regions and a range of approximately 14 cm in water. Interpretation of the RBE and OER data is discussed in detail in the text. Error bars represent standard deviations for RBE and OER values obtained in two to four separate experiments.
XBL 785-3163

Several general conclusions can be made from the data obtained:

(i) The biological effectiveness of charge-particle beams is greater with a 4-cm extended peak than with a 10-cm peak.

(ii) The RBE for carbon and neon beams increases in going from the proximal to the distal position in a 10-cm extended peak, although this effect is more pronounced for the carbon beam.

(iii) The OER decreases from the proximal to distal positions of a 10-cm peak for all three ion species, and reaches the lowest value of 1.2 in the distal argon peak.

(iv) The RBE for the argon beam decreases from the proximal to the distal ends of a 10-cm peak as a result of cell "overkill" in the high-LET (linear energy transfer) mid-peak and distal-peak regions.

(v) A "merit factor" can be defined to represent the efficiency of killing hypoxic cells in the peak region (i.e., the tumor location) relative to the efficiency of killing oxic cells in the plateau ionization region (i.e., the normal tissue zone). The merit factors are higher for carbon ions than for neon ions with a 22 to 23 cm range, but are similar for these two ions when the range is 11 to 14 cm. For argon ions, the merit factor varies by nearly a factor of two across a 10-cm peak as a result of both the RBE variation described above and the decrease in physical dose caused by the ridge filter used.

(vi) Survival data obtained for the three charged-particle beams can be combined to produce RBE versus LET_∞ curves for both oxic and hypoxic R1 cells, as shown in Figure 3. The peaks in the RBE versus LET_∞ curves occur at LET_∞ values of 100 to 200 keV/μm for oxic cells, and 200 to 400 keV/μm for hypoxic cells. At the highest LET_∞ values, in the argon peak region, the RBE decreases as a result of saturation of cell killing, ie., the "overkill" effect.

(vii) As shown in Figure 3, the OER decreases progressively for LET_∞ values greater than 20 keV/μm, but does not reach unity even in the distal argon peak where the LET_∞ = 600 keV/μm.

IN VIVO TUMOR VOLUME RESPONSE: FRACTIONATED RADIATION DOSES

The regression and regrowth characteristics of R1 tumors are being determined by measurements of tumor volume following graded fractionated doses of 225-kV x-rays and accelerated carbon and neon ion beams in the 4-cm extended peak ionization regions. Schedules of 5 fractions over a 4-day interval (5f/4d) and 10 fractions over an 11-day interval (10f/11d) have been studied. For both fractionation regimens, significant recovery was observed with x-rays; however, little or no recovery followed a 5f/4d radiation schedule with either peak carbon or peak neon ions, or a 6f/5d schedule with peak carbon ions. With a 10f/11d schedule, significant recovery was observed for the peak carbon ions, but not for the peak neon ions.

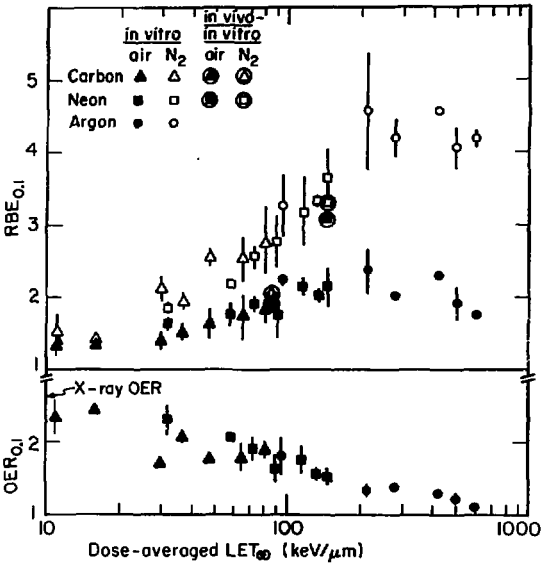

Figure 3. The variation in RBE and OER at the 10% survival level is plotted as a function of dose-averaged LET_∞. The data used to construct these curves were obtained from cell survival studies conducted throughout the Bragg curves of carbon, neon, and argon beams with ranges of 11 to 14 and 22 to 23 cm in water. RBE values are also shown for R-1 tumors irradiated in vivo and assayed for cell survival in vitro. The similarity of RBE values at the 10% survival level for tumors irradiated under air-breathing and hypoxic conditions is to be expected, since the chronically hypoxic cell fraction is 35%.

XBL 788-3452

HYPOXIC CELL SENSITIZERS *IN VIVO.*

As a preliminary to studying the enhancement of charged-particle radiation response by the hypoxic cell sensitizers misonidazole (Ro-07-0582) and Ro-05-9963 (the O-demethylated derivative of misonidazole), we have measured the toxicity and kinetics of these compounds in the WAG/Rij strain of rat. When administered as a single intraperitoneal dose, the acute lethal dose ($LD_{50/3}$) values for misonidazole and Ro-05-9963 are 750 and 2,750 mg/kg, respectively. The kinetics of drug uptake and clearance in plasma and tumor tissue were determined by means of a spectrophotometeric assay. For both misonidazole and Ro-05-9963, the plasma level reached a peak at approximately 15 minutes post-injection, and the tumor level is a maximum at approximately 30 minutes post-injection. Drug kinetics were also measured in lung tissue, and the uptake and clearance patterns for this organ closely paralleled that of the tumor.

STUDIES OF THE "SECOND WAVE" OF DECREASED GROWTH RATE FOLLOWING IRRADIATION

Following the initial burst of proliferation by surviving clonogenic cells, irradiated R1 tumors exhibit a marked reduction in growth rate, which is termed the "second wave of growth delay." A series of experiments was initiated to determine the underlying mechanism for this phenomenon. These studies include (i) measurement of the growth rate of retransplanted tumors, (ii) analysis of the effects

of host immunosuppression on tumor regrowth rate, and (iii) quantitative morphometric studies on cellular characteristics in irradiated tumors. Evidence to date indicates that the second wave of growth delay is not a consequence of either heritable non-lethal cellular damage, or an increased immunogenicity of the irradiated tumor cells. Morphometric evaluation of cellular characteristics has shown no abnormal features in the irradiated tumors except for a significant increase in the percentage of necrotic tissue relative to control non-irradiated tumors.

In summary, these studies are yielding evidence that there is a significant difference between the radiobiological response of R1 tumor cells to peak carbon ions and to peak neon ions. The OERs for neon ions are significantly lower than the OERs for carbon ions in the spread peak region. The OERs of argon ions in the spread peak region, while not unity, are considerably lower than any radiation modality yet used or contemplated for therapy. In general, beams with narrow peaks (e.g., 4 cm) will be more useful than those with broad peaks (e.g., 10 cm). Because of the less advantageous depth-dose characteristics for the neon beam compared to the carbon beam when the depth of penetration in tissue is large, carbon might be more advantageous than neon for deep-seated tumors.

LATE EFFECTS OF HIGH LINEAR-ENERGY-TRANSFER (LET) RADIATIONS

E. John Ainsworth and Edward L. Alpen

Several ongoing studies will provide data needed to estimate risk of radiation damage from heavy charged particles for space workers involved with the solar-powered satellite program. Experiments in progress will quantitate the carcinogenic/life shortening effects in mice of heavy charged particles; other studies will identify damage to the lens/cornea, the bone marrow, and blood vessels in the heart.

The Harderian gland is a small secretory organ located behind the eyeball in rodents. Because this gland shows high susceptibility to carcinogenesis following exposure to densely ionizing radiations, such as fission-spectrum neutrons, it is being used as a model system to define shapes of dose-response curves and relative biological effectiveness (RBE) when single doses of iron, argon, neon, carbon, or helium ions are given to the upper body of mice that have previously received transplants of two pituitary glands beneath their spleen capsule to promote tumor expression. Approximately 1,800 animals are involved in this collaborative study that involves the Lawrence Berkeley Laboratory, Argonne National Laboratory, and Oak Ridge National Laboratory.

Life-span shortening and tumorigenesis in mice are being evaluated following single doses of argon ions, neon ions, or carbon ions, and ^{60}Co gamma radiation. The extent to which radiation hazard is reduced, or increased, following dose fractionations is being assessed by administering weekly fractionated doses of carbon ions or ^{60}Co gamma radiation over 23 weeks, or approximately 25% of the life span of control animals. This experiment, which will involve a total of approximately 2,600 mice, could define the relative biological effectiveness (RBE) for heavy charged particles following single or protracted doses, and should help establish if the quality factor used currently for risk assessment for heavy charged particles in space is conservative. Dose-response relationships are also being determined for corneal and lens damage after exposure of mice to single doses of plateau argon ions, neon ions, or carbon ions, or 250-kV x-rays.

Since mammalian cells irradiated *in vivo* appear to show a maximum sensitivity to cell killing at lower values of LET_∞ than do mammalian cells irradiated *in vitro*, cell survival curves are being determined for both hematopoietic stem cells [colony-forming unit in the spleen (CFU-S)] and erythrocyte precursors [colony-forming unit—erythroid (CFU-E)] in mice exposed to argon ions, neon ions, carbon ions, and to ^{60}Co gamma radiation.

The ensemble of these studies will provide data critical to the assessment of risk for heavy charged particles, and complement other ongoing studies that concern cell killing and neoplastic transformation *in vitro* and previous studies of heavy-charged-particle damage in retina or in the central nervous system.

CELL SURVIVAL STUDIES WITH HEAVY-ION BEAMS

Cornelius A. Tobias, Eleanor A. Blakely, Frank Q.H. Ngo, and Ruth J. Roots

Our effort is directed towards a basic understanding of the molecular lesions and cellular kinetics of the fundamental biological responses to charged-particle beams. Our main investigation has been to study the dose-effect relationship for human cultured-cell monolayers at various values of residual range for monoenergetic beams of carbon (400 MeV/amu), neon (425 MeV/amu), and argon (570 MeV/amu). Cell survival was measured under aerobic and hypoxic conditions over a range of mean LET_∞ (linear energy transfer) from 10 keV/μm to 600 keV/μm. This allowed us to measure the aerobic relative-biological-effectiveness values (RBE) and the oxygen enhancement ratios (OER) over this LET range. Similar studies have been made for beams with extended Bragg peaks, using monolayers positioned at various points in a 4-cm or 10-cm peak region. In parallel with the cellular investigations, the induction and repair of DNA lesions have been studied for both the unmodified Bragg peak and the 10-cm extended Bragg peak.

Existing quantitative models were found to be inadequate for describing the time-dependent phenomena in cells exposed to ionizing radiations. We have proposed a model (RMR model) which is based on the idea that the fate of cells depends on the competition between eurepair (perfect repair) and misrepair of radiation-induced DNA lesions.

MAMMALIAN CELL RESEARCH

We have recently completed an extensive series of cell-survival studies with accelerated heavy ions. The dose-effect relationship for asynchronous human kidney T1 cells has been determined for monoenergetic beams of carbon (400 MeV/amu), neon (425 MeV/amu), and argon (570 MeV/amu). The "track segment" method of exposure was used at twelve different range values for each beam.

The interpretation of the above experiments disclosed the fact that the biological effects of heavy particles cannot be characterized by the two parameters usually employed: dose and LET. At the same LET and dose, the effects of neon and argon beams are different from each other. In the initial analysis it appeared that particle charge and velocity are better parameters than LET. For example, lethal effects in nitrogen depend on $velocity^{-4.6}$ whereas in air they depend on $velocity^{-1}$.

The relative biological effectiveness (RBE) values measured at the 10% survival level as a function of LET are shown in Figure 1 for cells irradiated under aerobic and hypoxic conditions. The maximum RBE falls between 100 and 200 keV/μm. The argon data diverge from the carbon and neon data due either to the velocity dependence of these effects or to the presence of different amounts of fragmentation—or both.

It was also demonstrated that the radiobiological "oxygen effect" is lowest for argon beams. It is important to minimize this effect for therapy. Figure 2 shows the oxygen-enhancement ratios calculated from the 10% survival levels for the carbon, neon, and argon beams. In addition, this figure contains data for comparison by Barendsen for irradiations of human kidnev T1 cells with alpha particles of various energies, and also data published by Todd who exposed the same cell line to various charged particle beams of constant velocity. Interestingly, the trend of our data follows that of Barendsen's remarkably well, except that Barendsen's OERs are lower for all LET points and also for x-rays. Todd's data, however, show a reduced OER at a much lower LET. We believe that the higher OERs found using Bevalac ions may be due in part to the presence of low-LET fragments in the Bevalac beams. Despite the separation of the curves at low LETs, all three studies agree that the OER becomes 1.2 or less at greater than about 200 keV/μm.

Radiobiological data for aerobic and hypoxic exponentially growing human kidney T1 cells in monolayer have been evaluated by Blakely et al, as a function of range for accelerated-charged-particle beams with extended Bragg peaks. Figure 3 depicts the specific Bragg ionization curves which were compared. For a maximum range of approximately 25 cm, cell survival was measured at points which cover the track length of carbon (400 MeV/amu), neon (557 MeV/amu), and helium (225 MeV/amu). The spread-Bragg-peak region for these beams was 10-cm wide. Cell survival was also measured for three ion beams with a maximum range of approximately 14 cm, with a 4-cm-wide extended Bragg peak. These included carbon (308 MeV/amu), neon (425 MeV/amu), and argon (570 MeV/amu).

Table 1 summarizes the RBE and OER data at the 10% survival level for the midpeak position of each beam.

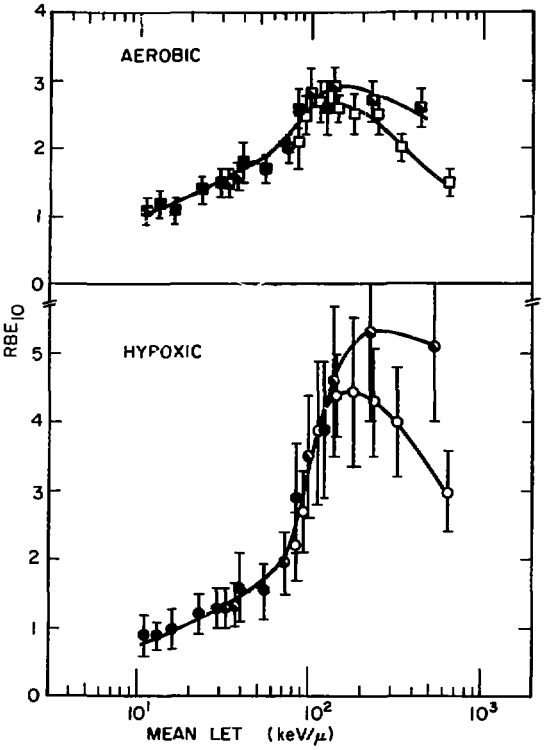

Figure 1. RBE at 10% survival as a function of the dose-average mean LET: carbon data (●, ■), neon data (◐, ◪), and argon data (○, □). Error bars are for 95% confidence limits.

XBL 787-3366

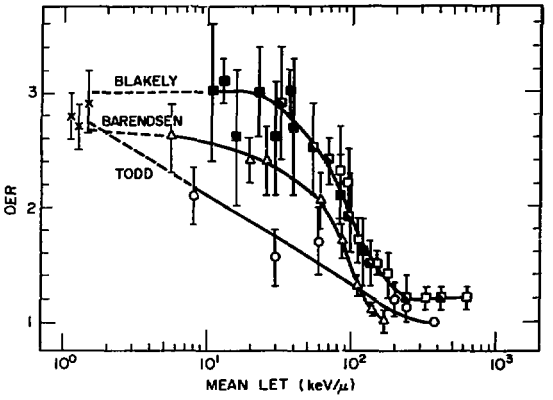

Figure 2. OER (95% confidence limits) versus dose-average mean LET: carbon (■), neon (◪), and argon (□) beams from the Bevalac; Barendsen low-energy helium ion data (Δ); Todd high-energy (up to 10 MeV/amu) heavy-ion data (○); and x-ray data (x).
XBL 787-3362

In general the results indicate the following points. (1) All charged particle beams studied have superior physical-depth-dose advantage over conventional radiation modalities at the same penetration depth. (2) The midpeak-to-plateau physical-dose ratio decreased slightly with increasing atomic number of the particle for both the maximum penetration depths studied. (3) Midpeak-to-plateau ratios of biological effectiveness (relative to 220 kVp x-rays) for all particle beams studied were greater than one (or in the single case of the argon beam, neon. (5) Dual opposed-port exposures of particle beams (simulated by crossfiring) demonstrated that more uniformly low OERs and survival can be the ratio was equal to one). A maximum advantage was observed for the 14-cm-range neon and carbon beams; in fact, the survival response to the carbon and neon beams is very similar. (4) Midpeak-to-plateau oxygen-gain ratios were all greater than one, with the greatest advantage observed for the argon and neon beams; the OER in the argon peak is significantly lower than it is for either carbon or achieved simultaneously over the cross-fired, extended-Bragg-peak region than from a single-port exposure.

MIXED MODALITY AND SPLIT-DOSE EXPERIMENTS

To further elucidate the mechanisms of heavy-ion radiations, we have done experiments with mixed modalities and split-dose experiments. For some time, it was believed that high-LET radiations produce primarily irreversible lethal lesions in the genome of cells. F.Q.H. Ngo used mixed-modality experiments (low- and high-LET radiations) to demonstrate for the first time that heavy-ion exposure produces sublethal injury to the cells. Because of the presence of these lesions, Ngo showed that heavy ions can potentiate the lethal effects of x-rays, and vice versa. Therefore, it is very clear that low- and high-LET radiations do not act completely independently, as was suggested by the earlier work of Barendsen based on alpha particles. Experiments with synchronized cells are now underway in order to quantify the degree of interaction.

Repair of radiation damage after low-LET radiation has been well documented with dose-fractionation experiments. An opposite effect was recently observed due to split doses with very high-LET particles. Using carbon, neon, or argon ions with dose-average LET higher than 85 keV/μm, Ngo showed a

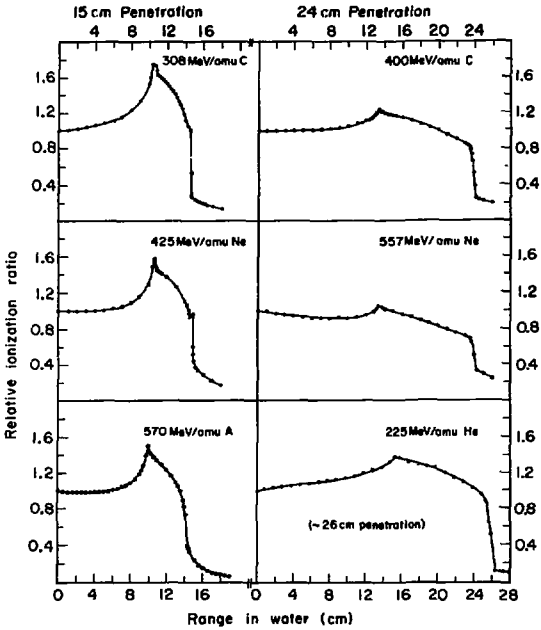

Figure 3. Specific Bragg ionization curves. XBL 785-3127A

Table 1. Midpeak OER and aerobic RBE values at 10% survival.

	14-cm range - 4-cm ridge filter		24-cm range - 10-cm ridge filter	
	OER	RBE	OER	RBE
Helium	—	—	2.6	1.2
Carbon	2.2	2.3	2.6	1.3
Neon	2.2	2.3	2.3	1.8
Argon	1.3	2.1	—	—

potentiation in cell killing for 3-hour, split-dose schemes, with the extent increasing with the total dose. The two-dose potentiation effect does not appear to be due to radiation-induced partial synchronization. These findings may influence the interpretation of repair measurements, or Elkind repair, particularly for fast-neutron or charged particles.

RELATIONSHIP OF DNA LESIONS TO CELL KILLING

We have completed experiments on the yield and repair of heavy-ion-induced DNA breaks in human kidney T1 cells exposed as monolayers to the same carbon, neon, and argon beams used for the OER and RBE studies reported above.

Figure 4 (panel A) illustrates that the rate of rejoining of DNA breaks is drastically reduced as the LET increases (1.5 hour post-irradiation incubation), and that about 25% of the initial number of breaks fail to rejoin at a $(Z^*)^2/\beta^2$ ratio of about 1,000, approximately equivalent to 100 keV/μm. These breaks are presumably DNA double-strand scissions.

In contrast, if the irradiations are made in a 10-cm spread Bragg peak of the same particle beams at energies to give a 24-cm range, the initial rate of rejoining approaches that observed after x-ray irradiations. This reflects the presence of a large component of low-LET radiation. Moreover, the final extent of breaks that fail to rejoin is below 10%.

THE REPAIR-MISREPAIR MODEL OF CELL SURVIVAL

A new model is presented for cell survival, lethality, and mutation caused by ionizing radiations: the repair misrepair model (RMR). We have shown that the fast events of physical energy transfer and of radiation chemistry are largely complete before the enzymes of a living cell can recognize relevant macromolecular processes, and before biochemical repair processes are under way. This allows the model to be separated into dose-dependent and time-dependent processes; the shape of the survival curves depends on both.

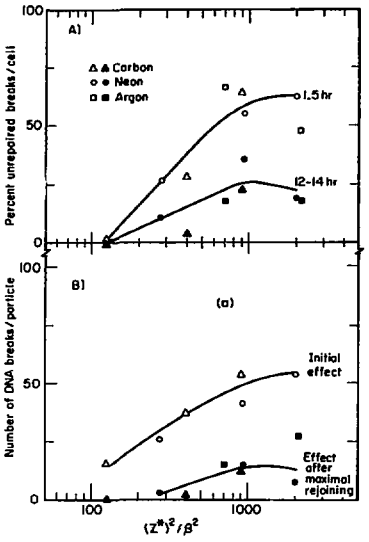

Figure 4. A) The percentage of the initial number of DNA breaks induced by accelerated heavy ions (2000 rad) left unrejoined after 1.5 or 11 to 12 hr of post-irradiation incubation plotted as a function of the energy deposition $(Z^*)^2\beta^2$. B) The number of DNA strand breaks per particle plotted against energy deposition $(Z^*)^2\beta^2$ after 2000 rad of particle irradiation. The open symbols represent the initial number of breaks; the solid symbols represent the number of nonrejoined breaks after 11 to 12 hr post-irradiation incubation. The graphs have been fitted by eye to the carbon and neon data because the argon data represent only one experiment. XBL 785-3111

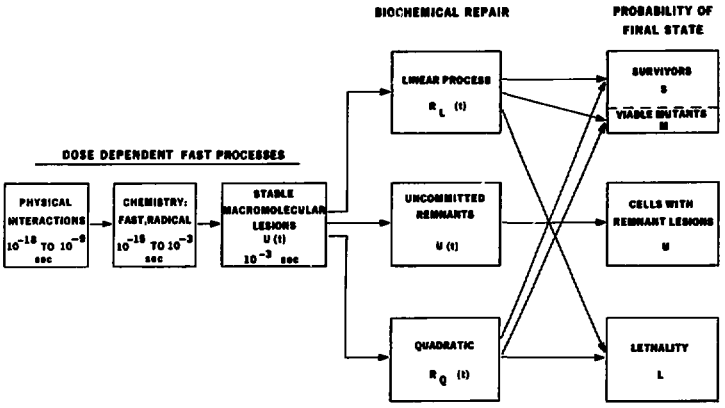

Figure 5. Schematic drawing of the repair-misrepair model, showing the dose-dependent fast processes, different types of biochemical repair, and the probabilities of the final states of the cell. *XBL 794-9463*

Initial macromolecular lesions are regarded as uncommitted because the eventual fate of cells remains uncertain for some time after exposure. The enzymatic repair processes yield either eurepaired states or misrepaired states with altered structures. Survival is a result of competition between eurepair and misrepair. A fraction of misrepair leads to lethality; other misrepair fractions produce mutants. The general features of the misrepair process are analogous to chromosome rejoinings. A schematic representation of this model is shown in Figure 5.

The detailed features of the RMR model cannot be explained within the confined space of this report. A central survival equation is, however, reproduced here:

$$S = e^{-\alpha D} \left\{ 1 + \frac{\alpha D}{\epsilon} (1 - e^{-\lambda t}) \right\}^{\epsilon\phi} .$$

Here S is survival probability and D is dose; α is a constant relating to the production of radiolesions in nucleoprotein; ϵ is the ratio of repair and quadratic misrepair; λ is the time rate of repair; t is time; and ϕ is a coefficient of linear misrepair.

We have applied RMR survival kinetics to a variety of radiobiological processes including the analysis of repair deficient mutants, the cell age response, the effects of accelerated heavy ions, split-dose survival from mixed modalities, and induction of mutations. The model provides a flexible framework for testing mechanisms of the biological effects of ionizing radiations and of other deleterious agents. Dose-rate effects have also been modeled. Work is in progress to adapt it to such processes as "repair inactivation" and "SOS repair."

REFERENCE

1. Blakely, E.A., Tobias, C.A., Yang, T.C.H., Smith, K.C., and Lyman, J.T. 1979. *Radiation Research* 80:122-160.

RADIATION AND MAMMALIAN CELL TRANSFORMATION

Tracy C. Yang and Cornelius A. Tobias

The primary objective of this research program is to study the potential role of radiation, particularly heavy ions, as an oncogen and as a co-carcinogen at cellular and molecular level. Ionization radiation can interact with chemical carcinogens and oncogenic viruses in inducing cell transformation, and has been found to be a highly potent co-carcinogen. At present very little is known of the co-carcinogenic effect of high-LET (linear energy transfer) radiation and the fundamental mechanism(s) that may be involved in the co-carcinogenic effect of radiation. Using an established cell line of mouse embryo fibroblasts (C3H10T1/2) as a model system, some systematic investigations on the interaction between radiation and oncogenic viruses (SV40) on cell transformation have been conducted.

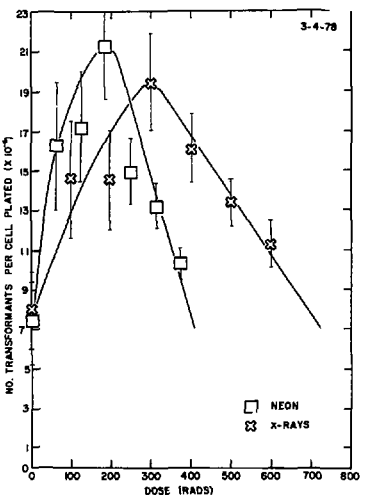

Figure 1. Effect of neon ions and x-rays on the number of transformants per cell plated in SV40-infected mouse embryo cells (C3H10T1/2). XBL 785-8403

In the past year, experiments with x-rays and high-energy neon beam (LET ≅ 34 keV/μm) have been done, and an enhancement of viral transformation was observed. This enhancement effect appeared to be both dose- and LET-dependent. The transformation frequency per cell irradiated generally increased with dose, reached a peak, and then declined (Fig. 1). The transformation frequency per survivor, however, increased rapidly with doses. Neon particles showed to be about two times more effective than x-rays in enhancing the viral transformation of cells (Fig. 2).

The importance of potential-damage repair system in the enhancement effect has been studied by infecting confluented cells with SV40 at various intervals after irradiation, and it was found that the enhancement effect was much reduced when the interval between irradiation and viral infection was prolonged (Fig. 3). Thus, the radiation-induced lesions, which are involved in the enhancement effect, are reparable.

Our data suggest that radiation may enhance the viral transformation by producing some LET-dependent DNA lesions, which provide additional sites for the integration of viral genes into cellular DNA. Further studies are underway to check this hypothesis.

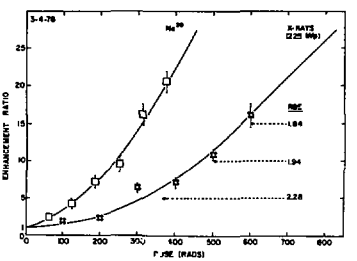

Figure 2. Enhancement effect of neon ions and x-rays on SV40 transformation of cells in vitro. Enhancement ratio = (transformants per survivor of irradiated cells)/(transformants per survivor of non-irradiated cells). XBL 784-8251

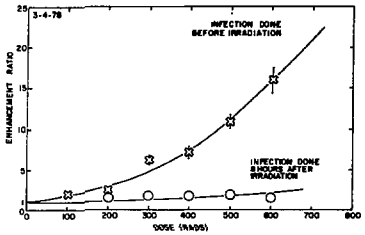

Figure 3. Reduction of the enhancement effect of x-rays by delaying the time of SV40 viral infection in cells at G_1 stage. XBL 784-6249

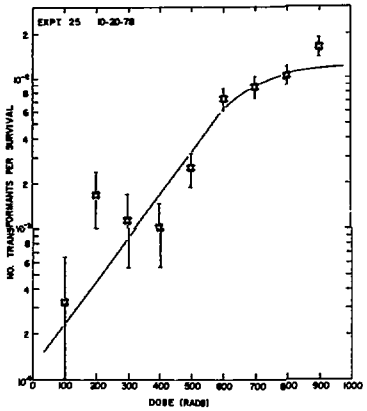

Figure 4. Direct transformation of mouse embryo cells with x-rays. Cells were irradiated at G_1 stage. XBL 791-7740

An investigation on the radiation-induced cell transformation has been initiated. Cells transformed by x-rays were found, and the transformation frequency per viable cell showed an exponential increase with dose, reached a maximum (about 10^{-2} transformants per survivor) at a dose of 600 rad, and then leveled off (Fig. 4). Experiments studying the effectiveness of high-LET radiation in transforming mammalian cells are in progress.

CLINICAL PHYSICS FOR CHARGED PARTICLE RADIOTHERAPY

George T.Y. Chen and John T. Lyman

The goal of the radiotherapy physics program is to assure precise dose localization to the specified target volume, while minimizing dose to surrounding normal structures. Calculation of dose distributions from multiport radiotherapy with charged particles and the quantitative assessment of processes which affect the calculated dose distributions are important steps toward this goal.

BEAM MODEL

To adequately treat a tumor, the narrow Bragg curve of a heavy-charged-particle beam must be modified to produce a more uniform effective dose over a broad region. The method currently used to achieve the desired modification involves passing a monoenergetic beam through a ridge filter to produce a polychromatic beam. The physical dose distribution is shaped over the desired region to compensate for the increase in relative biological effectiveness (RBE) with depth. Ridge filters have been designed for the various heavy-charged-particle beams. A different ridge filter is desirable for each particle beam and for each thickness of the treatment volume along the beam direction. As a practical matter, the ridge filters are generally built for treatment volume thicknesses from 4 to 14 cm, in 2-cm increments. Representative carbon beams used for treatment planning are shown in Figure 1.

Design of the ridge filter involves the use of a precisely measured Bragg curve and a corresponding theoretically calculated Bragg curve. The calculated curve is used to provide values of the mean energy loss, dE/dx, as a function of penetration depth. In order to produce a uniformly effective dose distribution over the desired region, there must be a means of predicting biologic effect as a function of the mean dE/dx and dose at each point in depth along the depth-dose distribution. To accomplish this we have used a linear-quadratic cell-

survival model. The linear and quadratic terms are both functions of the mean dE/dx and the particle velocity. The predicted RBE values at the 10% survival level are compared with RBE values obtained by various investigators at the 184-Inch Cyclotron and the Bevalac/Bevatron. These RBE values are stored in a computer databank ready for easy access and modification.

With the parameters of the heavy-charged-particle beam and a means of calculating a biologic effect in hand, it is a fairly straightforward procedure to calculate the expected biologic effect as a function of depth and then perform the necessary iterations to minimize the deviations from the desired biologic effect. The ridge filters are generally designed to produce a region where the cell survival will be uniform if the dose given is the appropriate dose for a 60% cell survival in the treatment volume.

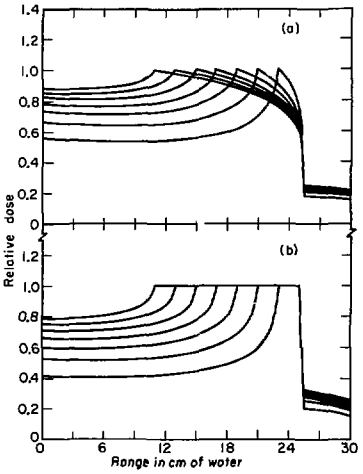

Figure 1. (a) Physical depth dose distributions for a series of carbon beams, (b) the corresponding isoeffect distributions, in CORE (Cobalt Rad Equivalent) units.

XBL 795-3475

TREATMENT PLANNING

Unlike photon radiotherapy, moderately small errors (~5 mm) in calculation of the required treatment range in particle therapy may have profound effects on dose distributions. Inadequate penetration depth could lead to substantial underdosing of the target volume, while overshoot could result in the undesirable irradiation of critical structures distal to the target. The role of clinical physics is to develop techniques for precise dose localization with this new therapy modality.

Computerized tomography (CT) plays an essential role in treatment planning in both target delineation and the quantitative assessment of inhomogeneities in the beam path. Quantification of inhomogeneities is used in the treatment planning code on a pixel-by-pixel basis to calculate the perturbations in beam penetration and the required depth along a beam ray from skin surface to target. CT data are proportional to linear attenuation coefficients at diagnostic photon energies, and are converted to water-equivalent path length per pixel by use of a calibration curve, as shown in Figure 2. The accuracy of this method has been established by experimental measurements on Rando phantoms to be ~3%.

CT scanners in the Bay Area are presently used for target volume definition and treatment planning. However, in collaboration with the Accelerator Division, approval and funds for an on-site CT scanner have been obtained. This specially modified unit will be capable of scanning patients in the upright treatment position, which is a more natural patient orientation when constrained to a fixed-horizontal therapy beam. Delivery is scheduled for late 1979.

GRAPHICS IN TREATMENT PLANNING

Image display hardware was installed this year and has extended the interactive treatment-planning capability. The therapist may now manipulate the image for best tumor definition and then enter the desired target volume via cursor. This process is done on all sequential CT slices over the tumor-bearing region. Beam entry angles and ion type are then selected. The treatment planning program utilizes target contour data to define field width, ridge-

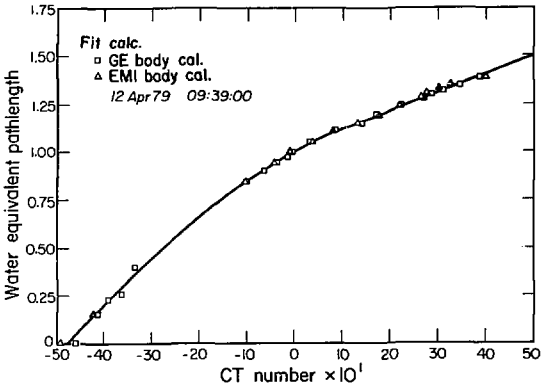

Figure 2. Conversion of CT numbers to water-equivalent pathlength per pixel is achieved through a calibration curve. XBL 789-11448

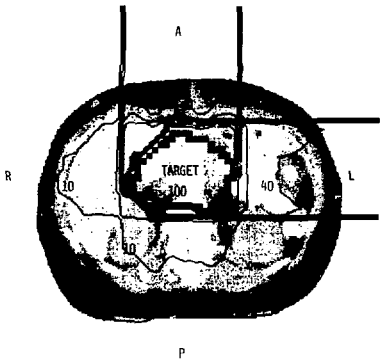

Figure 3. Carbon beam, irregular contour, fixed ridge filters. Isoeffect dose distribution for a two-field plan in the irradiation of a pancreatic carcinoma. The target is delineated by the broad line in the center of the body image. XBB:794-4289

filter size, and compensation required to shape the dose distribution to the contour. Data are also generated for automatic compensator fabrication on a computer-controlled milling machine. The sequential contour information may be used to define the required collimator shape. Calculated isodose distributions are displayed over the CT image, as shown in Figure 3.

PROCESSES AFFECTING DOSE DISTRIBUTION

Dose distributions described thus far are idealized in that static, CT-derived density data are used in the calculations. In reality, these plans are subject to a variety of processes which perturb the calculated distributions. Such processes have been under study to assess their magnitude and effect on treatment plans. One such process is respiration motion, which varies the skin-to-tumor depth by as much as 1 to 2 cm. To estimate the effect of breathing on treatment plans, respiration-modified, depth-dose curves were generated using a sinusoidal breathing model. Isoeffect distributions calculated with these modified beams show a broadened dose gradient at the distal end of the depth-dose curve, with little change elsewhere. For a maximum respiratory amplitude of 1 cm (from inhalation to exhalation), the 90% point on the distal gradient was moved by ~3 mm.

Compensation may also be misregistered relative to the target volume during daily treatment setup. This effect is simulated by a lateral displacement of the compensator. Resulting dose distributions are used to assess the magnitude of underdose and overdose.

BEAM SCANNING

In standard charged-particle delivery, a ridge-filter width is chosen to correspond to the maximum tumor dimension along the beam axis. This width is generally inappropriate for the target volume in other levels. In beam scanning, a pencil beam is moved across the portal, but the penetration depth and width of the spread-out Bragg peak are adjusted to match the target volume along each specific ray. In order to quantify its gain over fixed-ridge-filter methods, the treatment planning program was modified to simulate dose delivery through beam scanning.

This simulation was performed by using a family of ridge filters with 1-cm increments. A target volume was defined over 14 sequential CT scans in the treatment of a pancreatic carcinoma, and the total integral dose was calculated for the two methods of beam delivery. For the same target dose, the integral dose from a carbon beam to tissue outside the target volume was one-third less with beam scanning, as compared with fixed-ridge-filter techniques. The exact gain in beam scanning over fixed ridge filters is dependent upon the three-dimensional tumor volume, its placement relative to the body surface, and ion used. Representative treatment volumes in other sites, such as pelvis and head and neck, are presently under study.

HEAVY-ION RADIOGRAPHY

Cornelius A. Tobias, Jacob I. Fabrikant, William R. Holley, and Eugene V. Benton

Heavy-ion radiography is a newly developed noninvasive imaging procedure with increased resolution of minute density differences in soft tissues of the body. The method uses high-energy carbon and neon ions accelerated at the Bevalac, which are passed through the object to be radiographed, and come to rest in a stack of nuclear track detectors. When these detectors are developed, the stopping point distributions can be analyzed in terms of the electron density distribution of the object.

During the early phases of our program, it was necessary to focus our attention on the physical development of the method. Our program now applies heavy-ion radiography to treatment planning for cancer patients and for endocrine patients with pituitary tumors treated with particle radiotherapy at LBL. In addition, we are continuing our mammography program, and developing diagnostic noninvasive imaging procedures for imaging and accurate densitometry of skeletal structures (normal, malignant, and metastatic disease), brain and spinal neoplasms, and for imaging the moving heart. The potential of heavy-ion radiography is great, particularly for true three-dimensional reconstruction tomography as an adjunct to existing diagnostic imaging procedures in medicine. Eventually, applications will be made to the diagnosis, management, and treatment of cancer and cardiovascular disease in man, and also for the early detection of small soft-tissue malignancies at a low radiation dose to the patient.

HEAVY-ION RADIOGRAPHY AND TREATMENT PLANNING FOR PARTICLE RADIOTHERAPY

There is a close relationship between heavy-ion radiography and the studies currently being done with treatment planning for particle radiotherapy. The advantages of our imaging method applied to these programs are several: the same (or similar) ions are used for imaging and for radiotherapy; imaging can be carried out with the same patient using the same positioning and beam-delivery facilities that are used in treatment; the quantitative densitometric determinations in each minute volume of tissue results in the acquisition of an abundance of information on tissue structure and tissue inhomogeneities which can then be compensated for by physical or chemical means; heavy-ion radiography could replace the current use of computerized tomography (CT) densitometric data from x-ray reconstructions; and the potential for imaging tumors within normal tissues is enhanced by the enormous range provided by the improved density resolutions found with heavy-ion imaging.

We have successfully imaged tumors located deep within the body, particularly pancreatic carcinoma and brain tumors in patients scheduled for charged-particle radiation therapy. Figure 1 (top) is a single sheet of the detector stack from a carbon-ion radiograph of a patient with carcinoma of the head of the pancreas. A contour plot of the stopping power values of every third detector sheet (Fig. 1, bottom) demonstrates the low stopping-power values of the pancreatic neoplasm (T) and the higher values of the liver (L). The localization of the intestinal gas in the colon (C), which is essential for correcting for perturbations arising from tissue inhomogeneities, is readily identified.

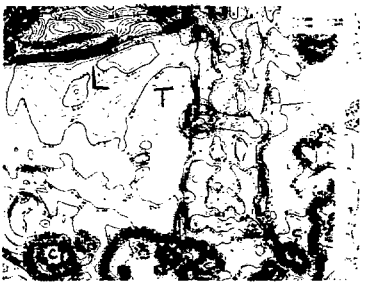

Figure 1. Above: carbon-ion radiograph of a patient with carcinoma of the head of the pancreas. This is one of the 150 plastic detector-sheets that were exposed. Below: contour plot of the data obtained from the radiograph. This figure demonstrates the low stopping-power values of the pancreatic neoplasm (T); the higher values of the liver (L); and the intestinal gas in the colon (C). XBB 782-1165A

HEAVY-ION MAMMOGRAPHY AND BREAST CANCER

Heavy-ion radiography of the breast represents a unique advancement in quantitative, noninvasive diagnostic imaging, with the potential of augmenting and improving the cancer detection rate with very low radiation dose to the patient. Thirty-four patients have received carbon-ion mammographic examinations. Heavy-ion mammographs proved capable of detecting breast cancers that appeared on x-ray mammograms either as a mass or because of the presence of microcalcifications. Heavy-ion imaging can delineate cancers of the breast that are less than 1 cm in diameter with difficulty, but it has the potential of detecting much smaller cancers because of its improved density resolution.

The important findings of the initial patient studies are (1) heavy-ion mammography is a low dose, reliable, and noninvasive imaging procedure that provides an enormous amount of quantitative information for image processing and analysis in each patient; (2) carbon-ion radiographs provide a greater sensitivity for detecting minute, contrasting tissue densities in the breast than x-ray mammographs; however, x-rays provide better lateral resolution and are relatively more sensitive to higher-atomic-number particles; (3) in all patients, the carbon-ion images demonstrated the same abnormal densities as did the x-ray mammographs; however,

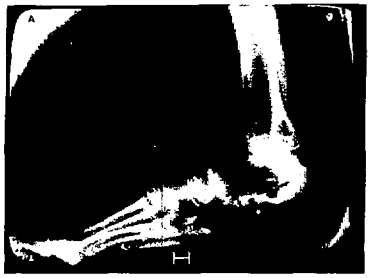

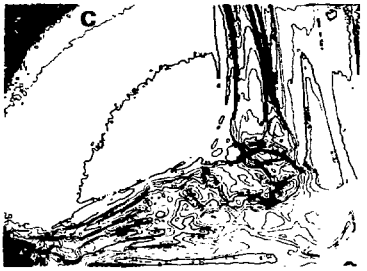

Figure 2. (A) Neon-ion radiograph; (B) x-ray image; (C) isodensity contour map derived from the neon-ion radiograph.
(A) XBB 780-13647
(B) XBB 792-1653
(C) XBL 7810-11938

the carbon-ion radiographs demonstrated abnormal densities in the breasts of two patients which were not detected by x-ray mammography; and (4) heavy-ion isodensity contour plots, measurement of tissue-stopping-power density-distribution profiles, and perspective density contours are three electronic quantitative display methods which provide valuable diagnostic information on internal structure of normal, diseased, and particularly neoplastic breasts.

TISSUE DENSITOMETRY

Some thirty organ specimens of normal and neoplastic human tissues have been investigated with both heavy-ion and x-ray radiography. Extremely low doses of only a few mrad of heavy ions are sufficient to detect density differences of 0.001 and less. Tissues and organs studied include brain, liver, kidney, breast, bone, muscle, skin, adipose tissue, and tendons. Mean radiation doses to specimens agreed with 30% of compared x-ray images, and only one glioma was not detected by either method. Except for a calcified adenocarcinoma metastasis to the liver, all remaining tumors were detected better by imaging with heavy ions than with x-rays. The ability of heavy-ion beams to detect small differences in tissue density at very low dose-levels makes them valuable for investigation of normal tissues, primary neoplasms arising in otherwise normal tissues, metastatic cancers in tissues and organs, and non-neoplastic diseases which give rise to small differences in tissue density.

SKELETAL HEAVY-ION RADIOGRAPHY

Because of the high absorption coefficient of x-rays in bone, skeletal x-ray radiography of abnormalities in bones and joints is reliable. We have been investigating the potential usefulness of heavy ions for skeletal radiography, not only for assessment of bone detail, but also for joint and associated soft-tissue detail. Figure 2 shows the comparison between a neon-ion radiograph, an x-ray, and an isodensity contour map derived from skeletal heavy-ion radiographs. The improved density resolution of the neon-ion beam has made it possible to visualize the entire skeleton, and the application

of our computer analysis and display methods of integrated images has made possible highly accurate images of bones, joints, tendons, and soft tissues in the leg and foot.

SPINAL CORD RECONSTRUCTION

Because of interest in the ability of heavy ions to image the spinal cord, intervertebral discs, and other structures of the vertebral column (particularly in trauma and neoplastic disease), we have carried out a few spinal cord reconstructions. In general, three types of studies are being carried out: computer integration and image display of the human spine (tissue specimens from autopsy material), heavy-ion radiography of the spine in patients who are undergoing heavy-charged-particle radiotherapy for cancer within the abdomen, and heavy-ion CT reconstruction of the human spine (in autopsy material at this time, with the view of ultimate application to humans).

Our initial study of the spine was carried out in conjunction with the study done on pancreatic carcinoma for the patient under heavy-particle radiotherapy. A very detailed anatomical carbon-ion image of the lower thoracic and upper lumbar spine was obtained (see Fig. 1). We have also made the first heavy-ion CT image reconstruction of the human spine. It demonstrated high resolution of both soft tissues and osseous structures. Differences in density were determined within the spinal canal, the outer cylinder of the cerebral-spinal fluid, the region of gray matter, and the region of white matter of the spinal cord.

CARDIAC HEAVY-ION RADIOGRAPHY

Initial studies have begun on fast-pulse, heavy-ion radiography of a dog heart *in vivo*, with a view of imaging and sizing myocardial infarction in ischemic heart disease and coronary thrombosis. We have obtained a neon-ion radiography image of the chest of a living dog (Fig. 3).

Figure 3. Neon ion radiograph of the chest of a living dog.
XBB 780-13068

The cardiac silhouette, great vessels of the mediastinum, vertebral column, muscles, fat, and skin are imaged. In the heart, the right ventricle, the aortic arch, and the dense, ventricular myocardial muscle-mass can be seen. The density in the thin-walled area lying posterior has the contour of the cardiac chamber. We are presently analyzing the digitized data, and the stopping-power values of the various cardiac tissues will be determined. Isodensity contour maps will be used for analysis of myocardial structure and blood, and density distribution plots for normal, ischemic, and infarcted myocardium will be made. Such imaging has the potential of providing a noninvasive imaging method for the experimental and clinical study of myocardial tissue ischemia, infarction and necrosis; for the detection and sizing of myocardial infarctions; for the evaluation of effectiveness of methods designed to limit myocardial infarct size; and possibly for evaluation of the functional anatomy of the normal and ischemic ventricular myocardium.

TREATMENT OF CANCER WITH HEAVY CHARGED PARTICLES

Joseph R. Castro

A systematic clinical trial of heavy-charged-particle radiation therapy of human cancers began at LBL in July 1975. The initial thrust of the project was to develop the physical, biological, and clinical bases to undertake helium-ion radiation therapy at the 184-Inch Synchrocyclotron as well as to use heavier ions such as carbon, neon, or argon, at the Bevalac. Much experience and hardware that could be rapidly modified for human cancer treatment existed at the 184-Inch because of the previous pituitary irradiation program. Some such hardware also existed at the Bevalac and, after completion of an appropriate patient facility, several patients have been treated there. Design refinements and other improvements continue to be made at both accelerators.

Radiobiological data, as well as assessment of skin, mucosal, and intestinal reactions observed in the trial, confirm that a radiobiological effect (RBE) for helium at 200 rad per fraction appears to be ~1.2. Pre-therapeutic evaluation of heavier ions such as carbon, neon, and argon has been carried out at the Bevalac by Tobias and associates as well as outside users. Experience so far has indicated an RBE which ranges between ~2.2 and ~4.0 for these heavier ions, depending upon how much the Bragg peak has been spread out.

Since 1975, 138 patients have been treated at LBL, including 65 during 1978. The tumor sites studied include brain, head and neck, esophagus, upper abdomen, and pelvis. Of the 138, 120 patients received either helium-ion irradiation or mixtures of photon x-ray and helium ions; 18 patients received irradiation with heavier particles such as carbon, neon, or argon. The distribution of these patients by tumor and anatomical site is shown in Table 1.

Table 1. Heavy charged particle patient accrual at Lawrence Berkeley Laboratory.

Disease	1975-77	1978	1979*	Total
Intracranial (including brain)	7	6	5	18
Head and neck (upper aero-digestive)	4	6	1	11
Esophagus	3	4	7	14
Pancreas and biliary	16	33	9	58
Stomach	2	2	1	5
Retroperitoneal and pelvic (colon, cervix, para-aortic)	11	10	1	22
Skin and subcutaneous nodules	3		1	4
Choroidal melanoma		4	2	6
	46	65	27	138

Helium or mixed photon/helium – 117
Carbon, neon, argon, ions – 18

*As of March 31, 1979.

The largest group of patients irradiated have been those with carcinoma of the pancreas. Most of these patients have had therapy with helium ions, although some of the earlier patients had the first part of their treatment (up to 5000 rad) with conventional radiation and were given a boost of helium ions (1000 to 2000 rad). In the past year, 3 patients had helium-ion irradiation plus carbon-ion irradiation as a portion of their overall treatment for advanced carcinoma of the pancreas. The treatment set-up is shown in Figure 1.

In September 1978, a randomized trial of adenocarcinoma of the pancreas was opened through the cooperation of LBL and the Northern California On-

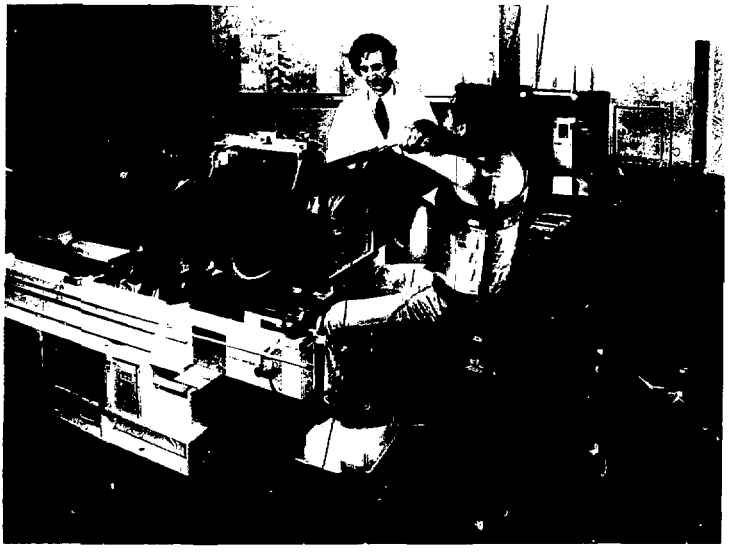

Figure 1. This photograph simulates a patient (John Lyman) in treatment position in the new Bevalac therapy room, and Chief Technologist, Bob Walton, preparing to insert an x-ray film cassette into the holder. Directly in front of the cassette holder is the individually poured cerrobend collimator which sits in front of the water column. Behind that is visible an ion chamber and a brass collimator. Behind the patient is visible one of three cameras which keep the patient in view, from different angles, at all times. The patient is supported with safety belts. He is made as comfortable as possible, without compromising immobilization, with foam rubber both on the chair and on the arm rest which keeps his arms above the treatment area. Above the patient's head, not visible in this photograph, is a microphone which is on at all times and which picks up even the softest voice from the patient, allowing him to be heard so that the staff can respond to the slightest need the patient may have. Also, you will notice a button in the hand of the patient. In an emergency, not only is the microphone available but the patient can press the button which activates a buzzer to which the staff immediately responds. CBB 794-5405

cology Group (NCOG-a cancer cente. .vithout walls, whose affiliates are throughout northern California and western Nevada). At this time there are five LBL/NCOG protocols: pancreas and cervis uteri (randomized); and esophagus, ocular melanoma, and Phase I-II (non-randomized). Later this year similar protocols will be activated by the Radiaion Therapy Oncology Group (RTOC) and LBL opening up nationwide randomization and increasing patient referral patterns.

In March 1979, the first patient was treated with 570-MeV/amu argon ions. The patient received 2000 rad in 4 fractions over 4 days. His skin reaction was carefully monitored; photographs were taken before, during, and after treatment, and skin erythema was scored with a Photovolt Reflexion Meter 670.

This year the Bevalac has scheduled regular treatment times that permit scheduling of a 4-fraction-per-week treatment series, as has been used at the 184-Inch. The Biomed therapy area itself is basically all new, including a Phii.ips ram-style treatment couch which has been modified to include a chair when desired; a patient waiting area; a fully outfitted examination room; a patient dressing room; and a treatment planning area.

Datatrieve-11, the Digital Equipment data retrieval program to store, modify and retrieve information about patients, is now in use. This program

stores patient information including name, identification number, status, treatment-site, and dose information. This entire database is password protected and can be accessed by privilege users only, thereby protecting patient confidentiality. Patient records can be sorted and printed out selectively. In addition, standard procedures now exist to edit data for each patient, thus making it possible, for example, to calculate and output the survival time for specific groups of patients.

Last summer, work was begun on improvements to building 55. These Phase II improvements have been completed and provide the clinical facility with examination rooms; rooms for patient impressions and lightcast molding; an x-ray simulation room which also is used for diagnostic x-ray studies and has itsown dark room for film developing; and a mini shop to complete the plaster impressions and/or fabricate materials for radiology, radiobiology, cancer therapy, etc. at the Bevalac as well as fabricate materials needed in building-55 clinical area. The modifications also include a patient dressing area and a clerical/technical support room. Next year, an upright CT (computerized tomography) scanner will be housed in building 55, to aid in treatment planning for patients who are treated in the upright position, but who can only be scanned at the present time in a horizontal position.

During 1979 new protocols have been opened and facilities have been updated and outfitted to allow more efficient patient therapy, examination, and followup. In the coming year an estimated 150 patients will be treated. Approximately 70 of these patients will be in one of the already established randomized protocols. Meanwhile, Phase I-II heavy particle studies will continue and Phase III protocols will be written as the appropriate data are accrued.

Magnetic Field Studies

BIOLOGICAL EFFECTS OF HIGH MAGNETIC FIELDS

Tom S. Tenforde

A large number of research and industrial technologies involve personnel exposures to magnetic fields at levels of 1 to 10 kG. These technologies include fusion reactors, magnetohydrodynamic systems, magnetic energy-storage rings, bubble chambers, isotope separation facilities, and various magnetic induction processes such as induction welding and induction furnaces for steel production. A biomagnetic program has therefore been undertaken to obtain data that will provide a basis for the establishment of occupational exposure guidelines in these diverse technologies. This program is focused on a broad-spectrum evaluation of physiological functions in small mammals exposed to high magnetic fields. A concentrated effort is also being made to analyze magnetic effects on the development of organisms and on the functional integrity of selected macromolecular systems and tissues with a demonstrated sensitivity to high magnetic fields.

Animal Physiology (Tom S. Tenforde, Cornelius T. Gaffey, Michael S. Raybourn, and Michael D. Edison)

Measurements of the electrocardiograms (ECG) of rats and dogs have demonstrated marked changes in the presence of a dc magnetic field, with the principal effect being an augmentation of the T-wave signal (Fig. 1, panels *a* and *c*). The highest field level used with dogs, 16 kG, produced a 750% increase in the amplitude of the T-wave signal (Fig. 1, panel *b*); with rats, the highest field level was 21 kG, which led to a 450% increase in the amplitude of the T-wave signal (Fig. 1., panel *d*). The threshold field levels above which this effect was observed were approximately 3 kG for rats and 800 G for dogs.

The change in the T-wave signal induced by a magnetic field was completely reversible, with no residual effect being observed immediately after reducing the field to zero. The magnitude of the increase in the T-wave amplitude was found to depend upon subject orientation in the field, with the

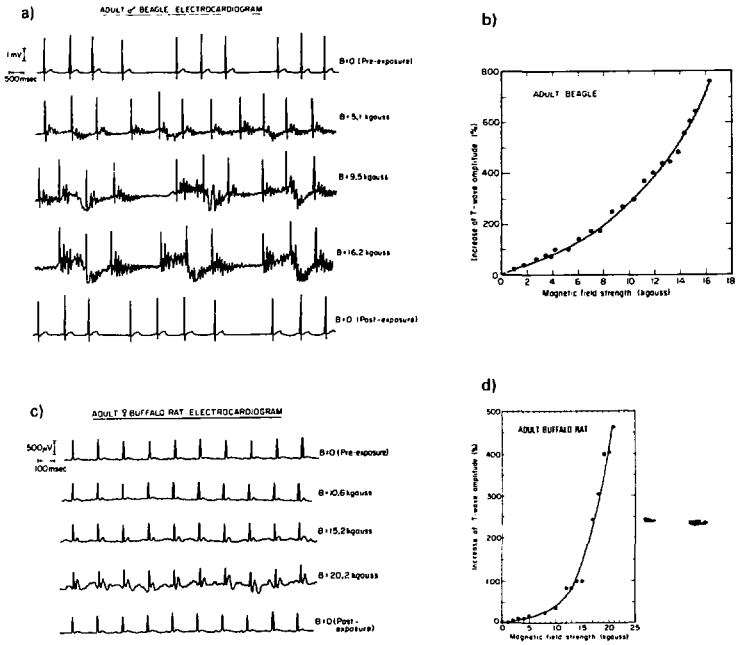

Figure 1. (a) Electrocardiograms of a dog (adult, male Beagle) in the pre-exposure or control state; during exposure to magnetic fields of 5.1, 9.5, and 16.2 kG strength; and promptly after cessation of the magnetic field exposure. The observed cardiac arrhythmia may result from the use of sodium pentobarbital anaesthesia.
(b) The percent increase in the T wave of an adult dog is plotted as a function of magnetic field strength.
(c) Electrocardiograms of a rat (adult, female Buffalo) in the pre-exposure or control state; during exposure to magnetic fields of 10.6, 15.2, and 20.2 kG strength; and immediately after cessation of the magnetic field exposure.
(d) The precent increase in the T wave of an adult rat is plotted as a function of magnetic field strength.
XBL 794-3409

greatest effect occurring when the lines of magnetic induction were perpendicular to the body axis. Future studies will focus on determining the point of origin of the augmented T-wave signal, as well as its underlying physical basis. Preliminary studies have also indicated that an acceleration of heart rate occurs in a dc magnetic field, and direct measurements of cardiac output will be made to evaluate the stress associated with this phenomenon.

The effects of magnetic fields on physiological function were also studied by measurements of deep-body temperature in adult mice. Non-magnetic telemetry transmitters were implanted in the abdominal cavity for continuous recording of body temperature, which was found to have a strong circadian variation from 35.5 to 37.5 °C (Fig. 2). The peak temperature occurred at approximately midnight, which is halfway through the 12-hour dark cycle and coincides with the period of peak activity. Continuous application of a 15.5-kG magnetic field for a 5-day period had no effect on either the amplitude or phase of the circadian variation in body temperature. No irregularity in the body temperature profile was observed during continuous mon-

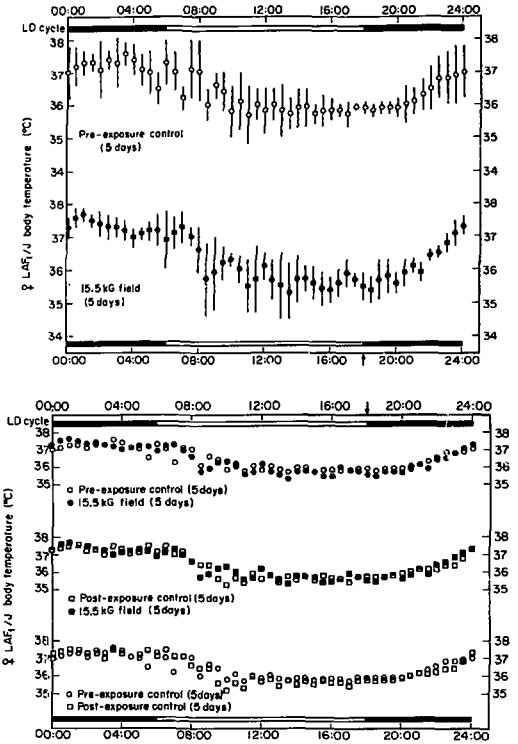

Figure 2. The deep-body temperature of an LAF1/J mouse was recorded by telemetry for 15 days, with continuous exposure to a 15.5-kG field during days 6 through 10. The average body temperature was recorded at 30-min intervals on each day during the 5-day pre-exposure control perind, the 5-day magnetic field exposure period, and the 5-day post-exposure control period. The points presented on the graphs represent 5-day average temperatures for each of these conditions. The error bars in the upper panel represent the standard deviation in body temperature recorded at a given time on 5 successive days. These plots demonstrate the circadian rhythm in body temperature, and the absence of any magnetic field effect. XBL 794-3410

itoring for a period of 5 days following the magnetic field exposure.

Several types of experiments were conducted to assess potential magnetic-field effects on nerve impulse propagation and the neurobehavioral characteristics of exposed animals. Action-potential measurements were made on a total of 12 frog-sciatic-nerve preparations while exposed to dc magnetic fields of 5-, 10-, 15-, and 20-kG strength. The long axis of the nerve was oriented perpendicular to the magnetic field lines, and the exposures were 30 minutes in duration. No magnetic field effect was observed on the action-potential amplitude in any of these nerve preparations (Fig. 3). Neurobehavioral studies with rodents, including the retention of memory of a learned task, failed to reveal any effect of a prolonged exposure to a 15.5-kG field. The examination of potential neurobehavioral effects of magnetic fields is being conducted in collaboration with E. Bennett (Laboratory of Chemical Biodynamics) and H. Davis (Psychology Department, UC Berkeley).

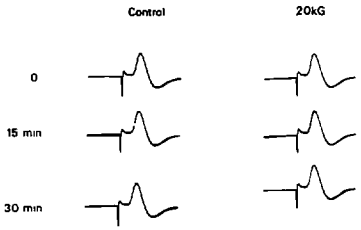

Figure 3. Action potentials are shown for two frog sciatic nerve preparations at 20°C. The oscillograms were taken at 0, 15 min, and 30 min after placement of the nerves in the recording chamber. The nerves were stimulated by application of a 0.1 msec rectangular voltage pulse to the central nerve area, and the evoked action potential was detected by an electrode at the peripheral nerve ending. In 12 separate repetitions of this experiment, no evidence was obtained for an effect of the applied magnetic field on the magnitude of the evoked action potential.

XBB 780–12959A

Developmental Studies With Plants and Insects (Tracy C. Yang and Laurie M. Craise)

In contrast to observations previously reported from several laboratories throughout the world, the continuous exposure of barley and corn seeds to a 16-kG dc field for periods of up to 4 days was found to have no effect on the subsequent development of plant roots and shoots. This result was obtained both for moist seeds that were germinating during the magnetic field exposure, and for dry seeds that were exposed to the field and subsequently soaked in water to promote germination. The absence of a magnetic field effect was found irrespective of the orientation of the seed axis relative to the lines of magnetic induction.

A total of ten experiments have been carried out to assess magnetic field effects on the development of the flour beetle *(Tribolium confusum)*. No effect of exposure to dc magnetic fields up to 21 kG strength has been observed on the hatchability of beetle eggs, and this result was independent of the orientation of the developing organisms in the field.

Molecular Studies (Ruth J. Roots and Raymond S. Farinato)

Physicochemical techniques are being used to detect conformational changes in magnetically anisotropic macromolecular systems that are subject to orientation in a dc magnetic field. Examples of such systems include the rhodopsin photopigments in the disk membranes of retinal rods, the membranes of chloroplast grana, and duplex DNA molecules. Our initial studies have been carried out with superhelical double-stranded DNA from the bacteriophage ϕX-174. High-resolution agarose gel electrophoresis indicated that no effect on molecular conformation resulted from a 2-hour exposure of ϕX-174 DNA to a 21 kG stationary field. Based on a bioassay for DNA infectivity in bacterial hosts, the functional capacity of ϕX-174 DNA molecules was also unaffected by the applied magnetic field.

In contrast to these results, the technique of electro-optical birefringence, in which the molecular relaxation time is monitored following induced alignment by a pulsed electric field, indicated that the rotational diffusion coefficient of ϕX-174 molecules was reduced following magnetic field exposure. This observation indicates that the magnetic orientation of nucleotide bases, previously reported by other investigators, may lead to a reduced number of superhelical turns in ϕX-174 DNA. However, the variation in relaxation times between different samples was sufficiently large that no firm conclusion can be drawn until several repetitions of this experiment have been carried out.

Biophysical Studies

CNS NEUROTOXICITY STUDIES WITH ENVIRONMENTAL POLLUTANTS AND RADIOSENSITIZING AGENTS

Michael S. Raybourn, Walter Schimmerling, and Julia A. Twitchell

We have developed an *in vitro* bioassay technique utilizing electrophysiological recordings from neural tissue that allows us to determine the direct interactions between various known toxins (as well as potentially harmful environmental agents) and quantitative indices of viable neuronal bioelectric activity. More specifically, we are using as an endpoint the spontaneous bioelectric activity that we can monitor from certain neurons (cerebellar Purkinje cells) in our neural cultures. Assuming that this model system gives us a reasonably representative picture of what the intact central nervous system (CNS) might do in response to these same toxic agents (buffered, of course, by the blood-brain barrier), we have been investigating at what dose levels certain common environmental agents (hypoxia, carbon monoxide, methyl mercury) alter the complex and dynamic CNS network functioning. It is this neural activity, of course, that underlies most, if not all, of our overt behavior.

Towards that end we have shown that variations in local oxygen tension and/or carbon monoxide (CO) concentrations directly affect the capacity of neurons to carry out their normal bioelectric functions. This is without any involvement of the blood hemoglobin system. Figure 1 depicts a sequential analysis of how this functional bio-electric activity is systematically altered by both hypoxic and CO-induced insults. These data are presented in the form an an inter-spike-interval histogram (ISIH), which is a measure of the temporal organization of action potential (i.e., spike) firing in a cell. This is an extremely sensitive measure of cell functioning.

In Figure 1A the effects of hypoxic insult (N_2 gas) can be compared to control conditions (air), both in terms of the overall rate of spontaneous activity (N = number of spikes in a 4-minute sample period) and in the relative temporal organization of that activity in the ISIH (RTC = return-to-control). In Figure 1B the effects of a 1,000-ppm CO gas-phase insult is shown for the same cell. Because of the fact that CO is photodisassociable from its presumed intracellular binding sites, we can modulate its effects by applying an external light (L) stimulus (L/ON, L/OFF). The L/OFF condition represents the maximum effect of CO on cellular functioning.

In our current studies we have found that local gas-phase concentrations of around 500 to 1000-ppm CO result in threshold alterations in neuronal function. This represents a CO concentration of approximately 1×10^{-4} CO that the cell is actually "seeing" at these threshold levels. Since the intact CNS is certainly more sensitive and dynamically equilibrated, subtle-to-significant behavioral manifestations of these agents may well occur at levels well below these values. These data suggest that such neurophysiological model systems are valuable in ascertaining the potentially deleterious effects of environmental pollutants and low-level radiations on the CNS.

Along that line we are beginning an assessment of what effects are seen in CNS tissues, *per se*, due to the clinical use of various radiosensitizing agents currently in use to potentiate radiotherapeutic treatment of cancer. Because these agents have been found to produce clinically relevant neuroleptic symptoms (ataxia, tremor, etc.), we are attempting to better define these dose-dependent effects. We also wish to address the biophysical basis for their neurotoxicity, in hopes of guiding future biochemical manipulations attempting to eliminate these side effects. Our preliminary results have, indeed, demonstrated that in addition to the previously known peripheral neuropathies, there is a severe dose-dependent toxicity to CNS tissues. These agents (misonidazole, metronidazole) greatly retard the growth and differentiation of our *in vitro* neural tissues and induce drastic modifications of cellular morphology in adult (i.e., mature) tissue (see Fig. 2).

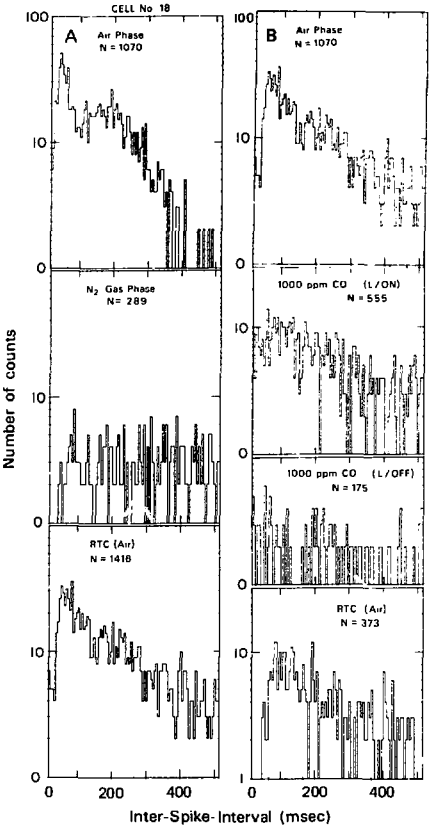

Figure 1. The inter-spike-interval histogram (ISIH), which is a measure of a cell's temporal firing pattern, is shown for the spontaneous activity of an in vitro cerebellar Purkinje cell under hypoxic (Fig. 1A) and carbon monoxide (Fig. 1B) insults versus the control condition (air phase). The total number of action potentials in a 4-min sample period is given under each condition. Air phase: 80% N_2 and 20% O_2; N_2 gas phase: 100% N_2; all gas flow rates = 150 ml/min. L/ON and L/OFF represent the presence or absence of an external light stimulus (see text). *(A) XBL 771-7381*
(B) XBL 771-7381A

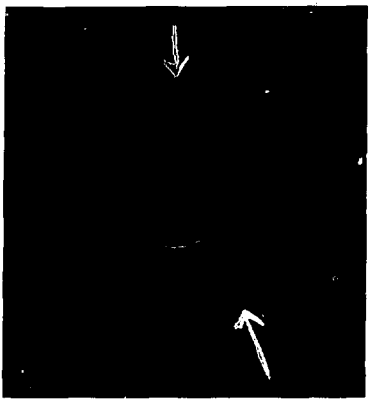

Figure 2. Phase contrast micrograph of a cultured cerebellar Purkinje cell (25 days in vitro) after 24 hours incubation with 10 mM metronidazole. Note extensive vacuolization, distorted cell shape, extensive swelling and cytoplasmic densification on the nuclear border.

XBB 789-12272

CELL-MEMBRANE BIOPHYSICS AND ENVIRONMENTAL AGENTS

Howard C. Mel

A variety of cell-membrane biophysical properties has been under investigation in relation to normal and abnormal cellular development, and in response to various physical and chemical agents. A principal tool for this kind of investigation, developed within this laboratory, is "resistive pulse spectroscopy" (RPS). By means of the RPS technique information can be obtained in a matter of seconds or minutes, for many thousands of cells, on cell size, cell deformability, cell-membrane fragility, and the kinetic details of several kinds of recovery processes that follow in sequence close upon the act of abrupt membrane disruption (e.g., by osmotic hemolysis of red blood cells). In this way it has become possible to rapidly monitor many cell-membrane characteristics and their changes—chemical, mechanical, osmotic, and electrical—to help clarify the intrinsic differences between normal and altered cells.

The technical details of the methodology were presented in some detail in the Annual Report for 1977 (LBL 7448). Some selected recent applications and results are as follows.

MERCURY EFFECTS

The red-blood-cell-membrane system is extremely responsive to small amounts of mercury when examined by RPS. The threshold for detection of effects of inorganic mercury on human blood cells has now been lowered to 10^{-9} M. In the process of accomplishing this, it was discovered that untreated control cells displayed systematic, multiphasic variations in fragility, size, and other biophysical properties, especially during the first hour after fresh blood samples are suspended at room temperature in isotonic media. The lowest-concentration effect (10^{-8} to 10^{-9} M $HgCl_2$ for instantaneous

exposure) is one of *protection* against the violent disruption induced by hemolytic stress. With time, or for higher mercury concentrations (e.g., $>10^{-4}$ M), the protection turns to an enhanced *fragility* compared with controls.

Systematic time-dependent size changes have also been detected (both shrinkage and swelling), indicating a highly specific kind of action of mercury on the transport regulatory processes under membrane control. Progress has been made in establishing a rational framework for predicting the general nature and magnitude of effects to be expected, with respect to the variables of cell concentration, time of incubation in mercury, concentration of mercury, and time of pre-incubation storage. The parameter: molecules of Hg per red cell is useful but not uniquely sufficient as a predictor, even after the time variables have been eliminated, contrary to previous suggestions in the literature. Some of these effects are depicted, for two different cell concentrations, in Figure 1. ("N.I." means "not incubated," i.e., instantaneously exposed to mercury; "I" means pre-incubated prior to testing.)

CROSSLINKING AGENTS

A systematic study of the kinetics of action of glutaraldehyde (GA) on red cells has just been completed, and a detailed publication covering the results has just appeared. Whereas cell-membrane *deformability* decreases monotonically upon exposure to GA, *volume* responses are complex and multiphasic, indicating several competing mechanisms of action. An empirical expression has been derived that accurately predicts the time of fixation as a function of concentration of GA. The nature of fixation, *per se*, has been clarified by this work, in part by subjecting the variously fixed cells to subsequent controlled physical stresses. One reason for interest in cross-linking agents is that they have been proposed for possible drug use, e.g., DMA (dimethyladipinate), an experimental anti-sickling agent. In low physiological concentrations this agent was found not to affect adversely the cell membrane deformability or other biophysical properties sensed by RPS, though in somewhat higher concentrations it proved extremely damaging to cells by these criteria. Some of these effects are indicated in Figure 2.

OSMOTIC, HEMOLYTIC AND RECOVERY RESPONSES OF RED CELL POPULATIONS

Dynamic osmotic hemolysis. The first stage of an extensive study on dynamic mechanisms of blood cell hemolysis and membrane repair has been completed.[2] New quantitative results have been obtained in several areas including on the nature of the prehemolytic and hemolytic processes, and on types of cell-membrane repair and recovery. Some notable findings: the most fragile subpopulation in a population of fresh cells, added to 125-mOSM (milliosmolal) PBS (phosphate-buffered saline) explosively ejects its cytoplasm according to first order kinetics, like a radioactive decay process, with a half-time of 14 seconds (see Fig. 3). The subsequent repair-recovery of the punctured viscoelastic membrane is demonstrated by the subsequent explosive rehemolysis of the restored ghosts, when they are re-exposed to hypotonic solutes of less than 125 mOSM. Our most recent work strongly suggests that, depending on the osmotic pressure and other conditions employed, a normal human population of cells contains subpopulations of cells possessing at least two longer time-constants for self destruction, as well.

Isotonicity and deformability. A common view, that isotonicity corresponds to 300 mOSM, must be revised downward to the lower value of 280 mOSM, which has been found to correspond to the point of experimental maximum in red cell deformability. This has led to the proposal that isotonicity be viewed as an evolutionary goal aimed at achieving this optimum condition, given the essential survival value of having high red-cell deformability.[1] Figure 4 is a plot of deformability, measured by RPS index, versus osmotic pressure, showing the clear maximum.

Restoration after hemolysis. Simultaneous investigations using "live cell cytology" and RPS have been carried out on normal red cells exposed transiently to hemolytic medium, sequentially restored to isotonic medium, then examined 30 to 180 minutes post-restoration. This work has revealed previously unsuspected subpopulations of intermediate cell-ghosts (i.e., objects having different residual hemoglobin content), where the dynamics indicate a complex pattern of transit from one cell class to another. It also appears that a very brief prehemo-

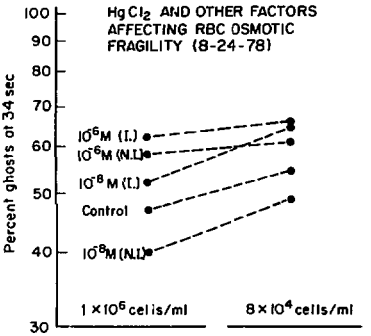

Figure 1. $HgCl_2$ and other factors affecting RBC osmotic fragility. The effects are depicted for two different cell concentrations. "N.I." means "not incubated" (i.e., instantaneously exposed to mercury); "I" means pre-incubated prior to testing. XBL 792-3179

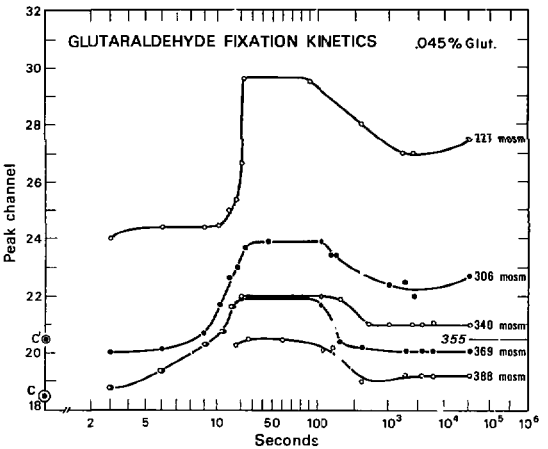

Figure 2. Resistive pulse spectroscopy (RPS) volume kinetics as a function of fixative medium osmolality. Fresh red blood cells (0.1 ml of stock solution) were added at time t = 0, to 10 ml of each fixative solution, with a final glutaraldehyde concentration of 0.045%. The osmolality of each solution is denoted to the right of each curve. The RPS spectral peak channels are plotted on a logarithmically compressed time scale. Point C represents the initial, native, unfixed RBC volume; C' the equivalent rigidified-cell volume, as determined from slow flow measurements. (Normal sample flow rate, 48 × 48 μm aperture.) DGL 745-4790A

lytic exposure to hypotonic solution, followed by immediate restoration to isotonic (thus preventing hemolysis), nonetheless leaves a permanent trace of membrane damage - loss of normal volume-regulation ability.

Members of the group include Howard C. Mel, Professor of Biophysics, Dr. James Yee, Steve Akeson, Jon White, Tom Reed, Gary Richieri, Sara Rabinovicci, and Rick Rensio.

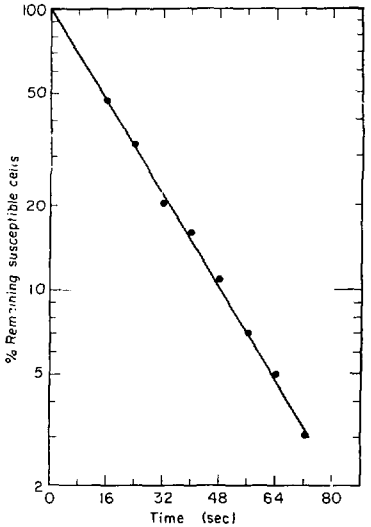

Figure 3. Early time osmotic fragility kinetics, measured by RPS. The most fragile subpopulation in a population of fresh cells, added to 125 mOSM PBS, hemolyzes and explosively ejects cytoplasm with a half time of 14 seconds.
XBL 782-2869A

REFERENCES

1. Yee, J.P. and Mel, H.C. 1978. *Blood Cells* 4: 485-497.
2. Yee, J.P. and Mel, H.C. 1978. *Biorheology* 15: 321-339.
3. Mel, H.C. and Jung, D.G. 1978. *Biophysical J.* 21: 119a.

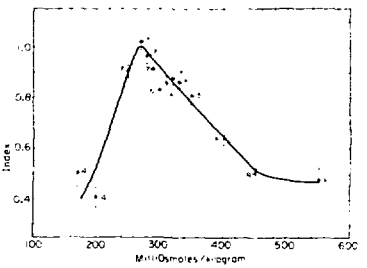

Figure 4. Red cell membrane deformability, measured by RPS index, versus osmotic pressure of suspending medium.
XBL 781-2782

7. STRUCTURAL BIOPHYSICS

This group, led by Dr. Thomas Hayes, uses various biophysical techniques to explore the high-resolution structure of biological macromolecules and cell organelles, a research effort which provides basic knowledge essential for our understanding of new methods of energy production and the possible effects of energy-related pollutants on living systems. Structural information is gathered from many sources utilizing several biophysical approaches. High-resolution electron microscopy, spectroscopic techniques, ultracentrifugal analysis, and optical activity measurements are among the tools employed by investigators working within this group.

Contributions come from chemical biophysics, relating to electron transfer and molecular states. Other facts come from a better understanding of the basic genetics of yeast cells. Additional information is derived from the application of low-temperature specimen preparation studies. The synthesis of findings from all of these various structural biophysical studies enables us to develop a knowledge of basic biological structure in its broadest sense. This basic knowledge is a necessary component in the research effort to find ways of producing more energy. It is also important for our understanding of the vulnerable points in our biological system and in our search to develop methods for early detection of pollutant effects.

In an effort to understand the basic mechanism of energy production, one investigator is studying plant systems which convert light energy into other forms of energy that are stored for future use. The powerful biophysical technique of electron paramagnetic resonance (EPR) spectroscopy is used to study basic characteristics of photosynthesis in plants. The increased knowledge concerning the energy-transforming properties of plant systems may lead to new insights in our search for applied energy systems.

Fly ash, the particulate effluent from smoke stacks of coal-burning power plants, contains particles ranging in size from submicrometer to 100 micrometers in diameter. The biological effect of such particulate contaminates occurs at the cellular level. Investigators are using scanning electron microscopy (SEM) techniques to measure the chemical elemental composition of individual fly ash particles at the site of their damaging action in tissues. This single-particle, single-cell analysis is important, since damage to even a single cell is significant in assessing the possible health effects of fly ash. SEM studies of particle morphology, frequency of occurrence of particles with detectable amounts of various elements, and the elemental ratios of elements in individual particles are providing unique information required for an accurate evaluation of fly ash toxicity.

By utilizing the special low-temperature SEM facility at Donner Laboratory, investigators can analyze large areas of frozen-hydrated biological samples directly. Because the sample itself is present, instead of only a replica of the surface, chemical elemental analysis by electron microbeam techniques is possible. Furthermore, sequential fracture planes can be examined in the same specimen without destroying the relationships between these planes. The important advantages of this direct frozen-hydrated SEM technique will be especially valuable in studying complex tissue systems, such as investigating the effect of environmental pollutants on the cell membranes of the lung.

The basic work in yeast genetics continues, including genetic mapping and studies of genetic recombination, mutagenesis, and radiation-sensitive strains. Studies of the DNA repair mechanism continue, with increased understanding of the control mechanism operating in DNA replication, repair, and recombination. One investigator has developed a method for forming thin, platelet-like crystals of DNA which are ideally suited for study by electron diffraction and electron microscopy, thus making possible the use of single crystal diffraction methods for determining the DNA structure.

Another investigator studied the optical activity of DNA aggregates and developed a novel method for determining the circular dichroism of systems whose CD (circular dichroism) spectra contain contributions from CD differential scattering. The technique can detect light over 4 steradians of acceptance angle and thus, for the first time, a complete correction for scattering is possible. The CD difference spectra, obtained from the scattering corrections and showing the contributions to different sections of the scattering envelope, contain information about the tertiary structure of the particle studied.

The objectives of the lipoprotein group are the development and refinement of techniques for the measurement and characterization of lipoproteins and the investigation of the function of lipoproteins

in the body, in both health and disease. Lipoprotein patterns present a very sensitive system that can be well monitored. Therefore, investigators are looking for lipoprotein changes that occur in the early stages of pollutant exposure, since this method could provide a very sensitive indicator of possible toxic response.

Another group of investigators focuses on the effect of radiation and pollutants on mammalian cells. They continue their study of mutagenic, carcinogenic, and teratogenic effects of environmental pollutants and other agents by making quantitative observations on the growth of mammalian cells in culture. Such studies help identify those agents that pose a health hazard, determine the level of exposure at which the hazard is first detectable, and explore the mechanism by which the cells are damaged.

The highlights of effort during the past year in these and other areas of investigational interest are presented in the following papers.

Electron Microscopic Studies

FLY ASH PARTICLE CHEMISTRY AND LUNG CELL EXPOSURE

Thomas L. Hayes, S. Jacob Bastacky, Clifford E. Lai, and Gerald L. Fisher*

Fly ash, the particulate effluent from the smoke stacks of coal-burning power plants, contains particles ranging in size from submicrometer to 100 micrometers in diameter. The overall composition of a particular fly ash sample depends on the method of combustion and the source of the coal, but heterogeneity of the materials precludes assumptions of a uniform distribution of elements among the particles. Rather, the particles vary considerably from particle to particle with respect to chemical elemental composition.

The biological effect of particulate contaminates such as fly ash occurs at the cellular level. While certain of the biological effects are only important when large numbers of cells are affected, other effects (e.g., carcinogenesis) are probably initiated by changes in a single cell or small group of cells. During phagocytosis of inhaled pollutant particles, the lung cell ingesting the fly ash interacts with only a few of the particles. The high degree of heterogeneity among the individual particles results in a distribution of toxic elemental components which may be very wide, with some cells receiving no particles containing a significant amount of a particular element, while other cells are subjected to a very high exposure to that element.

We have applied microanalytical scanning-electron-microscope techniques to determine the elemental composition and particle morphology of individual coal fly ash particles, and have used this information to estimate exposure for individual cells. The scanning-electron-microscope system used for these analyses includes a digital scan generator, multicolor mapping system, beam stop and light pen, beam locater, and the computer analysis system for peak-to-background ratio evaluations. Test particles of known composition were utilized to calibrate the system.

Fly ash particles selected ranged in size from approximately 20 micrometers down to submicron diameters. The particles were classified according to light-microscope characteristics, scanning-electron-microscope morphology, and elemental composition as determined by characteristic x-ray analysis. A field of fly ash particles is shown in Figure 1. Numerous spherical, glassy particles and an occasional amorphous particle are present. A higher magnification micrograph of a particle rich in car-

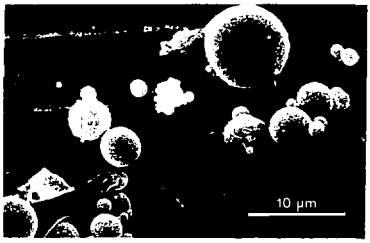

Figure 1. Fly ash particles from coal combustion. Scanning electron micrograph. Marker shows 10μm. (Magnification = 2,000×) XBB 780-13869

*Radiobiology Laboratory, University of California Davis.

bon is shown in Figure 2, and the fine structure of the surface of individual spherical particles is demonstrated in Figures 3 and 4. The rough and chemically active surface of such microparticles offers the site for adsorption and concentration of many of the atmospheric trace elements.

Individual-particle elemental chemistry was determined using a scanning electron microscope equipped with energy dispersive x-ray analysis. Standard operation at 20 kV and a specimen current of approximately 3×10^{-11} A allowed good imaging and adequate x-ray analysis. Heterogeneity among the particles with respect to elemental composition was evident in all samples studied. The spectra of two particles showing widely different chemical composition is shown in Figure 5. The computer printout for these particles listing elemental content of 12 elements is shown in Table 1. The segregation of chemical elements into specific particles of fly ash results in exposures of individual cells that ranges from essentially zero to values very much higher than the exposure estimated from the average, overall elemental composition as determined by multi-particle averaging techniques such as neutron activation analysis.

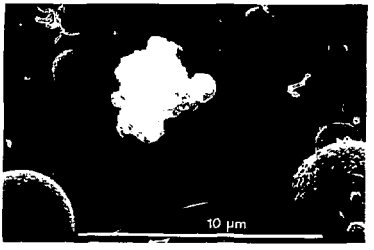

Figure 2. Carbonaceous particle in fly ash sample. SEM marker shows 10μm. XBB 780-13866
(Magnification = 5,000×)

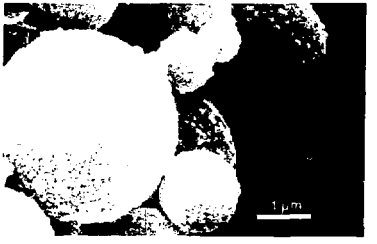

Figure 3. Surface structure of fly ash micro-spheres. SEM marker shows 1 μm. XBB 780-13875
(Magnification = 11,000×)

Figure 4. High magnification scanning electron micrograph of surface of fly ash particles. Marker shows 1μm. XBB 780-13879
(Magnification = 17,000×)

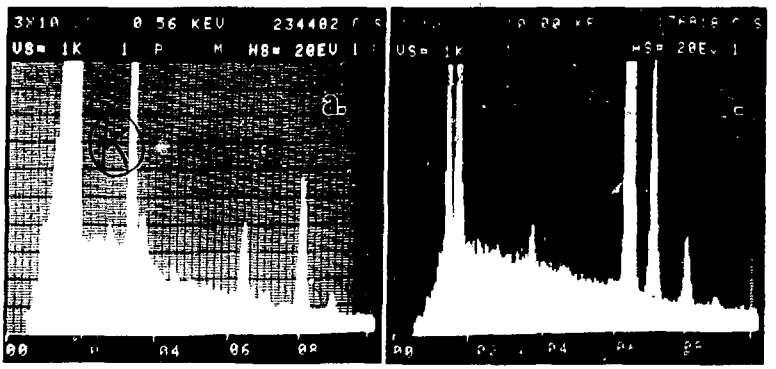

Figure 5. Characteristic x-ray spectra of two individual fly ash particles. (a.) Particle rich in potassium. (b) Particle rich in iron.
(a) XBB 796–7629
(b) XBB 796–7628

Table 1. Computer analysis of the characteristic x-ray spectra shown in Figure 5 indicates large variation in chemical element composition that is possible among individual particles of fly ash.

Elmt:	By diff.	Stoich.	Norm.	Direct (ratio bond)
		Particle number K M2.1B		
Na	4.13	4.37	5.04	4.11
Mg	0.72	0.77	0.88	0.72
Al	13.11	13.86	15.99	13.04
Si	19.44	20.57	23.73	19.34
P	0.16	0.17	0.20	0.16
S	0.00	0.00	0.00	0.00
Cl	0.00	0.00	0.00	0.00
K	3.93	4.16	4.80	3.91
Ca	0.41	0.44	0.50	0.41
Ti	0.34	0.36	0.42	0.34
Mn	0.00	0.00	0.00	0.00
Fe	1.79	1.89	2.18	1.78
		Particle number L RI.5		
Na	9.72	5.02	3.67	4.18
Mg	0.69	0.36	0.26	0.30
Al	9.46	4.88	3.57	4.06
Si	9.68	5.00	3.66	4.16
P	0.00	0.00	0.00	0.00
S	0.00	0.00	0.00	0.00
Cl	0.00	0.00	0.00	0.00
K	0.00	0.00	0.00	0.00
Ca	1.18	0.61	0.45	0.51
Ti	0.00	0.00	0.00	0.00
Mn	0.00	0.00	0.00	0.00
Fe	146.97	75.87	55.53	63.15

The individual cells of the lung that are associated with protection against particulate air pollutants fall into two general categories. In the larger airways the epithelium consists of cilliated cells which move a mucous coating up and out of the lung. Such cilliated cells (Fig. 6) can interact with the individual particles of fly ash and can be damaged if such particles contain relatively high concentrations of toxic elements. Recent sutdies have shown that serum extracts of fly ash particles exhibit mutagenic activity, and any soluble components of the particles may reach relatively deep structures within the cell or even be transported to underlying cell layers. The long, columnar cell body lying beneath the tufts of cilia is seen in the fractured specimen shown in Figure 7.

If the particle of fly ash penetrates to the very deep lung tissue made up of the individual air sacks or alveoli, the surface layer of cilliated cells which protect the larger airways is no longer present. The intricate structure of pores, septa, and aveolar openings (Fig. 8) is protected by the pulmonary macrophage phagocyte cell. Transport of fly ash particles by the pulmonary macrophage can result in deposition of such particles in other areas of the lung where actively dividing cells are located.

The alveolar macrophage is known to be sensitive to toxic trace elements. If it is true that such trace elements are associated with and concentrated in particles of specific matrix element composition, the individual particle concentration of these toxic trace elements can be estimated from measurements of the matrix element with which they associate. Particle morphology, frequency of occurrence of particles with detectable amounts of various elements, and elemental ratios of elements in individual particles provide unique information necessary for an accurate evaluation of fly ash toxicity.

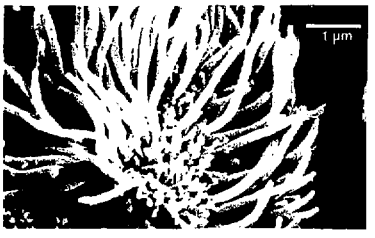

Figure 6. Ciliated cell from the larger airway of the lung. Marker shows 1μm. *XBB 771-399*
(Magnification = 11,000×)

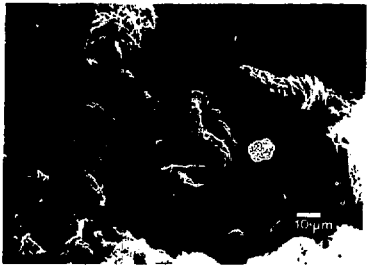

Figure 7. Columnar cell bodies with tufts of cilia are seen in fractured lining of airway. SEM marker shows 10μm.
XBB 780-14764
(Magnification = 5,000×)

Figure 8. Alveoli surfaces deep within the lung. No ciliated cells are present at this level. SEM marker shows 10μm.
XBB 780-14765
(Magnification = 7,700×)

LOW-TEMPERATURE SCANNING ELECTRON MICROSCOPY OF BIOLOGICAL MATERIALS HELD IN THE FROZEN-HYDRATED STATE

Thomas L. Hayes, James B. Pawley*, Gregory R. Hook, and Clifford E. Lai

Fracture surfaces of frozen biological material, which are usually studied only by replica techniques, may now be observed directly in the frozen, hydrated state utilizing the special low-temperature, scanning-electron-microscope facility at Donner Laboratory. The freeze-fracture replica technique, which led to the development of these new electron microscope methods, had developed into a standard tool of biological electron microscopy which was particularly useful for the study of membrane surfaces.

Although permitting high-resolution (2.5 nm) study of replicated specimens, the freeze-fracture replica technique always had certain technical limitations: 1) The carbon and platinum replicas are extremely fragile, and much care and patience are required to prepare them for electron microscopic observation. This is particularly true when large areas of complex tissue such as lung tissue must be replicated. 2) The carbon and platinum replica, despite its very real appearance, is not the actual sample. The sample itself has been completely destroyed in preparing the replica; it cannot be subjected to chemical elemental analysis by electron beam techniques, nor can the investigator monitor the fracture process and make subsequent fractures of the same sample.

The replication step can be completely eliminated, and the limitations mentioned above greatly reduced, if the freeze-fracture surface is studied directly in the scanning electron microscope. In this way, large fracture surfaces can be viewed, and the sample itself is present for x-ray analysis. Second or third fracture planes using the same specimen can be examined.

Following the lead of early investigators using the low-temperature electron microscope, we have used the yeast *Saccharomyces cerevisiae* as our first sample for study utilizing direct observation in the frozen-hydrated state. Although freeze-fracture scanning electron microscopy (SEM) will be applied next to the study of complex tissue systems such as lung, we first examined the yeast cell because the structure and possible artifact of the freezing process have been well described in this system.

*Now at High Voltage Electron Microscope Facility, University of Wisconsin, Madison, Wisconsin.

Cells from a 24-hour culture were fixed in gluteraldehyde for 30 minutes, and then rinsed and placed in 30% glycerol for 24 hours for cryoprotection during the freezing step. The frozen sample was carried through all of the preparative steps associated with freeze fracture and coating in the chamber attached directly to the scanning electron microscope. This method provides for the specimen stub temperature to be below −170°C, and in the vacuum environment, during all of these procedures.

Figure 1 shows the yeast cells after cryofracture and viewed directly in the scanning electron microscope at temperature of −170°C. It is well known that such cryofracture of ice produces a surface where the cell membrane splits down the middle to reveal the two interior surfaces of the membrane. The surface which is attached to the protoplasm of the cell has been designated the P-face, and the face that is attached to the half of the membrane facing the environment is designated the E-face. In the yeast cell, invaginations into the cell membrane are seen as indentations in the P-face and as ridges in the E-face. Both types of inner-membrane surface structures can be seen in Figure 1. A higher-magnification view of the E-face is shown in Figure 2. Although the characteristic 40 to 45 nm ridges on the E-face are readily visible, we have not yet been able to visualize the intramembrane particles that are known from high-resolution TEM (transmission electron microscopy) replica investigations.

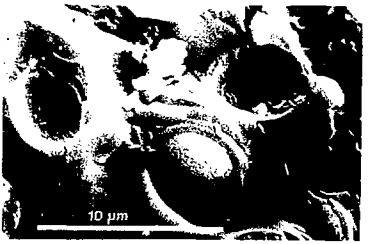

Figure 1. Fractured yeast cells viewed directly in the frozen-hydrated state (−170°C). Both interior surfaces of the membrane produced by cryofracture are shown. Scanning electron micrograph. Marker shows 10μm.
(Magnification = 4,000×) *XBB 787-8437*

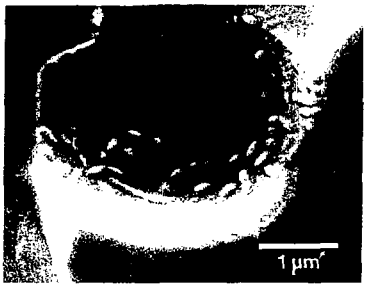

Figure 2. Split membrane surface (E-face) of yeast cell showing characteristic ridges. SEM at −170°C. Marker shows 1μm. *XBB 787-8432*
(Magnification = 17,000×)

Direct viewing of the frozen-hydrated surface permits high-angle intersection of the planes of the fracture to be represented without destroying the relationships between these planes. In Figure 3, a 90° bend in the fracture plane can be visualized, whereas such an acute angle between adjacent planes would make replication of this field extremely difficult. Replicas in general are quite fragile and tend to break up into small pieces, particularly along lines of intersection of the planes of fracture.

Figure 3. Direct viewing of intersecting fracture planes in frozen-hydrated yeast specimen. Three dimensional information would be very difficult to obtain by standard replica technique. SEM at −170°C. Marker shows 1μm.
XBB 787-8430
(Magnification = 7,000×)

Etching (by radiant heating and/or by conductive heating of the entire tissue block) can be carried out to reveal underlying tissue components. In Figure 4 the yeast sample has been etched to a depth where the entire yeast cell has emerged from the ice field.

If the frozen surface exhibits very large excursions in depth and a complicated, intricate three-dimensional structure, production of a replica is extremely difficult. Figure 5 shows a set of thin needle-like crystals (probably ice growth) associated only with the P-face, and not the E-face, of the cells. This structure (Fig. 6) is important in understanding the effects of the underlying cell protoplasm on possible ice-crystal growth; such thin, needle-like crystals would be very difficult to replicate and study by the conventional freeze-etch technique.

Observation of the frozen-hydrated surface directly will permit the application of electron microbeam techniques for the analysis of elemental composition of surface particles. Figure 7 shows the surface of the common plant, *Pelargonium domesticum,* following exposure to fly ash (a common pollutant particle resulting from coal combustion). The leaf can be quick-frozen and maintained in the frozen state while scanning electron microscopy and x-ray analysis for elemental composition are carried out. Figure 8 shows a higher-magnification image of the particles on the frozen-hydrated surface.

Results to date indicate that large areas of frozen-hydrated biological samples can be analyzed by scanning electron microscopy without replication.

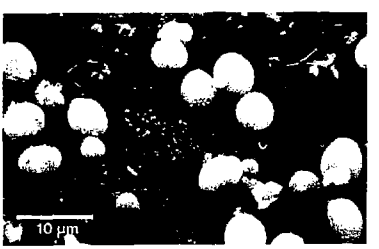

Figure 4. Sublimation of ice matrix can be carried out in the SEM. Deep-etched yeast sample shows entire cells emerging from the ice. SEM at −170°C. Marker shows 10μm. *XBB 787-8431*
(Magnification = 1,500×)

Because the sample itself is present (rather than only a replica of the surface), sequential fracture planes are available and chemical elemental analysis by electron microbeam techniques is also possible. The reduction in preparative artifacts, the integrity of relationships between large parts of the complex tissue, and the availability of the sample for chemical analysis are important advantages of this direct frozen-hydrated SEM technique.

Figure 5. Needle-like crystals develop on the P-face but not the E-face of the split membrane of the yeast cell. SEM at −170°C. Marker shows 1µm. *XBB 787–8438*

(Magnification = 8,500×)

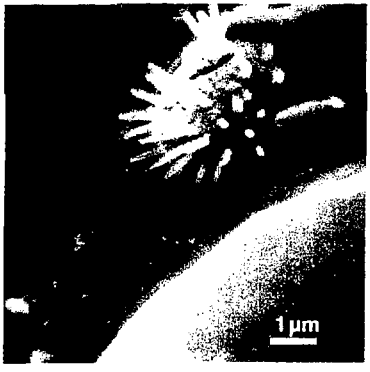

Figure 6. Long, needle-like crystals are shown on the yeast membrane P-face. Microstructures of this depth and intricacy are very difficult to study by surface replication techniques and require direct microscopy in the frozen-hydrated state. SEM at −170°C. Marker shows 1µm.

XBB 787-8440

(Magnification = 9,500×)

Figure 7. Micro-hairs and gland structures on the leaf of the common plant Pelargonium domesticum. Exposure to fly ash has resulted in clusters of particles on the surface. Marker shows 100µm. *XBB 778–7652*

(Magnification = 74×)

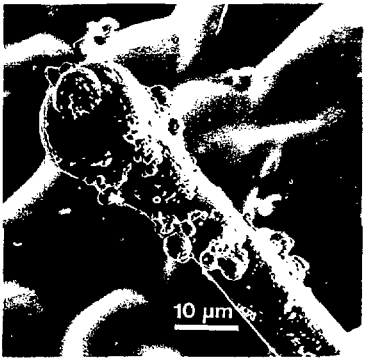

Figure 8. Particles of fly ash are shown adhering to the gland structure on Pelargonium leaf surface. Specimen viewed directly following quick freezing. No preparative fixation or drying steps were needed, and the number and distribution of pollutant particles could be maintained. Marker shows 10µm. *XBB 778–7643*

(Magnification = 1,350×)

THE ELECTRON UTILIZATION EFFICIENCY IN SCANNING-TRANSMISSION ELECTRON MICROSCOPY (STEM) AND CONVENTIONAL-TRANSMISSION ELECTRON MICROSCOPY (CTEM)

Robert M. Glaeser

The electron wave function at the detector plane of the STEM is, under normal conditions (far field limit and weak scattering approximation), the Fourier transform of the projected potential convoluted with the Fourier transform of the incident wave function. For crystalline objects, the wave function at the detector plane is thus a regular array of discs, which may partially overlap with each other, depending upon the unit cell dimensions and the incident probe size. The overlapping portions of the discs will show constructive and destructive interference, depending upon the probe position and the relative (crystallographic) phases of the respective diffraction spots.

The collection efficiency of the STEM is very high. However, only a fraction of the diffracted electrons (i.e., those in the overlapping regions) are utilized to produce structural information. In the case of crystalline biological specimens, the diffraction pattern rarely extends beyond ~2.5 Å resolution, and therefore the majority of the diffracted electrons fall into the bright-field cone of a high-resolution STEM. A larger probe-size will permit a greater fraction of diffracted beams to fall outside of the bright-field cone, but the use of a larger probe size reduces the area of overlap of the diffraction discs, and thereby reduces the utilization efficiency. In either case, the utilization efficiency is much less than the collection efficiency.

In CTEM, on the other hand, the utilization efficiency is equal to the collection efficiency, apart from losses in efficiency due to the contrast transfer function. If the first zero in the transfer function falls beyond (1/2.5Å), the CTEM will have nearly perfect utilization efficiency with respect to the periodic structural information of most biological materials.

I am pleased to acknowledge the collaboration of B.K. Jap in this research project.

MORPHOLOGICAL MODEL OF THE SURFACE-LAYER ARRAY IN *SPIRILLUM SERPENS*

Robert M. Glaeser

The outer membrane of *Spirillum serpens*, strain VHA, possesses a surface-layer protein which forms a two-dimensional, hexagonally ordered array. The center-to-center distance in the array is ~145 Å. The array appears to be composed of a single protein of molecular weight ~140,000. The surface-layer protein is operationally a "peripheral" membrane protein, in that it is removed by treatment in 1.5*M* guanidine HCl. Murray has shown that reconstitution of the solubilized protein (as ordered arrays attached to the outer membrane material) requires Ca^{++}.

A morphological model of the surface-layer protein has been developed on the basis of (1) computer-processed images of frozen-hydrated specimens, (2) side views of frozen-hydrated specimens and negatively stained specimens, and (3) a partial analysis of tubular ("helical") forms of the surface-layer array. The model is based upon ~20 Å resolution data, and clearly shows the regions of protein-to-protein contact between the morphological subunits. The morphological unit is a hollow cylinder with six spokes at the outer end, and looks very similar to the surface-layer structures ("mushrooms") on *Micrococcus radiodurans*.

Recent work has led to the isolation of very large sheets of the surface-layer protein from *S. serpens*, which should facilitate the task of getting a higher-resolution model of the structure. Preliminary work on the surface-layer lattice of *Caulobacter* will also be presented. This structure shows some similarities to the *S. serpens* material, but it appears to be a considerably more complicated and very delicate structure, which may involve two or more proteins in its composition.

I wish to acknowledge the participation of D. Grano in the image processing work. W. Chiu and K. Taylor have done most of the electron microscopy. W. Wu is continuing the work on *S. serpens*, while the *Caulobacter* work is a collaboration with J. Smit.

DNA and Genetic Studies

THE OPTICAL ACTIVITY OF DNA AGGREGATES

Marcos F. Maestre and Charles Reich

During the past year, a novel method was developed for determining the circular dichroism (CD) of systems whose CD spectra contain contributions from CD differential scattering. The technique, as shown in Figure 1, can detect light over 4π steradians of acceptance angle and thus, for the first time, a complete correction for scattering is possible. These methods were applied to DNAs and poly[d(A-C)•d(G-T)] particles in 80% ethanol (ETOH). From the results obtained, the former are proposed to have an "A"-type secondary structure. This is significant in view of proposals in the literature concerning the structure of DNA during transcription. The polynucleotide particles are shown to exhibit behavior similar to that of cholesteric liquid crystals. The CD difference spectra, obtained from the scattering corrections and showing the contributions to different sections of the scattering envelope, contain information about the tertiary structure of the particles studied.

Moreover, the novel techniques—which include Fluorscat curettes, fluorescence-detected circular dichroism (FDCD) methods, back-scattering capturing devices, and beam-mounted goniometer detectors—were used to study the circular dichroism of DNA films with twisted structures, DNA-polylysine complexes, and condensed DNA aggregates in ethanolic buffers of defined salt concentrations.

The results of these measurements were: DNA films can be made to have very large ellipticities or CDs (~ ± 500) at sharp, specific wavelengths. The sign of these ellipticities is related to the handedness of the twists: right-handed twist gives large positive rotations, left-handed gives negative rotations. The DNA films show nodal angles at which the interaction with light is minimal. The scattering patterns of both films, DNA-polylysine particles, and DNA-ETOH condensates show that the main interaction is light scattering produced by a resonance phenomenon similar to that produced in cholesteric liquid crystals and twisted nematic liquid crystals. From these results we propose that the so-called psi-type CD spectra are a manifestation of a side-by-side packing of DNA molecules with a long-range twisting order whose helical parameters match the helical parameter of circularly polarized light at specific resonance or critical wave lengths. A model is depicted in Figure 2. Application of the Bragg Law for cholestric liquid crystals gives the periodicity of the long-range ordered structure.

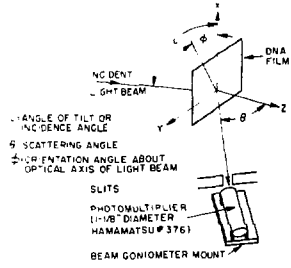

FIG. 1a

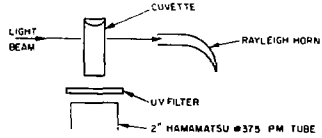

FDCD DEVICE

FIG. 1b

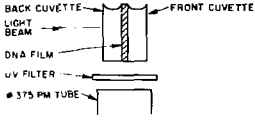

FDCD BACK REFLECTION DEVICE

FIG. 1c

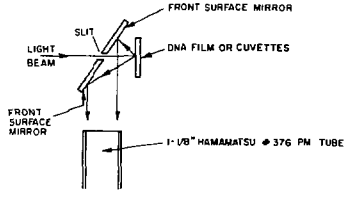

BACK REFLECTION MIRROR DEVICE

FIG. 1d

Figure 1. Schematics of the differing techniques and devices used in the measurement of the CD scattering components. All these devices were used in a modified Cary 60-Dichrograph.
XBL 7810–11721

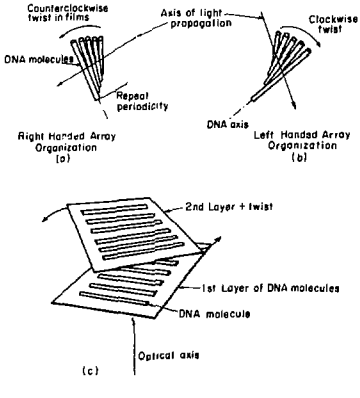

Figure 2. Proposed model of DNA packing in films and aggregates. Figures 2(a) and 2(b) give the sense imposed upon the film by mechanical twisting. 2(c) represents the actual interpretation given to twisted nematic on cholesteric liquid crystals as applied to the DNA fibers in a twisted DNA film.
XBL 7811–3693

DNA REPAIR

Junko Hosoda

Helix-destabilizing protein (HDP) of bacteriophage T4 not only is essential for DNA replication, repair, and recombination, but also controls activities of other enzymes (proteins) involved in these processes. Therefore, we intend to gain a better understanding of the control mechanisms operating in these three processes through studying the structures and functions of this HDP.

Based on our previous observations, we proposed that T4 HDP has two protruded regions, A and B, which control activities (of the HDP itself as well as other proteins) through protein-protein interactions. A-region is highly acidic, at the carboxy terminal, and 55 to 60 amino-acid residues long. B is basic, at the NH_2 terminal, and 16 to 21 amino-acid residues long.

During the current research period, we examined (with the aid and cooperation of R.L. Burke and B.M. Alberts at University of California at San Francisco Medical School) activity of a HDP molecule which lost A-region [we call it *I or *I(−A)] in an *in vitro* T4 DNA replication system.

This system is made of seven purified, T4 gene products. Two of the products (gp41 and gp61) are related to RNA-primer formation; five [gp32, 43 (DNA polymerase), 44, 45, and 62—called the five-protein system] carry out DNA chain elongation in both directions. Leading-strand synthesis is in the direction of replication fork movement, and lagging-strand synthesis—backward synthesis—is started with RNA primer. In the complete seven-protein system, 41–61 makes primer and interacts with the five-protein system to accelerate the rate of leading-strand synthesis two- to three-fold. The seven-protein system replicates DNA at a rate and with fidelity comparable to that *in vivo*.

The pathways from a variety of template DNAs are summarized in Figure 1. Reactions marked with "X" are inhibited in the *I-substituted systems. They are the reactions related to RNA-primer formation (step a-1) and the use of RNA as a primer (step a-2) of the DNA chain. Once a stable DNA primer is given, the *I-system can synthesize both leading strands (steps 1-c, 2-c, and 3-c) and lagging strands (steps 1-b and 2-b). Synthesis rates and protein component requirements differ for the intact and the *I-substituted system.

For instance, lagging-strand synthesis with DNA primer (1-b and 2-b) can be done by polymerase alone—but addition of gp32, under certain conditions, accelerates the rate. Addition of *I completely inhibits this reaction. This incompatibility of polymerase and *I may be related to loss of affinity for each other. The *I + polymerase mixture does become active when three other proteins (44/62 + 45) are present. The five-protein system with *I substitution is always more active than the normal five-protein system in the temperature range 25 to 30°. These data indicate that removal of A does not inhibit formation of the five-protein complex or its activity, and that the relationship between polymerase and gp32 is different within than outside of the replication complex. Addition of 41 + 61 to a *I-substituted system did not accelerate the rate of leading-strand synthesis, as it did with the intact (gp32) system.

Gp61, polymerase, and gp32 are DNA-binding proteins; of the three, gp32 binds the strongest. However, gp32 has to release DNA when RNA primer is made and when DNA polymerase elongates the DNA chain. Our present interpretation of the *in vitro* replication data is that 41 + 61 and polymerase interact with gp32 to induce conformational change in A-region. Because of that conformational change, the negative charges in A-region are located in a position that leads to release of the DNA by gp32.

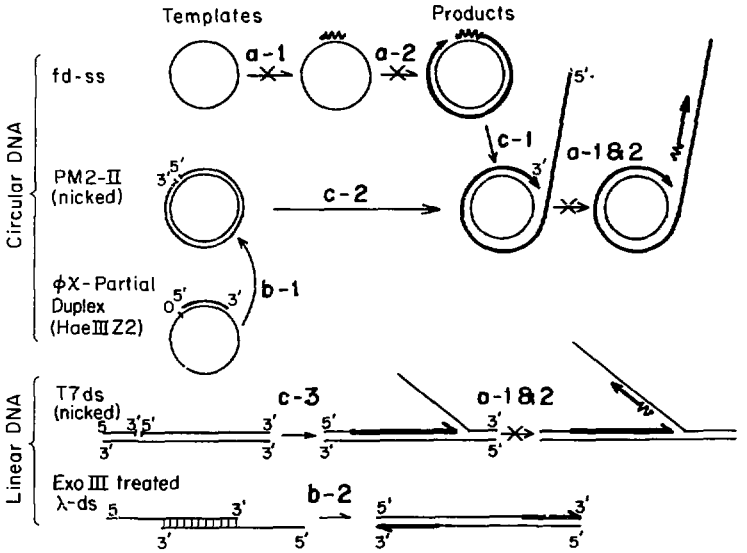

*Figure 1. Activity of *I-substituted in vitro replication system.* XBL 795-1482

CRYSTALLIZATION OF DNA FOR ELECTRON DIFFRACTION STUDIES

Kenneth H. Downing

The double-helical model for the structure of DNA has been widely accepted since its introduction by Watson and Crick. The model has been found to be consistent with a wide range of physical and biochemical data. The basic parameters of the structure were derived from rather limited x-ray diffraction data, and extensively refined using stereochemical constraints. This relatively indirect structural determination has left the double helix open to sporadic criticism. For example, models have recently been proposed in which the two antiparallel DNA strands are arranged in a series of helical segments with alternating handedness, rather than in one continuous helix. These new models have at least a great aesthetic appeal, as they reduce the complications involved in separating the two strands during replication and transcription. They may be compatible with virtually all of the physical data as well.

Determination of the structure of DNA using more direct methods would be clearly desirable, especially by single-crystal diffraction methods. Single crystals of DNA, except for very short oligonucleotides, have not been produced large enough for x-ray work. However, we have produced crystals ideally suited for study by electron diffraction and electron microscopy, and have obtained preliminary electron-diffraction patterns from single crystals.

Structure determination using thin, two-dimensional crystals, by electron diffraction and microscopy, has recently been applied with success to some proteins, for example the bacteriorhodopsin of the purple membrane. Not only can diffraction data be obtained from the crystals, but an image

can be recorded at an electron dose low enough to avoid severe radiation damage to the crystal. While this image is in general statistically noisy, spatial averaging by computer yields the phase information lacking in x-ray crystallography, vastly simplifying the data interpretation.

Thin, platelet-like crystals of DNA can be formed when a solution of sonicated DNA, containing just enough ethanol to cause precipitation of the DNA, is heated, redissolving the DNA, and slowly cooled to room temperature. Examples of crystals formed by this procedure are shown in Figure 1. There is an obvious variability in size and morphology of the crystals, though all show the six-fold symmetry indicating that the DNA strands are aligned perpendicular to the broad faces of the crystals. X-ray diffraction of these crystals has confirmed the impression that there are at least two types of crystals, i.e., two slightly different strand separation distances.

Gel electrophoresis shows that after extensive sonication, the DNA has been sheared to short segments of nearly uniform size, around 200 base pairs. A successive ethanol-fractionation procedure (as used in generating the different fractions for Figure 1a-e from one initial sonicate) has almost no effect on the distribution of strand lengths, although the resultant fractions are different in their melting curves, indicating that some separation by base composition has occurred.

Figure 1 gives the clear impression that some of the crystals are much thinner than others. Since all DNA strands are about the same length, it appears that in some crystals the strands are folded back and forth through the crystal, while in others the strands run straight through, giving the crystal a thickness equal to the length of the DNA strand. This folding may have important implications for the packaging of DNA *in vivo*. Characterization of the conditions allowing or enhancing the folding is continuing. This characterization will answer such questions as whether the "snowflake" appearance of some crystals (Fig. 1b) is a result of changes in a characteristic folding length during crystallization, or an effect of base composition. The folding is certainly affected by the rate of cooling during crystallization. More rapid cooling results in smaller, thicker crystals.

Apart from the biological significance, this is important for the electron diffraction work, as the crystals of Figures 1d and 1e would probably be too thick to use with the mathematical approximations involved in the computer processing. Crystals sufficiently thin can be formed under conditions favoring strand folding, or by using shorter DNA strands. For example, crystals have been made with synthetic DNA, the alternating copolymer poly d(AT)•poly d(AT), trimmed to uniform 148 base-pair segments. Further work will involve use of even shorter segments of this DNA.

As a first step toward the crystallographic structure determination, preliminary electron-diffraction patterns have been obtained from single crystals of these DNA preparations. To overcome the sensitivity of the crystals to dehydration, the crystals are examined in the frozen-hydrated state in the cold stage of the electron microscope. Figure 2 is one of the first diffraction patterns. It shows the hexagonal

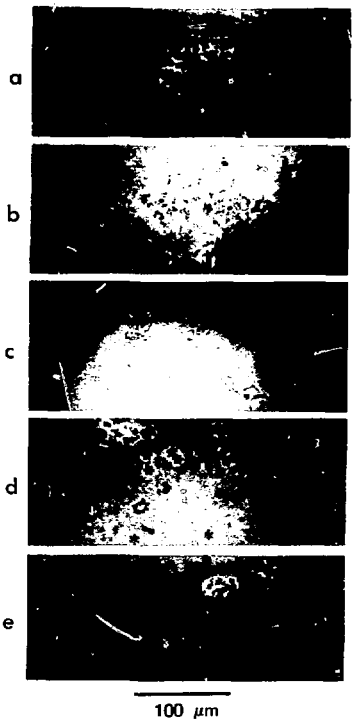

Figure 1. DNA crystals prepared as described in text. Bar = 100μm. *XBB 792-1505*

nature of the strand packing, with a 23.1 Å Bragg spacing. Reflections have been recorded to 5.0 Å spacings. Not only are these the first diffraction patterns (x-ray or electron) from single crystals of highly polymerized DNA, but also they can be obtained with the beam parallel to the DNA-strand axis, the direction least accessible to x-ray diffraction from fibers.

The diffraction patterns illustrate the feasibility of performing a direct structure analysis using electron diffraction and electron microscopy. The data analysis will involve application of computer software which was developed for similar studies of proteins and membranes.

Figure 2. Electron diffraction pattern from a single crystal of sonicated calf thymus DNA, obtained with the beam parallel to the strand axes. XBB 790-14706

GENETIC STUDY ON YEAST *(SACCHAROMYCES CEREVISIAE)*

Robert K. Mortimer

GENETIC MAPPING

Three years ago, I decided to discontinue research on gene mapping, except to provide mapping strains to other investigators and to periodically collate and publish mapping information from various laboratories. The recent research on cloning of yeast genes and the use of cloned genes to effect transformation of yeast strains has forced a re-evaluation of this decision. For example, several groups are trying to clone centromeres, using genes that are closely linked to centromeres as a method of selecting these DNA regions.

Chromosome III has the following gene order in the centromere region: *leu2-cdc10-centromere-SYF2* with distances of 2.5, 0.5, and 0.5 cM, respectively. *cdc10* represents one of the cell-cycle genes and *SUF2* is a frameshift suppressor. The gene *leu2* controls one of the leucine biosynthetic enzymes and has been cloned on the bacterial plasmic colEI. Another gene in this region, *pgkI* (phosphoglycerokinase), has also been cloned. From the available mapping information regarding *pgkI*, it has been provisionally located across the centromere from *leu2*. Several DNA restriction-fragments have been cloned that overlap *leu2* and *pgkI* and, if the provisional location of *leu2* relative to *pgkI* is correct, some of these should contain the centromere of chromosome III. Several crosses are currently being analyzed to map *leu2, pgkI,* and the centromere more precisely. This information will be of considerable value to the investigators working on the clones segments from this region.

We are also in the process of developing a set of haploid strains (7 to 10) that collectively carry 66 genetic markers spaced at approximately 50 map

units over the entire yeast genome. With such a set of strains it should be possible to map a gene with relative ease, because linkage can be easily detected for distances less than 25 map units. These strains should be available within the year.

GENETIC RECOMBINATION

S. Fogel and I have recently completed a detailed study of gene conversion in *Saccharomyces*. Over 23,000 unselected meiotic tetrads derived from 21 hybrids were analyzed. These hybrids were each heterozygous for several (8 to 13) genes, and a total of 221,751 segregations at 30 heterozygous sites were examined. Aberrant segregation frequencies ranged from 0.6% to 18.2% for sites in different locations. For different alleles at the *arg4* locus, conversion frequencies range from 1.6% to 8.3%, an expression of polarity. The percentage of aberrant events associated with post-meiotic segregation (p.m.s.) ranged from 0 to 54%, and this parameter appeared to be primarily a property of the allele. However, for *agr4-16* the p.m.s frequency was strongly dependent on the presence of additional heterozygosity at the locus. If only *arg4-16* was heterozygous, p.m.s. events per totals aberrant events was in the range of 50%. If alleles both proximal and distal to 16 were also heterozygous, this value was only 8%. Intermediate values were seen with either proximal or distal heterozygosity.

These results suggest that the mismatch associated with *16* is a poor signal for repair and that mismatches on either side can provide repair which extends to include *16*. The frequency with which outside marker exchange was associated with conversion ranged from .27 to .74. When these values were corrected for incidental exchanges in the flanking intervals, the corresponding values ranged from .18 to .66. Calculations show that there is sufficient crossing-over associated with gene conversion events to account for all crossing over in yeast—thus, gene conversion is a signal of the basic recombination event.

Our results were considered with respect to the predictions of various molecular models of genetic recombination and were found to be most compatible with models that invoke both asymmetrical and symmetrical stretches of hybrid DNA.

Our current work on this problem is concentrated on *arg4* and involves an examination of strains that have transformed with plasmids which contain this gene. Two stable transformants have been analyzed genetically. In both cases it can be shown, by genetic and colony hybridization procedures, that the plasmid has been integrated in the neighborhood of the normal map-position of this gene. Eventually, I plan to study heterozygous diploids of these integrated plasmids, to determine if conversion at *arg4* is altered by the presence of nonhomologous DNA. Additional stable transformants will be isolated with the hope of finding some that have been integrated at other sites in the genome. These also will be analyzed for genetic recombination. Our earlier work at *arg4* indicated that a region near the distal end of the gene acted as a promoter of recombination events. Study of the transformed strains should help determine if this is the case.

MUTAGENESIS

The nondisjunction strain has been grown in parafluorophenylalanine (pFPA), and than plated on either canavanine medium or on medium containing 1.5-M ethylene glycol. Ambiguous results were obtained using the first approach because canavanine-resistant diploids appeared that still carried the suppressor. This has since been shown to be due to heterozygosity for genes that modify suppressor efficiency. We are currently making crosses to eliminate these genes. However, the hypertonic medium gave very clear results. Nearly all the diploids that grew in this medium had the phenotype expected for loss of both suppressors (canavanine-resistant, *ilv*$^-$, *lys*$^-$, and *ade*$^-$). The frequency of the putative nondisjunctants increased with increasing pFPA exposure. However, genetic analysis of several of the strains that had lost both suppressors failed to yield the centromere-linked lethal expected for a missing chromosome. Our current hypothesis is that strains go from 2n to 2n-1, but because the monosome is less healthy, or because of additional events that double-up, the remaining chromosome (2n - 1 → 2n) is at a selective advantage. We are testing this hypothesis by examining resistant clones at an earlier stage, and by using shorter exposure to the pFPA.

Additional strains that detect mitotic gene-conversion, mitotic crossing-over, and mutation have been constructed and are now being tested with a number of known mutagens.

RADIATION-SENSITIVE STRAINS

We have isolated several new x-ray-sensitive mutants. Many show a temperature-conditional response to x-rays—they are sensitive if incubated at 36° but show a normal response if incubated at 23°, or vice versa. One of these mutant strains showed

a very unusual response when put into crosses. The strain appeared to have diploidized, and so gave good viability only if crossed to diploids. However, the spores from these tetraploids were found also to behave as tetraploids (instead of diploids). Through a number of additional experiments, we have shown that the original strain contains a mutation that causes endoduplication (diploid→tetraploid), and that the expression of this mutation is temperature dependent. This mutation appears to be independent of the x-ray-sensitivity mutation carried by the strain. To our knowledge, this is the first such mutant isolated in yeast and it could prove to be of considerable importance in studies of cell division regulation.

We have completed setting up for O'Farrel 2-D gel analysis and plan to look at several of the *rad* mutants to determine if any can be associated with a specific protein.

Studies on Photosynthesis and Hydrocarbon Production

RESONANCE STUDIES IN PHOTOSYNTHESIS

Alan J. Bearden

Two major problems in green-plant photosynthesis have been the focus of research: the molecular structure and mechanism of the oxygen-evolving (water-splitting) complex, and the structure and mode of operation of each of the two photochemical reaction centers present in plants. Electron paramagnetic resonance (EPR) spectroscopy is particularly advantageous in studies of both these problems, as it permits identification chemically of the reaction participants—provided these participants have unpaired electron spins—together with information about the molecular architecture at the point of operation.

In order to increase the amount of information that EPR spectroscopy can give in these photosynthetic experiments, we have concentrated on a new study of this spectroscopic method with the view of increasing both the sensitivity and the information content of the method, and also to be able to make measurements on a shorter time-scale (down to a fraction of a microsecond). These studies and the subsequent reconstructions have produced a spectrometer capable of measurements at sensitivities approaching twenty to fifty times those previously possible.

One student, K. Rose, has been able to measure spin-lattice relaxation times of paramagnetic entities such as the oxidized reaction-center chlorophyll ($P700^+$) over a temperature range from 4 K to 300 K, using both power-saturation and microwave-power saturation recovery methods. A first result, important to an understanding of Photosystem I reaction-center structure, is that the state of reduction or oxidation of neighboring components such as plastocyanin or the iron-sulfur centers does not produce changes in the spin relaxation kinetics of $P700^+$, indicating that these paramagnetic components lie greater than 5 nm apart in the photosynthetic membrane.

A related study by another graduate student, M. Crowder, and a visiting professor, R. Prince (University of Pennsylvania)—using thin films of oriented chloroplasts—shows that the iron-sulfur centers of Photosystem-I acceptors (Centers A and B) are definitely oriented in the membrane. This result is in contrast to studies in other laboratories.

Studies of the oxygen-evolving complex by similar techniques are not yet unambiguous. We are attempting two things: to study the orientation of EPR Signal II, and to find EPR signatures of the S-states which participate in this important process. Using laser flashes, we are trying to correlate the EPR spectra obtained with either flash number or occupation level of S-states.

Further studies of reaction-center kinetics, using photosynthetic materials enriched in a single photosystem (Photosystem I or Photosystem II) activity and single or double laser flash irradiation, are underway to answer the questions of turnover even at low temperatures (4 to 50 K) in plant systems. In addition we are investigating a method of determining quantum yields at low temperatures, as these yields will ascertain the relative importance of various donor-acceptor processes.

This work includes the efforts of a principal investigator, five graduate students, and a part-time laboratory technician, as well as support from Donner Laboratory support activities. A portion of this research is supported by a grant from the National Science Foundation.

HYDROCARBON BIOSYNTHESIS IN GUAYULE

Thomas E. Bauer

Guayule *(Parthenium argentatum)* is a shrub native to semiarid regions of North America. While the plant's small stature and scruffy appearance (Fig. 1) are unimpressive, the plant's ability to produce hydrocarbons is very impressive. Guayule can produce rubber in amounts up to 20% of its dry weight, and it produces a similar amount of lower molecular-weight hydrocarbon resins which may be useful as substitutes for petroleum in some chemical feedstock applications.

Figure 1. Aerial growth habit of Guayule. (Photographed by A. B. Ledling.) XBB 769-8549

In 1977, the National Academy of Sciences issued a report on guayule which called for its development as a domestic source of national rubber. The report, together with a world-wide shortage of natural rubber and the increasing cost of petroleum-derived synthetic rubber, has spurred guayule development projects in California, Arizona, and Texas.

The rubber produced by guayule is essentially identical to that obtained from the rubber tree *(Hevea brasiliensis)* of Southeast Asia and South America. However, the anatomy of rubber production, and consequently the method of extraction of the rubber, are quite different in the two species. In *Hevea*, the rubber forms in long, thin tubes, called latex vessels, which ring the tree just inside the bark. The rubber is tapped by slashing the bark and collecting the latex "sap" which runs out. In guayule, rubber is formed in individual cells of the stems and roots, and the whole plant is harvested and ground to extract the rubber. Figures 2a and 2b are transmission and scanning electron micrographs of rubber in stem cells of guayule.

Research in the structural biophysics group is contributing to guayule development at both the applied and basic levels. At the applied level, we have contracted with the California State Department of Agriculture to develop a rapid field-assay for the rubber content of guayule plants. Basic research into the mechanisms of rubber biosynthesis has produced evidence of unique properties of guayule's chloroplasts, which may have important implications for the general problem of hydrocarbon production via photosynthesis.

During the last year, we studied the subcellular effects of a recently discovered family of chemicals which significantly increases rubber production in guayule. Figure 3a is an electron micrograph of typical chloroplasts in a palisade cell of guayule leaf before treatment. Within the chloroplasts are small black inclusions, called plastoglobuli, labeled with a "P" in the figure. Figure 3b is an electron micrograph of palisade chloroplasts 13 days after treatment with one of the rubber production-stimulating chemicals. The plastoglobuli, which are partially composed of material derived from the same precursors as rubber, enlarged dramatically as a result of the treatment. The treatment also caused the formation of rubber, labeled with an "R" in the figure, in leaf cells which are normally devoid of rubber.

These results, together with information gained from earlier research, suggest that the chloroplasts of guayule have the unique capacity to directly source hydrocarbon (terpene) precursors. Experiments designed to test this hypothesis are in progress. Confirmation of this chloroplast function will have immediate significance for guayule development and long-term implications for efforts to photosynthetically produce hydrocarbon fuels.

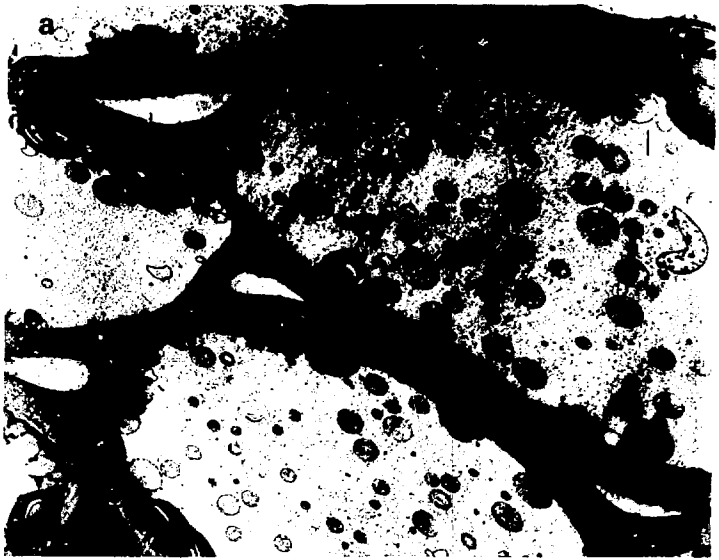

Figure 2. (a) Transmission and (b) scanning electron micrographs of rubber globules in guayule stem cells.
(a) XBB 794–4509
(b) XBB 794–5610 A

Figure 3. Transmission electron micrographs of guayule leaf chloroplasts (a) before and (b) 13 days after the plant was treated with a rubber production stimulant.
(a) XBB 794-5613
(b) XBB 794-5615

LIPOPROTEIN STUDIES

The objectives of this lipoprotein group are the development and refinement of techniques for the measurement and characterization of lipoproteins and the investigation of the function of lipoproteins in the body, both in health and in disease. In the blood, fats (or lipids) are bound to protein, and circulate in the form of complexes known as lipoprotein molecules. Recently, popular concern has turned from one aspect of these molecules—the cholesterol level and deposits on vein and artery walls—to a focus on other aspects as possible indicators of and contributors to cardiovascular disease. The role of lipoproteins in metabolism is far more complex and more important than that, of course, and is only beginning to be understood. Methods for accurately measuring their levels, properties, changes, and effects (to give only a few parameters) are still being worked out.

A special need is establishing norms—which means studying normal subjects and accumulating a sufficiently large representative sample from which to compare, establish, and characterize abnormalities. An additional focus of study is the transport of mutagens (and carcinogens) by serum macromolecules and the relationship of this to pollutant effects in man.

LIPOPROTEIN METHODOLOGY AND BIOMEDICAL APPLICATIONS

Frank T. Lindgren, Mason M-S. Shen, and Ronald M. Krauss

One of our targets has been the development of a fully automated system for a variety of measurements; today our fully computerized microdensitometry facility, with double disc, magnetic tape, CRT keyboard, and hard copier system, is being used in several research programs at Donner Laboratory. A new electron-microscopy particle-sizing technique using a sonic digitizer has been developed, and with this system we have also improved the schlieren film-reading procedure for standard runs of low- and high-density lipoproteins (LDL and HDL). This will also allow a more accurate study of subfractions that have been observed in these lipoprotein classes.

In addition to these highly complex, expensive ways of studying lipoproteins, we have been evaluating, in collaboration with P.D. Wood and S.B. Lewis, simplified methods for quantifying lipoproteins, with comparison to the analytic ultracentrifuge as a standard. These efforts to develop, calibrate, and apply simplified and inexpensive methods for measurement of lipoprotein may provide practical clinical tests for early evaluation of cardiovascular disease risk as well as a way of observing changes in individuals who are undergoing therapy in an attempt to reduce such risk.

Because of the importance in identifying differences among subfractions of the atherogenic LDL class, we have developed a density-gradient preparative ultracentrifugal procedure for isolation of six LDL subclasses, ranging in density from 1.02 to 1.06 g/ml. A typical subfraction is shown in Figures 1a and 1b which demonstrates minimal degradation of the fractions as compared with the original total LDL fraction.

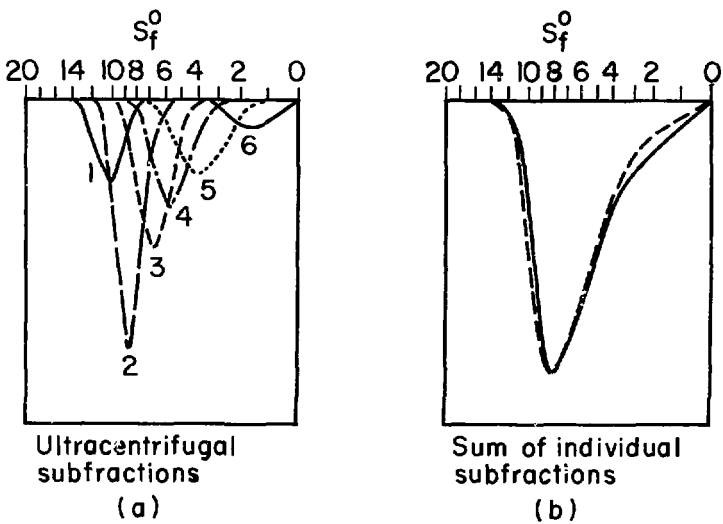

Figure 1. (a) Analytical ultracentrifugal patterns of LDL subfractions from a 24-year-old normal female subject. (b) Normalized summation of analytical ultracentrifugal patterns of LDL subfractions (———) compared with the total LDL pattern (- - - - - -) from the same subject. XBL 795-3460

However, in applying the LDL subfractionation, we have noticed discrepancies in data on composition, particle size, and density as recorded with different methods of measurement, especially in electron microscopy as compared to analytic ultracentrifugation. These discrepancies, studied in detail by M. Shen, suggest that the process of centrifugation may lead to lipoprotein distortion and degradation. Such a possibility is of great importance, since most current work in the field has been based on some type of centrifugal fractionation and/or measurement. Further studies are planned which will help resolve this question.

A number of studies are being continued with outside collaboration. Perhaps of most general interest currently is the longitudinal study with P. Wood of Stanford University on the effects of physical conditioning (specifically, long-distance running) in both males and females. Duration and intensity of physical activity are being correlated with changes in HDL subfraction levels in an effort to discover what level of activity is required for a measurable, and potentially beneficial, change in HDL levels.

INTERRELATIONSHIPS AMONG SUBGROUPS OF SERUM LIPOPROTEINS IN NORMAL SUBJECTS

Ronald M. Krauss

The incidence of coronary events has been shown to be positively associated with low-density lipoprotein (LDL) cholesterol and negatively with high-density lipoprotein (HDL) cholesterol. However, since the major lipoprotein classes are recognized as containing a range of particles of differing composition and density, this project looked for possible definable subgroups within the classes that would have significant intercorrelations and that might have implications for prediction and prevention of coronary disease.

Computer analysis of the results of analytic ultracentrifugation, used to measure serum lipoproteins in a normal population, defined three subgroups of LDL and two subgroups of HDL based on flotation rates. In addition to these measurements, subfractions of LDL have been isolated from serum of normal subjects, and have been characterized by physical and chemical techniques.

The pattern of differences in HDL and LDL subfractions between the sexes was the initial clue to the finding of correlations among the subgroups *within* age and sex categories. Women have lower levels of all subfractions except the larger and less dense HDL (HDL^{2-9}) and LDL (LDL^{7-12}).

These data indicate the possibility that the decrease in HDL (which has been implicated in coronary disease risk) represents a decrease in the HDL^{2-9} subfraction and a concomitant increase in LDL^{0-7} and VLDL. Higher levels of HDL seen in women and runners (in another study being carried on jointly with P. Wood of Stanford University) represent increased HDL^{2-9}, with decreased LDL^{0-7} and VLDL. This raises the possibility that LDL^{0-7} includes LDL subspecies with atherogenic potential that are partly responsible for the coronary risk previously associated with reduced levels of HDL.

STRUCTURE AND FUNCTION OF HIGH DENSITY LIPOPROTEINS

Alex V. Nichols, Patricia J. Bianche, and Elaine L. Gong

The risk of coronary heart disease (CHD) is positively correlated with plasma levels of the cholesterol-rich, low-density lipoproteins, and negatively correlated with plasma levels of high-density lipoproteins (HDL). Our research has been concerned with the structure and function of HDL subclasses, their origin and metabolism, and their interactive properties which might bear on their inverse association with the risk of CHD. For a long time, the HDL class has been considered to consist of two major subclasses, HDL_2 and HDL_3. Early population studies suggested differential contributions by these two subclasses to the inverse relationship with CHD risk.

In the course of studies directed towards a fuller physical-chemical characterization of the major HDL subclasses, D.W. Anderson, working in our labora-

tory, identified three major HDL subclasses by gradient-gel electrophoresis. Two of these were subcomponents of the HDL_2 subclass and were designated HDL_{2b} and HDL_{2a}; the third subclass remained as the previously defined HDL_3 subclass. These observations added considerably to our understanding of the heterogeneity of the HDL class, and provided a framework for the further evaluation of HDL metabolism and of specific HDL subclasses as risk factors in CHD.

In the past period, we evaluated the feasibility of using gradient-gel electrophoresis for both resolution and quantification of HDL subclasses. A much larger and more diverse population subsample was used in this study than in the initial work. Figure 1 shows a representative stained gel after electrophoresis of a plasma d ≤ 1.20 g/ml ultracentrifugal fraction. The three bands corresponding to HDL_{2b}, HDL_{2a}, and HDL_3 are indicated.

Unexpectedly, an additional component, encountered at a migration distance slightly beyond the HDL_3, was frequently observed. We have preliminarily designated this previously unreported subclass as "HDL_4." Bands in the sample application region correspond to very low-density and low-density lipoproteins, while the sharp band beyond the HDL components corresponds to human serum albumin. A densitometric scan of the gel presented above is also shown. The four major HDL peaks are clearly distinguished; diameters based upon those of reference proteins are indicated. In some subjects a minor, fifth peak was detected in the densitometric scans just beyond the "HDL_4' subclass (possibly "HDL_5").

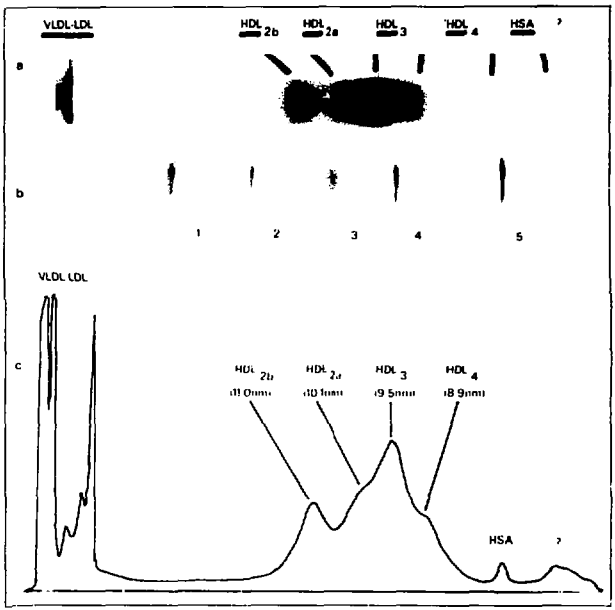

Figure 1. (a) Stained gel, following GGE of a serum d≤1.200 fraction. (b) Stained gel, following GGE of the reference protein mixture: (1) thyroglobulin, (2) apoferritin, (3) catalase, (4) lactate dehydrogenase, and (5) bovine serum albumin. (c) Densitometric scan (GGF pattern) of stained gel in (a) above, showing particle diameters for the four HDL peaks. XBB 798-9868

In certain individuals, the "HDL_4" subclass can be a major contributor to the total mass of the HDL class. Densitometric scans from two subjects, which show a relative elevation in the "HDL_4" subclass, are shown in Figure 2. The analytic ultracentrifugal patterns corresponding to these gradient-gel electrophoretograms are also shown. The analytic ultracentrifugal patterns show little direct evidence of subclasses within the major peak, and would therefore appear to consist almost exclusively of the HDL_3 subclass. In addition, plasma concentrations of the very low-density lipoproteins in subjects with gradient-gel electrophoretograms similar to those shown in Figure 2 were substantially elevated relative to the group's mean level for these lipoproteins.

Calibration of the above HDL subclasses by gradient-gel electrophoresis was explored, and a computer-assisted quantification of the major HDL subclasses in a group of normal subjects was established. High correlation was observed between plasma concentrations of the HDL subclasses determined by gradient gel electrophoresis and by analytic ultracentrifugation. Unlike the other subclasses, which show strong negative correlations with very low-density lipoproteins, the "HDL_4" and "HDL_5" showed strong positive correlations with plasma levels of very low-density lipoproteins. The latter observation suggests a metabolic linkage between these HDL subclasses and the triglyceride-rich, very low-density lipoproteins.

Our observations provide new evidence for the physical-chemical and possibly metabolic heterogeneity of the HDL class, and indicate that gradient-gel electrophoretic analysis may be useful in further investigation of HDL subclass function in health and disease.

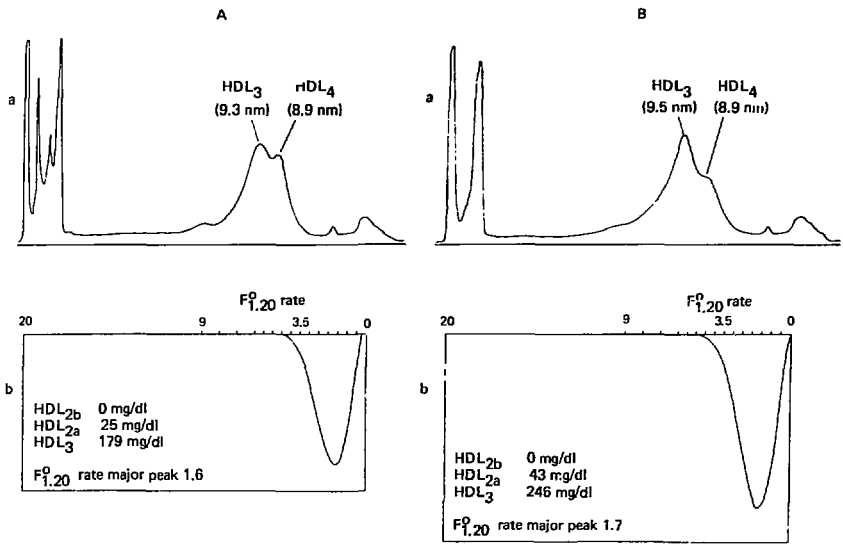

Figure 2. (A) and (B) Patterns from two different subjects, in each case. (a) GGE pattern exhibiting a relatively high level of the "HDL_4" subclass; and (b) ANUC pattern of the total HDL class obtained for the same serum d≤1.200 fraction that gave the GGE pattern in (a).

XBL 798-10819

LIPOPROTEIN TRANSPORT OF MUTAGENS

Helen M. Shu

The function of plasma lipoproteins in the transport of polar (phospholipid) and apolar (triglyceride and cholesteryl ester) lipids and their relationship to atherosclerosis have been subjects of intensive investigation in recent years. However, little attention has been directed toward their role in transporting compounds foreign to the body. In light of the increasing public health concern with carcinogens as well as the suggested role of mutagens in atherogenesis, we have studied the interaction between plasma lipoproteins and the carcinogen, benzo(a)pyrene.

When ^{14}C-benzo(a)pyrene is incubated with human whole blood, the majority of the benzo(a)pyrene is taken up by the lipoproteins, with the low- and very low-density lipoproteins taking up the most and the high-density lipoproteins taking up the least. The distribution of benzo(a)pyrene among the lipoprotein classes correlates with total lipid volume. Details of these findings, as well as a discussion of the potential significance of such benzo(a)pyrene-lipoprotein complexes in cellular uptake of benzo(a)pyrene and in benzo(a)pyrene turnover in humans, are given in reference 1.

Currently we are further characterizing the benzo(a)pyrene-lipoprotein complex by fluorescence spectroscopy. Since benzo(a)pyrene fluoresces, we can probe its location in the lipoprotein particles by quenching its fluorescence with compounds possessing different solubilities. For examples, benzo(a)pyrene in the lipoprotein core will be quenched by the most apolar quenchers, while these quenchers will not affect benzo(a)pyrene in the more polar environment near the lipoprotein surface. We hope to determine whether benzo(a)pyrene location differs in different lipoprotein classes, whether the concentration of benzo(a)pyrene in lipoprotein affects its location, and whether metabolites of benzo(a)pyrene are located in more polar regions of the lipoprotein particles.

REFERENCE

1. Shu, Helen P., and Nichols, Alex V. 1979. Benzo(a)pyrene Uptake by Human Plasma Lipoproteins *in vitro*. *Cancer Research* 39 (4):1224–1230.

CHARACTERIZATION OF FETAL CALF AND NEWBORN CALF SERUM LIPOPROTEINS

Trudy M. Forte and Julia Bell-Quint

Tissue culture studies frequently use 10 to 20% fetal calf serum in the media in order to establish good, viable cell monolayers. To a lesser extent, newborn calf serum is also used in cell culture studies. However, our knowledge of the lipoprotein constituents present in either fetal or newborn calf serum is scanty. To remedy this situation we decided to characterize the physical and chemical properties of fetal and newborn calf lipoproteins.

In addition, we felt that such a study might provide new insights into the metabolism of lipoproteins during development.

Sources of sera used in these investigations included: Gibco frozen fetal-calf serum, fresh fetal-calf serum, Gibco frozen newborn-calf serum, fresh newborn-calf serum (between 1 and 9 days postpartum) and adult-steer serum. Since Gibco frozen serum lipoproteins and fresh serum lipoproteins were similar in their chemical and physical properties, the data were pooled.

The analytical ultracentrifugal distributions of fetal calf, newborn calf and mature steer lipoproteins are shown in Figure 1. These distributions indicate that fetal calf serum contains only S°_{f} 0-20 or low-density lipoproteins (LDL) and $F^{\circ}_{1.20}$ or high-density lipoproteins (HDL). Both HDL and LDL are low in concentration, and the total lipoprotein concentration is only one-fifth that of the mature animal.

Electron microscopy revealed that fetal calf LDL are large (260 Å diameter) and form unusual linear arrays with parallel edges (Fig. 2). Newborn and mature-steer LDL are heterogeneous, spherical particles with considerably smaller mean diameters (190 to 200 Å). Newborn HDL are small, spherical particles approximately 80 Å in diameter (Fig. 3). Since no discoidal HDL particles were noted in the HDL region, we concluded that the fetal liver has an active lecithin:cholesterol acyltransferase enzyme system. This is corroborated by the fact that the cholesteryl ester content of the HDL is exceedingly high.

Fetal calf serum contains no very low-density lipoproteins (VLDL); however, these particles appear after birth when the calf is suckling. Lack of VLDL in the fetal serum, together with the presence of LDL which contain no triglyceride, indicates that the fetal liver synthesizes LDL *de novo*. The independent synthesis of LDL has thus far been difficult to demonstrate in humans or in other animal models.

Apoprotein distributions in the various fetal calf, newborn calf and steer lipoproteins are shown in Figure 4. Fetal calf LDL contains only apoprotein B; this protein in tissue-culture cells binds to B-protein receptor sites on cell membranes, which then triggers LDL internalization. The internalized LDL further regulates cholesterol synthesis by the cells. Fetal calf HDL possesses two major apoprotein bands, one corresponding to apoprotein A-I and the other to apoprotein C-II. The other minor C-protein bands (C-III proteins) are missing. These latter bands appear after birth and are seen in both the VLDL and HDL. These findings suggest that at birth the dietary change from carbohydrates to fats stimulates synthesis of additional lipoproteins and apoproteins. Furthermore, since apoprotein C-III's and VLDL appear simultaneously in the newborn calf, these apoproteins may be required for VLDL synthesis and release by the liver.

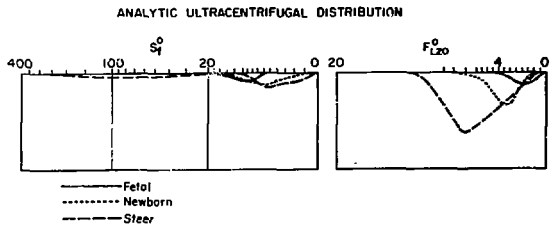

Figure 1. Serum lipoprotein distributions from fetal calf (———), newborn calf (-----), and mature steer (— — —). Flotation interval S_f^0 20 – 400 = VLDL; S_f^0 0 – 20 = LDL; and F^0 0 – 20 = HDL. XBL 794-3372

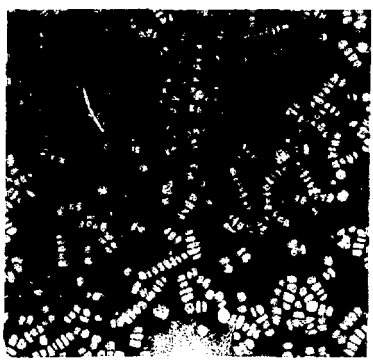

Figure 2. An electron micrograph of negatively stained low-density lipoprotein from fetal calf. They show unusual flattened particles (arrows). Bar marker = 1000 Å. XBB 794-5148

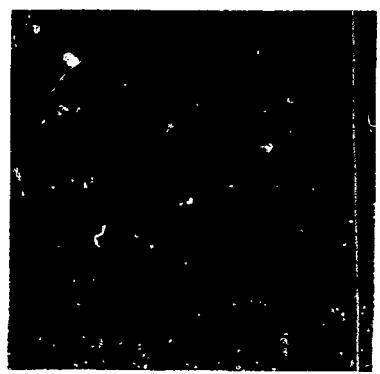

Figure 3. An electron micrograph of negatively stained high-density lipoproteins from fetal calf serum. Bar marker = 1000 Å. XBB 794-5150

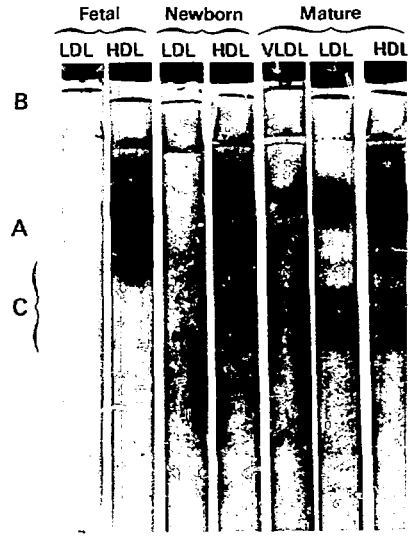

Figure 4. Polyacrylamide gel electrophoresis patterns of tetra-methylurea soluble proteins from fetal calf, newborn calf, and mature steer. Apoprotein-B is precipitated on top of gels from LDL and VLDL. The fetal calf has none of the minor C-protein bands seen in the adult and newborn.
XBB 792-1335

SYNTHESIS AND METABOLISM OF LIPOPROTEINS BY MONOLAYER CULTURES OF RAT HEPATOCYTES

Julia Bell-Quint and Trudy M. Forte

We have recently completed studies outlining the basal conditions required for lipoprotein secretion by the cultured hepatocytes. In these studies, very low-density lipoproteins (VLDL), low-density lipoproteins (LDL), and high-density lipoproteins (HDL) were secreted by hepatocytes in a time-dependent manner; the chemical composition and structure of the particles (Fig. 1) were similar to rat plasma lipoproteins. After 3 and 9 hours of incubation, 64% of the total lipoprotein mass consists of VLDL, 13% of LDL, and 23% of HDL (Fig. 2). The secreted LDL represent the first evidence that these particles are produced *de novo* by parenchymal cells. After 24 and 48 hours, no VLDL are detected in the culture medium and significantly larger triglyceride-rich particles are isolated in the LDL region. These findings are compatible with lipolysis of secreted VLDL by hepatic lipase and the formation of lipoproteins of intermediate density.

In contrast, no substantial changes occur in the secretion rate or composition of HDL particles isolated after 24 and 48 hours of incubation. The inclusion of sodium oleate in the culture medium of hepatocytes incubated for 24 and 48 hours stimulates the secretion of VLDL to the levels obtained at 3 and 9 hours. The secreted VLDL contain the same apolipoproteins (B,E, and C) as plasma VLDL; however, the relative proportions are different. The hepatocyte LDL contain primarily apolipoprotein B and in this respect are significantly different from plasma LDL which contain large concentrations of apolipoprotein E.

The apolipoprotein content of the hepatocyte HDL particles is similar to that of plasma in the large concentration of apolipoprotein A-1 present; however, the secreted particles contain less apolipoprotein E and measurable amounts of apolipoprotein B (Fig. 3). The incorporation of [^{3}H]-leucine into the

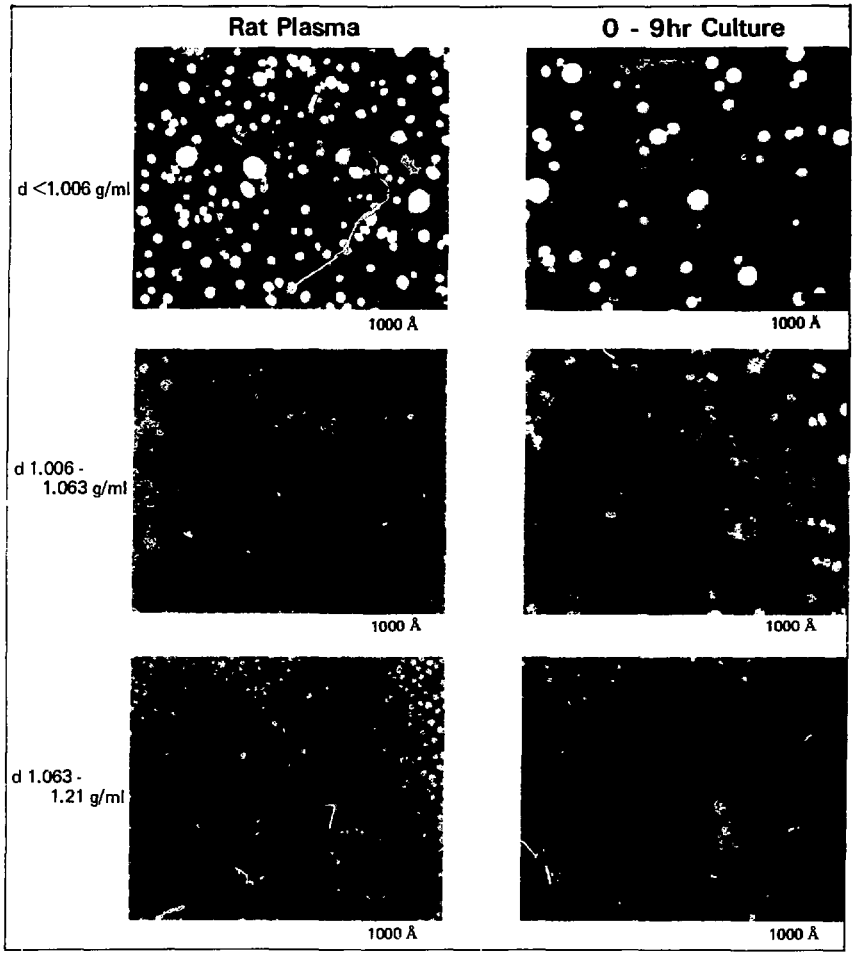

Figure 1. Comparison of electron-microscopic structure of rat plasma lipoproteins with those secreted by cultured rat hepatocytes.
XDB 7811–14022

apolipoproteins of the secreted lipoproteins at all incubation periods (Fig. 4) and the complete inhibition of [^{3}H]-leucine incorporation by cycloheximide suggests that secreted lipoproteins result from *de novo* synthesis.

Electron microscopy examination of the hepatocyte monolayers was carried out to correlate structural-functional events. Scanning electron microscopy revealed that after an initial 18 hours in culture medium supplemented with fetal calf serum, the parenchymal cells re-establish polarity and form bile canaliculi (Fig. 5). Thin-section studies of cells maintained in culture medium containing lipoprotein-deficient fetal calf serum indicate that VLDL are present within the cisternae of the Golgi and are later secreted into the intercellular spaces. The rough and smooth endoplasmic reticulum are normal even after 3 days in culture. Glycogen particles were absent in the cultured cells and may explain the decrease in the absence of exogenous fatty acids.

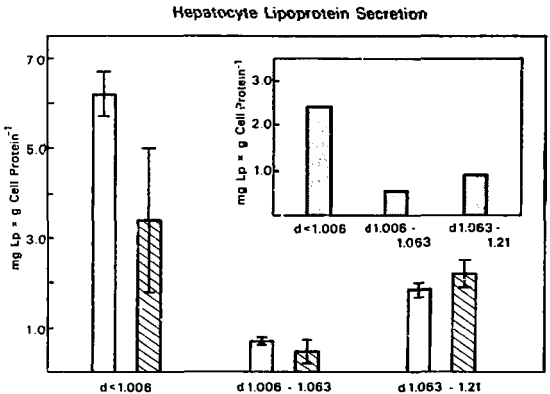

Figure 2. Lipoproteins isolated from the culture media at 9 hours are represented by open bars, and 18-hour lipoproteins by hatched bars. The data presented are means ± S.E. of 4 experiments. d<1.006 = VLDL; d 1.006–1.063 = LDL; d 1.063–1.21 = HDL. Inset: Lipoprotein secretion after 3 hours of incubation. XBL:792-3098

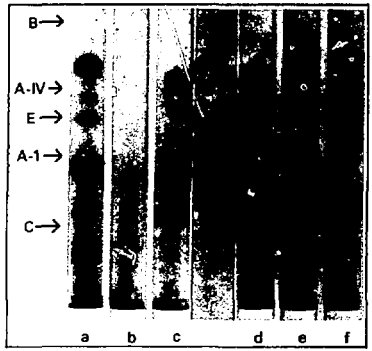

Figure 3. Rat plasma and hepatocyte culture media apoproteins assessed by 10% SDS-polacrylamide gel electrophoresis. Samples in each set are: a, b, c, plasma VLDL, LDL, and HDL; d, e, f, hepatocyte VLDL, LDL, and HDL lipoproteins. XBB 792-1338

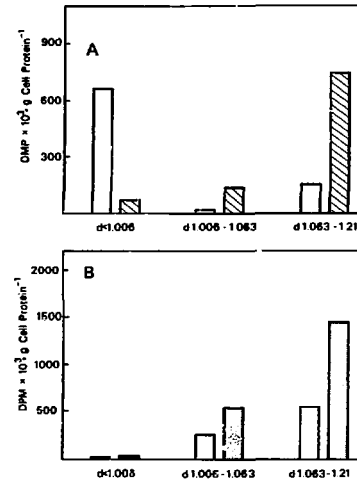

Figure 4. Incorporation of [^{3}H] -leucine into hepatocyte culture media lipoprotein protein. (A) Protein radioactivity in lipoproteins after 9 hours of incubation (open bars) and after an additional 18 hours of incubation in fresh medium (hatched bars). (B) Labeled protein in lipoproteins after 24 hours (open bars) and after an additional 48 hours of incubation in fresh medium (stippled bars). XBL 792-3104

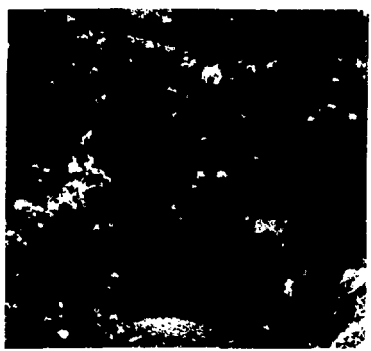

Figure 5. Scanning electron micrograph of rat hepatocyte monolayer cultures. Several parenchymal cells can be seen surrounding a small lumen (small round hole in center of picture) which is similar to the bile canaliculus.
XBB 780-14019

Effect of Radiation and Pollutants on Mammalian Cells

SOLAR, NEAR ULTRAVIOLET, AND FLUORESCENT LIGHT DAMAGED MAMMALIAN CELLS

H. John Burki

This study was initiated in 1979. The initial experiments are being performed with easily available light sources such as fluorescent lights (white, yellow, black light, blue, and green) and light from germicidal ultraviolet (UV).

ASYNCHRONOUS CELL STUDIES

We have completed studies which show that yellow light is not mutagenic in CHO (Chinese hamster ovary) cells. Therefore, the active wavelengths which induce mutations are those that are shorter than 5,000 Å and can pass through ordinary glass and plastic (greater than 3,000 Å). This initially defines the wavelengths of most interest to us.

We have begun to study the effects of near UV on the induction of mutations of the point mutation type [ouabain and diphtheria toxin (DT) resistance], since fluorescent lights appear to be more effective in inducing these effects than in inducing those mutations associated with chromosomal changes [6-thioguanine (6TG) resistance]. For example, moderate doses of fluorescent light double the background of 6TG resistance but raise the DT resistant clones by a factor of 10. We consider these data preliminary at this time.

Far-UV appears to induce mutations to the three drugs above at a similar rate. In contrast to the near-UV results, the dose response curve from far-UV appears to be linear, at least up to intermediate doses ($20^J/M^2$). All three sites show a similar response.

SYNCHRONOUS CELL STUDIES.

We have completed several experiments to determine the "age response" for mutagenesis induced by germicidal UV light. The results show that the response to UV is a function of both when in its cycle the cell is irradiated and the genetic locus studied.

Resistance to 6TG and ouabain are induced somewhat more strongly in the G1 period and early S period than in the rest of the cell cycle. However, induction to resistance to diphtheria toxin shows a dramatic peak only in the G1 period. The reason for these differences is unclear at this time. The possibility is that genetic recombination occurs more readily in G1 than at other stages of the cell cycle, and that the peak for DT resistance induction is associated with this type of "error prone repair."

TRITIUM DAMAGE IN SYNCHRONOUS CHINESE HAMSTER CELLS *IN VITRO*

H. John Burki

ASYNCHRONOUS CELL STUDIES

We have investigated the dose-response relationship for the induction of 6-thioguanine (6TG) resistance in Chinese hamster cells after exposure to 50-kV x-rays at 300 rad per minute. We found that the induction was curvilinear with dose, as has been reported for 300-kV x-rays by Hsie et al.[1] However, we found an RBE (relative biologic effect) of about 2, which is what we expected from the comparative LET (linear energy transfer) distributions of the two radiations. We were not able to induce resistance to ouabain or diphtheria toxin by x-ray exposure. These results are control experiments for eventual studies of tritium exposure. The curve for induction of mutations was curvilinear, similar to that found for the alkylating carcinogen ethylnitrosurea (ENU), but unlike that for ultraviolet (UV) light—suggesting that different mechanisms exist in the cells for handling different types of damage.

The dose response for exposure to ENU was determined for resistance to ouabain and to 6TG. Both dose-response curves were curvilinear with dose, with the ouabain resistance being induced at

about one-tenth the rate of the 6TG resistance. A number of control experiments were performed to determine the optimum expression time for the mutations and the gradual loss of mutants from a mixed population of cells with extended expression times. It is interesting to note that because the ouabain resistance is a dominant trait, it is possible to obtain mutations immediately after ENU exposure without the need of an "expression period."

SYNCHRONOUS POPULATIONS

Using the automatic cell-synchronizing system and constantly monitoring the degree of the cells' synchrony on a given day with flow-microfluorimetry, Coulter size spectroscopy, and uptake of tritiated thymidine, we have performed a number of mutagenesis experiments for cells synchronized at 1-hour intervals throughout the cell cycle of 12 hours.

Preliminary results after acute exposure to x-rays show that the induction of resistance to 6TG is strongly cell-cycle dependent. The sensitive period is the G1 period of the cell cycle. This characteristic age-response for mutagenesis is new and different from the age response found for x-ray induced cell killing. Since the results occur in the G1 period before the replication of the gene for HPRT (hypoxanthineribosyl transferase), which is associated in most cases with 6TG resistance, the results suggest that the mechanism is associated with the induction of deletions and the induction of genetic recombination, a process which may be error-prone in mammalian and other eucaryotic cells.

There appears to be little cell-cycle dependence in the induction of 6TG resistance by ENU, which is very different from the results for x-rays and for UV. The G1 sensitivity does seem a little higher for high doses of ENU at the ouabain locus. These results suggest either that the mechanisms by which ENU induces mutations are not dependent on the biochemistry of the cell cycle, or that the time constant for the induction is very long. The former is more likely, since control experiments showed that the half-life for ENU for inducing mutations is less than 1 hour and may be as short as 15 minutes.

REFERENCE

1. Hsie, A.W., O'Neill, J.P., Couch, D.B., San Sebastian, J.R., Brimer, P.A., Machanoff, R., Fusce, J.C., Riddle, J.C., Li, A.P., Forbes, N.L., and Hsie, M.H. 1978. *Radiation Research* 76: 471.

EFFECTS OF POLLUTANTS ON SOMATIC MAMMALIAN CELLS

Donald A. Glaser

The overall goal of this project is to detect and measure mutagenic, carcinogenic, and teratogenic effects of environmental pollutants and other agents by making quantitative observations on the growth of mammalian cells in culture. Automated techniques for carrying out large-scale experiments in cell biology developed in this laboratory are being used to make quantitative measurements of growth rate and morphology on each of 100,000 colonies of mammalian cells per experiment. The extensive instrumentation and computer facilities necessary for this work comprise our NIH-funded National Research Resource: "Facility for Automated Experiments in Cell Biology." Collaboration with a number of other laboratories engaged in studying the same biological problems allow correlation of our observations with those made using more conventional methodologies, and ensures the widest possible use of our facilities.

In the last year, we have concentrated on isolating and characterizing two classes of animal-cell mutants that have defective systems of protection against the effects of mutagenic and carcinogenic agents. One class is defective in repair of ultraviolet (UV)-induced damage, the second in resistance to polycyclic aromatic hydrocarbon toxicity. The general utility of these mutants is twofold. First, they can be used in basic studies to determine the specific roles of individual protein molecules in complicated enzyme systems, since each mutant is defective in only one of the protein species involved in the repair or detoxifying processes. Secondly, they promise to be useful as highly sensitive probes or tester strains for mutagenic or toxic materials, since they lack one of the systems which protects the normal cell from these substances.

Among other effects, ultraviolet irradiation is mutagenic, due to a variety of chemical modifications which it can induce in DNA, the genetic material. There exist several DNA-repair enzyme systems, without which the cells suffer increased damage when exposed to UV. Using standard replica plating techniques, we have isolated two mutants of the Chinese hamster ovary (CHO) cell line

which have greater than normal UV sensitivity, and using our automated Cyclops system, we have found an additional twenty-five such mutants. Examination of the UV survival curves (percent cell survival versus UV dose) of these mutants suggests that there are four classes, with the most sensitive being ten times as sensitive as the original parental cell, and the least being about twice as sensitive.

Preliminary characterizations, done by J. Cleaver of the UCSF Medical School, indicate that all our mutants exhibit a reduced level, and some no detectable amount, of excision-repair DNA synthesis. Future work is directed toward the characterization of the sensitivity of these mutants to other agents that damage DNA, and to the isolation of double mutants which are also defective in a second DNA-repair system.

Many toxic compounds are rendered harmless to the cell by enzymatic conversion to harmless products. Ironically, some of the chemical intermediates formed in the detoxification process can be more harmful than the original material. Thus the polycyclic aromatic hydrocarbon, benzo(a)pyrene (BP), is not itself carcinogenic, but is converted to a carcinogenic compound (activated) by a member enzyme of a detoxification system, aryl hydrocarbon hydroxylase (AHH). We have continued our work with two rodent hepatoma cell lines, isolating mutants with decreased sensitivity to BP, which we have shown is due to greatly reduced levels of AHH activity.

The mutants we have presently isolated have also lost the ability to activate aflatoxins, but retain the ability to activate azo dyes. We have found the mutant phenotypes to be recessive. This should allow us to determine the number of genes involved in these activation processes, by fusing cells to make hybrids between pairs of mutants, and testing for complementation between the mutants. We are also in the process of isolating cell mutants deficient in the ability to activate azo dyes, in order to extend our study of this class of compounds.

APPENDICES

Appendix A: 1978–1979 Publications

CONTRIBUTIONS TO JOURNALS, BOOKS, AND PROCEEDINGS

Aidells, B.D., Konrad, M.W., and Glaser, D.A. Growth and morphology of colonies of Chinese hamster ovary cells growing on agar is affected by insulin. Proc. Natl. Acad. Sci. *76*:1863–67 (1979).

Anderson, D.W., Nichols, A.V., Pan, S.S., and Lindgren, F.T. High density lipoprotein distribution: resolution and determination of three major components in a normal population sample. Atherosclerosis *29*: 161–179 (1978).

Atkins, H.L., Budinger, T.F., Lebowitz, E., Ansari, A.N., Green, M.W., and Fairchild, R. Thallium-201 for medical use. III. Human distribution and physical imaging properties. J. Nucl. Med. *18*: 133–140 (1977).

Barnes, B.D., Parker, H., and Anger, H.O. Neurologic diagnosis using the 80-lens optical camera. Neurology *27*: 26–31 (1977).

Bassel, J., Phaff, H.J., Mortimer, R.K., and Miranda, M. Examination of hydrocarbon-utilizing mutants of *Saccharomyces cerevisiae*. Intl. J. Systematic Bacteriology *28*: 427–432 (1978).

Bastacky, J. and Hayes, T.L. Scanning electron micrographs. *In* Lenfaut, Claude J.M., Chronic obstructive pulmonary disease. American Lung Association Bulletin *64*: 2–9 (1978).

Blakely, E.A., Tobias, C.A., Yang, T.C.H., Smith, K.C., and Lyman, J.T. Inactivation of human kidney cells by high-energy monoenergetic heavy-ion beams. Radiation Research *80*: 122–160 (1979).

Bradley, D.D., Wingard, J.C., Pettitti, D.V., Krauss, R.M., and Ramcharan, S. Serum high density lipoprotein cholesterol in women using oral contraceptives, estrogens and progestins. New Eng. J. Med. *299*: 17–20 (1978).

Braun, Gisela, Shulgin, Alexander T., and Sargent, Thornton, III. Synthesis of ^{123}I-labelled 4-iodo-2,5-dimethoxyphenylisopropylamine. J. Labelled Compounds and Radiopharmaceuticals *14*:767–773 (1978).

Brecher, G., Tjio, J.H., Haley, J.E., Narla, J., and Beal, S.L. Transplantation of murine bone marrow without prior host irradiation.

Budinger, T.F. Physiology and physics of nuclear cardiology. *In* Willerson, J.T., ed., Nuclear cardiology. Cardiovascular Clinics, F.A. Davis & Co., Philadelphia (1979).

——. Thresholds for physiological effects due to RF and magnetic fields used in NMR imaging. IEEE Trans. Nucl. Sci. *NS-26*: 2821–2825 (1979).

——, **Derenzo, S.E., Gullberg, G.T., and Huesman, R.H.** Trends and prospects for circular ring positron cameras. IEEE Trans. Nucl. Sci. *NS-26(2)*: 2742–2745 (1979).

——, **Greenberg, W.L., Derenzo, S.E., Gullberg, G.T., and Huesman, R.H.** Quantitative potentials of dynamic emission computed tomography. J. Nucl. Med. *19*: 309–315 (1978).

Burki, H.J. and Aebersold, P.M. Bromodeoxyuridine-induced mutations in synchronous Chinese hamster cells: temporal induction of 6-thioguanine and oubain resistance during DNA replication. Genetics *90*: 311–321 (1978).

—— **and Lam, C. King.** Comparison of the lethal and mutagenic effects of gold and white fluorescent lights on cultured mammalian cells. Mutation Research *54*: 373–377 (1978).

Case, G.D., Dixon, J.S., and Schooley, J.C. Interactions of blood metalloproteins with nitrogen oxides and oxident air pollutants. Environ. Res. *20*: 43–65 (1979).

Castro, J.R. and Lawrence, J.H. Heavy ion radiotherapy. *In* Lawrence, J.H. and Budinger, T.F., eds. Recent advances in nuclear medicine, vol. 5. New York, Grune & Stratton, Inc., chapter 5 (1978).

Chapman, J.D., Blakely, E.A., Smith, K.C., Urtasun, R.C., Lyman, J.T., and Tobias, C.A. Radiation biophysical

studies with mammalian cells and a modulated carbon ion beam. Radiation Research *74*: 101–111 (1978).

——, **Urtasun, R.C., Blakely, E.A., Smith, K.C., and Tobias, C.A.** Hypoxic cell sensitizers and heavy charge-particle radiations. Brit. J. Cancer *37, Suppl. III*: 184–188 (1978).

Chatterjee, A. and Magee, J.L. Relationship of track structure of heavy particles to the physical distribution and chemical effects of radicals. *In* Booz, J. and Ebert, H.G., eds. Sixth symposium on microdosimetry. Brussels (1978).

Chervenak, R.P., Nelson, K.G., and Goodman, J.W. Colony-forming units in the spleen and bone marrow of young (C57 BL/6 x DBA/x) F_1 hybrid mice. Biomedicine Express *29*: 121–123 (1978).

Chiu, Wah. Factors in high resolution biological structure analysis by conventional transmission electron microscopy (CTEM). *In* Johari, O., ed. Scanning electron microscopy/1978, vol. 1. Chicago, SEM Inc., AMF, O'Hare, pp. 569–580 (1978).

—— **and Glaeser, R.M.** Electron exposure–dependent contrast transfer. *In* Proc. ninth international congress on electron microscopy, vol. 1. Toronto (1978).

—— **and Hosoda, J.** Crystallization and preliminary electron diffraction study to 3-7Å of DNA helix-destabilizing protein Gp32*I. J. Mol. Biol. *122*: 103–107 (1978).

—— **and Hosoda, J.** Electron microscopy of a DNA *helix destabilizing protein crystal (GP32*I). In Proc.* ninth international congress on electron microscopy, vol. 2. Toronto, pp. 178–179 (1978).

—— **and Jeng, T.W.** Electron diffraction of crotoxin complex at 1.6 Å. *In* Bailey, G.W., ed. Thirty-seventh ann. proc. electron microscopy soc. amer., San Antonio, pp. 122–123 (1979).

Curtis, S.B., Tenforde, T.S., Parks, D.L., Schilling, W.A., and Lyman, J.T. Response of a rat rhabdomyosarcoma to neon- and helium-ion irradiation. Radiation Research *74*: 274–288 (1978).

Davis, David. Analysis of iron content in individual human red blood cells by electron microprobe and scanning electron microscope. Micron *9*: 175–190 (1978).

Davis, Jefferson W. Studies with amino acids. 1. Synthesis of valine. J. Organic Chem. *43*: 3980–3982 (1978).

Deans, Stanley R. A unified radon inversion formula. J. Math. Phys. *19*: 2346–2349 (1978).

——. Gegenbauer transforms via the radon transform. SIAM J. on Mathematical Analysis *10*: 577–585 (1979).

Derenzo, S.E., Budinger, T.F., Cahoon, J.L., Greenberg, W.L., Huesman, R.H., and Vuletich, T. The Donner 280-crystal high resolution positron tomograph. IEEE Trans. Nucl. Sci. *NS-26(2)*: 2790–2793 (1979).

Downing, Kenneth H. Resolution of photographic emulsions at low electron exposure. *In* Bailey, G.W., ed. Thirty-seventh ann. proc. electron microscopy soc. amer., San Antonio, pp. 126–127 (1979).

——. Possibilities of heavy atom discrimination using single-sideband techniques. Ultramicroscopy *4*: 13–31 (1979).

Durbin, P.W. (Member, Panel on Hanford Wastes). Radioactive wastes at the Hanford Reservation: a technical review. Natl. Acad. Sciences (1978).

——. A summary of actinide biological research 1943–1977. *In* Workshop on research needs in actinide biology (CONF-770491, Seattle, Wash., April 5–7, 1977). U.S. Dept. of Energy (1978).

Ebbe, Shirley Experimental and clinical megakaryocytopoiesis. Clinics in Haematology *8*: 371–394 (1979).

—— **and Phalen, E.** Regulation of megakaryocytes in W/W^v mice. J. Cell. Physiol. *96*: 73–79 (1978).

—— **and Phalen, E.** Does autoregulation of megakaryocytopoiesis occur? Blood cells *5*: 123–138 (1979).

——, **Phalen, E., and Howard, D.** Parabiotic demonstration of a humoral factor affecting megakaryocyte size in $S1/S1^d$ mice. Proc. Soc. Biol. Med. *158*: 637–642 (1978).

Echlin, P., Pawley, J.B., and Hayes, T.L. Freeze-fracture scanning electron microscopy of *Lemna minor* L. (Duckweed). *In* Scanning electron microscopy/1979/II. Chicago, SEM Inc., AMF O'Hare, pp. 69–76 (1979).

Fabrikant, J.I. Cell cycle of spermatogonia in mouse testis. Investigative Radiolcgy *14*: 189–191 (1979).

Fisher, J.W., Adamson, J.W., Camiscoli, J.F., Fried, W., Gordon, A.S., Schooley, J., and Zanjani, E. Cooperative erythropoietic assay of several steroid metabolites in polycythemic mice. Steroids *30*: 833–845 (1977).

Forte, T.M., Nordhausen, R.W., Nichols, A.V., Endemann, G., Miljanich, P., and Bell-Quint, J.J. Dissociation of apolipoprotein A-1 from porcine and bovine high density lipoproteins by guanidine hydrochloride. Biochim. Biophys. Acta *573*: 451–463 (1979).

Frank, J., McFarlane, S.C., and Downing, K.H. A note on the effect of illumination aperture and defocus spread in bright field electron microscopy. Optik *52*: 49–60 (1978).

Frantz, A., Gordon, G.C., Linfoot, J., and Strott, C. Pituitary workup: when, why, and how. Patient Care *12(20)*:80–95 (1978).

Freeling, M. Allelic variation at the level of intragenic recombination. Genetics *89*: 222–226 (1978).

—— and Cheng, D.S.K. Radiation-induced alcohol dehydrogenase mutants in maize following allyl alcohol selection of pollen. Genet. Res. *31*: 107–129 (1978).

Garcia, J.F. Assays for erythropoietin. *In* Fisher, J.A., ed. Kidney hormones II. New York, Academic Press (1977).

——. Erythropoietin. *In* Jaffe, B.M. and Behrman, H.R., eds. Methods of hormone radioimmunoassay, 2nd ed. New York, Academic Press (1979).

——, Sherwood, J., and Goldwasser, E. Radioimmunoassay of erythropoietin. Blood Cells *5*: 405–419 (1979).

Glaeser, Robert M. Prospects for extending the resolution limit of the electron microscope. J. Microscopy *17*:77–91 (1979).

——. Radiation damage with biological specimens and organic materials. *In* Hren, J.J., Goldstein, J.I., and Joy, D.C., eds. Introduction to analytic electron microscopy. New York, Plenum Publ. Corp., chapter 16, pp. 423–436 (1979).

——, Chiu, W., and Grano, D. Structure of the surface layer protein of the outer membrane of *Spirillum serpens*. J. Ultrastructure Research *66*: 235–242 (1979).

—— and Hayward, S.B. Measurement and reduction of radiation damage in frozen hydrated crystalline specimens. Proc. ninth intl. congress electron microscopy *3*: 70–77 (1978).

—— and Jap, Bing K. The utilization efficiency of diffracted electrons in STEM and CTEM. *In* Bailey, G.W., ed. Thirty-seventh ann. proc. electron microscopy soc. amer. San Antonio, pp. 120–121 (1979).

——, Jap, B.K., and Ho, M.H. Single scattering approximations: the domains of validity for structural analysis of protein crystals by electron diffraction. Proc. ninth international congress on electron microscopy, Toronto *1*: 186–187 (1978).

Goodman, J.W., Basford, N.L., and Shinpock, S.G. On the role of thymus in hemopoietic differentiation. Blood Cells *4*: 53–64 (1978).

——, Basford, N.L., Shinpock, S.G., and Chambers, Z. An amplifier cell in hemopoiesis. Experimental Hematology *6*: 151–160 (1978).

——, Shinpock, S.G., and Basford, N.L. Thymic involvement in control of bone marrow growth. Use of T-cell-depleted hybrid mice. Exptl. Hematol. *7*: 17 (1979).

Gullberg, Grant T. The reconstruction of fan-beam data by filtering the back-projection. Computer Graphics and Image Processing *10*:30–47 (1979).

Hankinson, O. (Communicated by D.A. Glaser) Single-step selection of clones of a mouse hepatoma line deficient in aryl hydrocarbon hydroxylase. Proc. Natl. Acad. Sci., *76*: 373–376 (1979).

Hayes, T.L., Pawley, J.B., and Fisher, G.L. The effects of chemical variability of individual fly ash particles on cell exposure. *In* Johari, O., ed. Scanning electron microscopy/1978, vol. 1. Chicago, SEM Inc., AMF O'Hare, pp. 239–244 (1978).

——, Pawley, J.B., and Hook, G.R. Biological applications of a low temperature SEM. Beitrage zur Electronenmikroskopischen Direktabbilding von Oberflachen *11*: 277–280 (Verlag RA Remy, Munster, Germany) (1978).

——, Tobias, C.A., and Yang, T.C. Heavy ion microscopy of hydrated cells with SEM imaging of the contact radiograph. *In* Johari, O., ed. Scanning electron microscopy/1978, vol. 1. Chicago, SEM Inc., AMF O'Hare, pp. 233–238 (1978).

Hayward, S.B. and Glaeser, R.M. Radiation damage of purple membrane at low temperature. Ultramicroscopy *4*: 201–210 (1979).

——, Grano, D.A., Glaeser, R.M., and Fisher, K.A. Molecular orientation of bacteriorhodopsin within the purple membrane of *Halobacterium halobium*. Proc. Natl. Acad. Sci. *750*: 4320–4324 (1978).

Heinen, R.J., Herbert, P.N., Fredrickson, D.S., Forte, T., and Lindgren, F.T. Properties of the plasma very low and low density lipoproteins in Tangier Disease. J. Clin. Investig. *61*: 120–132 (1978).

Herbert, Peter N., Forte, Trudy, Heinen, Robert J., and Fredrickson, Donald S. Tangier disease: one explanation of lipid storage. New Eng. J. Med. *299*: 519–521 (1978).

Ho, Ming-Hsiu, Jap, Bing K., and Glaeser, Robert M. Electron diffraction from protein crystals: theoretical investigation of the importance of dynamical effects. *In* Bailey, G.W., ed. Thirty-seventh ann. proc. electron microscopy soc. amer. San Antonio, pp. 118–119 (1979).

Hosoda, J. and Moise, H. Purification and physicochemical properties of limited proteolysis products of T4 helix destabilizing protein (Gene 32 Protein)* J. Biological Chemistry *253*:7547–7555 (1978).

Hughes, A.M., Tenforde, T.S., Calvin, M., Bissell, M.J., Tischler, A.N., and Bennett, E.L. Inhibition of adenocarcinoma TA3 ascites tumor growth by rifamycin derivatives. Oncology *35*: 76–82 (1978).

Ismail, Latife, Sargent III, Thornton, Dobson, E.L., and Pollycove, M. Altered metabolism of the methionine methyl group in the leukocytes of patients with schizophrenia. Biological Psychiatry *13*: 649–660 (1978).

Kennedy, W.L., Alpen, E.L., and Garcia, J.F. Erythroid colony production *in vitro* as a function of exposure time to erythropoietin. Blood Cells *4*: 143–154 (1978).

Krauss, R.M., Lindgren, F.T., Wingerd, J., Bradley, D.D., and Ramcharan, S. Effects of estrogens and progestins on high density lipoproteins. Lipids *14*: 113–118 (1979).

Leith, J.T., Woodruff, K.H., Howard, J., Lyman, J.T., Smith, P., and Lewinsky, B.S. Early and late effects of accelerated charged particles on normal tissues. International J. Radiation Oncology Biology Physics *3*: 103–108 (1977).

Lindgren, Frank T. The prognosis for quantitative lipoprotein electrophoresis. *In* Peeters, H., ed. The lipoprotein molecule. New York, Plenum Publ. Corp. (1978).

Llacer, J. Theory of imaging with a very limited number of projections. I.E.E.E. Trans. Nucl. Sci. *NS-26* (1979).

——, Chatterjee, A., Jackson, H.C., Lin, J.C., and Zunzunegui, M.V. An imaging instrument for positron emitting heavy ion beam injection. IEEE Trans. Nucl. Sci. *NS-26* (1979).

Lyman, J.T. and Howard, J. Dosimetry and instrumentation for helium and heavy ions. International J. Radiation Oncology Biology, Physics *3*: 81–85 (1977).

Magee, J.L. and Chatterjee, A. Theory of the chemical effects of high-energy electrons. J. Physical Chemistry *82*: 2219–2226 (1978).

—— and Chatterjee, A. Theory of electron tracks with explicit consideration of track end effects. *In* Booz, J. and Ebert, H.G., eds. Sixth symposium on microdosimetry. Harwood Academic Publ., for the Commission of the European Communities (1978).

Malachowski, M., Tobias, C.A., and Leith, J.T. Effects of radiation upon the light-sensing elements of the retina as characterized by scanning electron microscopy. Life Sciences and Space Research *15*: 175–191 (1977).

Malkin, R. and Bearden, A.J. Membrane-bound iron-sulfur centers in photosynthetic systems. Biochimica et Biophysica Acta *505*: 147–181 (1978).

Mamoon, A.M., Schlapfer, W.T., Gahwiler, B., and Tobias, C.A. Nerve tissue in culture; studies on spontaneous bioelectric activity. Adv. Biol. Med. Physics *16*: 1–40 (1977).

Marshall, S. and Linfoot, J.A. Influence of hormones on urinary tract infection. Urology *9*: 675–679 (1977).

McNulty, P.J., Pease, V.P., Bond, V.P., Schimmerling, W., Vosburgh, K.G., Crebbin, K., Everette, W., and Howard, J. Delivery of single accelerated particles. Nuclear Instr. Meth. *155*: 325–329 (1978).

Mel, H.C. and Mohandas, N. Physical separation and characterization of reticulocytes and other cell fractions from rat bone marrow and the 1-g Mini-Staflo. *In* Catsimpoolas, N., ed. Methods of cell separation, vol. 2. New York, Plenum Publ. Corp., pp. 271–298 (1979).

—— and Yee, J.P. Commentary on modification of erythrocyte physico-chemical properties by millimolar concentrations of glutaraldehyde, by W.D. Corry and H.J. Meiselman. Blood Cells *4*: 481–483 (1978).

Nichols, Alex V. Interconversion of plasma lipoproteins. *In* Peeters, M., ed. The lipoprotein molecule (NATO-ASI). New York, Plenum Publ. Corp., pp. 157–167 (1978).

——, Gong, E.L., Forte, T.M., and Blanche, P.J. Interaction of plasma high density lipoprotein HDL_{2b} (d

1.063-1.100 g/ml) with single-bilayer liposomes of dimyristoylphosphatidylcholine. *Lipids 13*: 943–950 (1978).

Ogrydziak, D., Bassel, J., Contopoulou, R., and Mortimer, R. Development of genetic techniques and the genetic map of the yeast *Saccharomycopsis lipolytica*. Molec. Gen. Genet. *163*: 229–239 (1978).

Pawley, J.B. Design and performance of presently available TV-rate stereo SEM systems. *In* Johari, O., ed. Scanning electron microscopy/1978, vol. 1. Chicago, SEM Inc., AMF O'Hare, pp. 157–166 (1978).

——, Hayes, T.L., and Hook, G. Preliminary studies of coated complementary freeze-fractured yeast membranes viewed directly in the SEM. *In* Johari, O., ed. Scanning electron microscopy/1978, vol. 2. Chicago, SEM Inc., AMF O'Hare, pp. 683–690 (1978).

Peterson, D.D., Denton, E.V., Tran, M., Yang, T., Freeling, M., Craise, L., and Tobias, C.A. High-LET particle dosimetry in ASTP-biostack III zeamays experiment. Radiat. Eff. *34*: 139–142 (1977).

Pritchard, L.L. and Goodman, J.W. Dose-dependence of the augmentation of hemopoiesis by thymocytes. Experimental Hematology *6*: 161–171 (1978).

Raybourn, M.S., Cork, C., Schimmerling, W., and Tobias, C.A. An *in vitro* electrophysiological assessment of the direct cellular toxicity of carbon monoxide. Toxicology and Appl. Pharmacology *46*: 769–779 (1978).

Roots, R., Yang, T.C., Craise, L., Blakely, E.A., and Tobias, C.A. Impaired repair capacity of DNA breaks induced in mammalian cellular DNA by accelerated heavy ions. Radiation Research *78*: 38–49 (1979).

Ross-Riveros, P. and Leith, J.T. Response of 9L tumor cells to hyperthermia and X irradiation. Radiation Research *78*: 296–311 (1979).

Ruch, W., Mixter, R.C., Russell, R.M., Garcia, J.F., and Gale, C.C. Aminergic and thermoregulatory mechanisms in hypothalamic regulation of growth hormone in cats. Am. J. Physiol. *233*: E61–E69 (1977).

Sachs, M. and Freeling, M. Selective synthesis of alcohol dehydrogenase during anaerobic treatment of maize. Mol. Gen. Genet. *161*: 1–1–115 (1978).

Sanders, R., Sheldon, G.F., Garcia, J., Schooley, J., and Fuchs, R. Erythropoietin synthesis in rats during total parenteral nutrition. J. Surg. Res. *22*: 649–653 (1977).

Sargent, T. III, Lim, T.H., and Jenson, R.L. Reduced chromium retention in patients with hemochromatosis, a possible basis of hemochromatotic diabetes. Metabolism *28*: 70–79 (1979).

—— and Stauffer, Henry. Whole-body counting of retention of ^{67}Cu, ^{32}P and ^{51}Cr in man. Int. J. Nuclear Med. and Biol. *6*:17–21 (1979).

Sheldon, G.F., Saunders, R., Fuchs, R., Garcia, J., and Schooley, J. Metabolism, oxygen transport, and erythropoietin synthesis in the anemia of thermal injury. Am. J. Surg. *135*: 406–411 (1978).

Shinpock, S.G. and Goodman, J.W. Ability of thymic lymphocytes to alter CFU kinetics in radiation chimeras. Cell and Tissue Kinetics *11*: 111–119 (1978).

Shu, Helen P. and Nichols, Alex V. Benzo(a)pyrene uptake by human plasma lipoproteins *in vitro*. Cancer Research *39*: 1224–1230 (1979).

Smith, H.S. In vitro properties of epithelial cell lines established from human carcinomas and nonmalignant tissue. J. Natl. Cancer Inst. *62*: 225–230 (1979).

——, Owens, R.B., Nelson-Rees, W.A., Springer, E.L., Hackett, A.J., and Dollbaum, C.M. Epithelial cell cultures from human carcinomas. *In* Nieburgs, H.E., ed. Detection and prevention of cancer, vol. 2. New York, Marcel Dekker, pp. 1465–1479 (1978).

——, Springer, E.L., and Hackett, A.J. Nuclear ultrastructure of epithelial cell lines derived from human carcinomas and nonmalignant tissue. Cancer Research *39*: 332–344 (1979).

Sommer, F.G., Capp, M.P., Tobias, C.A., Benton, E.V., Woodruff, K.H., Henke, R.P., Holly, W., and Genant, H.K. Heavy-ion radiography: density resolution and specimen radiography. Investigative Radiology *13*: 163–170 (1978).

Sosinsky, G.E. Disappearance of two dimensional crystalline patches on the yeast plasma membrane during lag and early log phase. *In* Bailey, G.W., ed. Thirty-seventh ann. proc. electron microscopy soc. amer. San Antonio, pp. 150–151 (1979).

Statham, P.J. and Pawley, J.B. A new method for particulate X-ray microanalysis based on peak to background measurements. *In* Johari, O., ed. Scanning electron microscopy/1978, vol. 1. Chicago, SEM Inc., AMF O'Hare, pp. 469–478 (1978).

Stockman, J.A., III, Garcia, J.F., and Oski, F.A. The anemia of prematurity—Factors governing the erythropoietin response. New Engl. J. Med. *296*: 647–650 (1977).

Tenforde, Tom S., ed. Magnetic field effects on biological systems. New York, Plenum Press (1979).

——. Review of "The geomagnetic field and life: geomagnetobiology." Medical Physics *6*: 463–464 (1979).

——, **Curtis, S.B., Woodruff, H.K., Parks, D.L., Daniels, S.J., Crabtree, K.E., Schilling, W.A., and deGuzman, R.J.** Studies on the regrowth rate, morphological characteristics, and transplantation properties of rat rhabdomyosarcoma tumors following large doses of x-rays. Int. J. Radiat. Biol. *35*: 589–596 (1979).

——, **Yee, J.P., and Mel, H.C.** Electrophoretic detection of reversible chlorpromazine: HCl binding at the human erythrocyte surface. Biochimica et Biophysica Acta *511*: 152–162 (1978).

Tobias, C.A. Human and scientific concepts of time. Adv. Biol. Med. Physics *16*: 267–287 (1977).

——, **Benton, E.V., and Capp, M.P.** Heavy ion radiography. *In* Lawrence, J.H. and Budinger, T.F., eds. Recent advances in nuclear medicine, vol. 5. New York, Grune & Stratton, Inc., chapter 3, pp. 71–102 (1978).

——, **Blakely, E.Z., Yant, T.C.H., Chatterjee, A., Smith, K.C., Craise, L.M., Madfes, I.A., and Abrams, F.E.** The effects of accelerated heavy nuclei of neon and argon on mammalian cells in culture. Proc. intl. symposium on radiobiological research needed for the improvement of radiotherapy, IAEA, Nov. 22–26, 1976 and Radiobiological research and radiotherapy, vol. 2. Vienna, IAEA, pp. 3–18 (1977).

Tsugita, A. and Hosoda, J. DNA binding site of the helix destabilizing protein gp32 from bacteriophage T4. J. Mol. Biol. *122*: 255–258 (1978).

Tsui, E. and Budinger, T.F. Transverse section imaging of mean clearance time. Phys. Med. Biol. *23*: 644–653 (1978).

—— **and Budinger, T.F.** A stochastic filter for transverse section reconstruction. IEEE Tran. Nucl. Sci. *NS-26(2)*: 2687–2690 (1979).

Wiedemann, E., Saito, T., Linfoot, J.A., and Li, C.H. Specific radioimmunoassay of human β-endorphin in unextracted plasma. J. Clin. Endocrinol. Metab. *49*: 478–480 (1979).

——, **Uthne, K., Tang, R.G., Spencer, M., Saito, T., and Linfoot, J.A.** Serum somatomedin activity by rat cartilage bioassay and human placental membrane radioreceptor assay in acromegaly and Cushing's disease. *In* Giordano, G., Van Wyk, J.J., and Minuto, F., eds. Somatomedins and growth; London, Academic Press, pp. 289–294 (1979).

Wolf-Priesnitz, J.W., Schooley, J.C., and Wiedemann, L.J. Inhibition of erythropoietin production in unanesthetized rabbits exposed to an acute hypoxic-hypercapnic environment. Blood *52*: 153–162 (1978).

Woodruff, K.H., Leith, J.T., Powers-Risius, P., Havens, V., Lyman, J.T., Howard, J., and Tobias, C.A. Comparison of heavy particle with x-irradiation on the hamster lung. Amer. J. Pathology *95*: 765–774 (1979).

——, **Leith, J.T., Smith, P., Havens, V., Lyman, J.T., Howard, J., and Tobias, C.A.** Chronic effects of heavy-ion and x-irradiation in the hamster lung. ERDA Symposium Series *43*: 533–551 (1977) and Proceedings, 16th Annual Hanford Biology Symposium, Richland, Washington.

Yang, T.C., Welch, G., Tobias, C.A., Maccabee, H., Hayes, T., Craise, L., Benton, E.V., and Abrams, F. The feasibility of heavy charged-particle microscopy. Ann. New York Acad. Sci. *306*: 322–339 (1978).

Yano, Y. Effect of transport on the distribution of radioions and radiometabolites. Proc. First Intl. Symposium on Radiopharmacology, May 21–24, 1978, Innsbruck, Austria, and *In* Colombetti, L.G., ed. Principles of radiopharmacology, vol. 2. CRC.

—— **and Roth, E.P.** An alumina column ^{82}Rb generator. Intl. J. Appl. Radiat. and Isotopes *30*: 382–385 (1979).

Yee, J.P. and Mel, H.C. Kinetics of glutaraldehyde fixation of erythrocytes: size, deformability, form, osmotic and hemolytic properties. Blood Cells *4*: 485–497 (1978).

—— **and Mel, H.C.** Cell-membrane and rheological mechanisms: dynamic osmotic hemolysis of human erythrocytes, and repair of ghosts, as studied by resistive pulse spectroscopy. Biorheology *15*: 321–339 (1978).

LBL REPORTS ISSUED

Alonso, J.R., Chatterjee, A., and Tobias, C.A. High purity radioactive beams at the bevalac. LBL-8951 (March 1979) 3p.

——, **Howard, J., and Criswell, T.** The bevalac radiotherapy facility. LBL-8961 (March 1979) 3p.

——, **Tobias, C.A., and Chu, W.T.** Computed tomographic reconstruction of beam profiles a multiplane wire chamber. LBL-8947 (March 1979) 3p.

Budinger, T.F., Derenzo, S.E., Yano, Y., Huesman, R.H., Cahoon, J.L., Greenberg, W.L., and Moyer, B.R. Measurement of heart muscle damage using the Donner 280-crystal ring detector and rubidium-82. LBL-7476 (1978).

——, **Wong, P., and Yen, C.** Magnetic field effects on humans: epidemiological study design. LBL-8319 (October 1978) 23 p.

Burki, H.J. Ionizing radiation-induced 6-thioguanine resistant clones in synchronous CHO cells. LBL-8896 (March 1979) 15p.

——, **Moustacchi, E., and Cleaver, J.E.** Tritiated uracil, tritiated thymidine, and bromodeoxyuridine induced mutations in eucaryotic cells. LBL-8811 (February 1979) 17 p.

Chen, G.T.Y., Singh, R.P., Castro, J.R., Lyman, J.T., and Quivey, J.M. Treatment planning for charged particle radiotherapy. LBL-7493 (May 1979) 32 p.

Derenzo, Stephen E. Precision measurement of annihilation point spread distribution for medically important positron emitters. LBL-9169 (April 1979) 5 p.

——. Tabulation of side shielding optimization and comparison of detector materials for circular positron emission tomographs. LBL-9201 (1979).

Fabrikant, J.I. Perspectives of decision-making and estimation of risk in populations exposed to low levels of ionizing radiations. LBL-8667 (January 1979) 40p.

——. Somatic effects—other than cancer: fertility. LBL-8704 (January 1979) 19p.

——. Somatic effects—cancer: pharynx and hypopharynx. LBL-8711 (January 1979) 6 p.

——. Somatic effects—cancer: II. Introductory material A. Mechanisms of radiation carcinogenesis; B. Concepts of somatic effects. LBL-8715 (January 1979) 14 p.

——. Somatic effects—cancer: Q. ovary. LBL-8743 (January 1979) 8 p.

——. Degeneration and regeneration of the spermatogonial stem-cell system after exposure to ionizing radiation. LBL-8850 (February 1979) 25p.

——. Health effects of low-level ionizing radiation. LBL-9018 (April 1979) 8 p.

——. The 1979 report of the Advisory Committee on the Biological Effects of Ionizing Radiation (The BEIR Report). The effects on populations of exposure to low levels of ionizing radiation. Implications for nuclear energy and medical radiation. LBL-9084 (April 1979) 41 p.

—— **and Land, C.E.** Somatic effects—cancer; pancreas. LBL-8710 (January 1979) 11p.

—— **and Lyman, T.J.** Somatic effects—cancer: estimates of radiation doses in tissues and organs in the single-course radiotherapy patients treated for ankylosing spondylitis in England and Wales. LBL-8709 (January 1979) 9 p.

—— **and Sloan, M.H.** Somatic effects—cancer: salivary glands. LBL-8708 (January 1979) 11 p.

Farinato, R.S. and Roots, R.J. Analysis of the products of gamma-irradiated X-174RFI DNA in solution by electrooptics, neutral sucrose gradient sedimentation analysis, and agarose gel electrophoresis. LBL-7470 (1978).

Gaffey, C.T., Montoya, V.J., and Welch, G.P. Correlation between RBE and LET of heavy ions in blocking frog nerve conduction. LBL-9091 (May 1979) 17 p.

—— **and Tenforde, T.S.** Changes in the electrocardiograms of rats and dogs exposed to dc magnetic fields. LBL-9085 (1979) 9 p.

Grano, David A. Three-dimensional reconstruction in electron microscopy. Ph.D. Thesis, LBL-9322 (May 1979) 385 p.

Greenburg, W.L. An ultrafast Fourier transform parallel processor I. LBL-7442 (April 1978).

Gullberg, Grant T. The attenuated radon transform: theory and application in medicine and biology. Ph.D. thesis, LBL-7486 (1979) 230 p.

—— **and Huesman, Ronald H.** Emission and transmission noise propagation in positron emission computed tomography. LBL-9783 (June 1979) 13 p.

Hackett, A.J. and Springer, E.L. Scanning and transmission electron microscopy of human metastatic mammary carcinoma. LBL-8877 (February 1979) 9 p.

Hayward, Steven B. Low temperature electron microscopy and electron diffraction of the purple membrane of *Halobacterium Halobium*. Ph.D. Thesis, LBL-7487 (September 1978) 94 p.

Hollis, D.F. The interaction of the Eco RI restrictive enzyme from *E. coli* with nucleotides. Ph.D. Thesis, LBL-8484 (November 1978) 155p.

Jayko, M., Appleby, A., Christman, E., Chatterjee, A., and Magee, J. Radiation chemistry of particles accelerated by the Bevalac. LBL-7432 (April 1978) 22p.

Kennedy, William L. Hemopoietic cell precursor responses to erythropoietin in plasma clot cultures. Ph.D. Thesis, LBL-8668 (January 1979) 143 p.

Lim, T.H. Kinetic model building using advanced nuclear medicine techniques—the kinetics of chromium (III) in the human body. LBL-7473 (June 1978) 26p.

Linfoot, J.A. Advances in the understanding of diabetic complications. UCLRL Report #7433; American Diabetes Assoc., Northern California Affiliate, Inc., *7(2)*: 1, 5, 7(1978).

Magee, John L. and Chatterjee, Aloke Chemical track effects in condensed systems and implications for biological damage. LBL-9078 (May 1979) 8 p. (Presented at 6th International Congress of Radiation Research, Tokyo, Japan May 13–19, 1979.)

Olson, J.E., Schimmerling, W., and Tobias, C.A. Laser action spectrum of reduced excitability in nerve cells. LBL 9166 (July 1979) 15 p. (To be submitted for publication.)

Schimmerling, W. and Curtis, S.B. (co-editors) Proceedings of workshop on the radiation environment of the satellite power system. LBL-8581 (September 15, 1978).

Smith, A.R., Schimmerling, W., Henson, A.M., Kanstein, L.L., McCaslin, J.B., Stephens, L.D., Thomas, R.H., Ozawa, J., and Yeater, F.W. Neutron flux density and secondary-particle energy spectra at the 184-Inch Synchrocyclotron medical facility. LBL-6721 (July 1978).

Smith, H.S., Owens, R.B., Nelson-Rees, W.A., Springer, E.L., Dollbaum, C.M., and Hackett, A.J. Epithelial cell cultures from human carcinomas. LBL-8878 (February 1979) 13p. (To be published as a chapter in Molecular biology of tumor viruses, J.W. Watson and J. Tooze, Eds. New York, Cold Spring Harbor Lab.

Wolf-Priessnitz, J. Superimposition of carbon dioxide on acute isobaric hypoxia: plasma erythropoietin, acid-base status, and P_{50} in the unanesthetized rabbit. PH.D. Thesis, LBL-07460 (June 1978) 74 p.

Appendix B: Biology and Medicine Division Staff

DIVISION HEAD

Edward L. Alpen

DIVISION ADMINISTRATION STAFF

Janice C. DeMoor
De A. Eggers
Laurie E. Graves
Allan W. Long
Georgia A. Newell
Mark D. Sessler
Robert W. Springstreen
Baird Whaley
Herbert Wiener

DIVISION SCIENTIFIC STAFF

E. John Ainsworth
Hal O. Anger

Mary E. Barker
John B. Bassel
S. Jacob Bastacky
*Thomas E. Bauer
Alan J. Bearden
Eugene V. Benton
Eleanor A. Blakely
James L. Born
George Brecher
Thomas F. Budinger
H. John Burki

Joseph R. Castro
Aloke Chatterjee
George T. Y. Chen
William T. Chu
Gisela K. Clemons
Gerald M. Connell
Stanley B. Curtis
Hunter O. Cutting

Jefferson W. Davis
*Stanley R. Deans
Stephen E. Derenzo
Jonathan S. Dixon
Kenneth H. Downing
Patricia W. Durbin
Shirley N. Ebbe

Jacob I. Fabrikant
Raymond S. Farinato
Trudy M. Forte
Michael Freeling

Cornelius T. Gaffey
Joseph F. Garcia
Walter George
Robert M. Glaeser
Donald A. Glaser
Joseph D. Goldstein
Joan W. Goodman
Martin H. Graham
David A. Grano
Grant T. Gullberg

Adeline J. Hackett
Thomas L. Hayes
Stephen B. Hayward
Lester Hollander
William R. Holley
Junko Hosoda
Jerry Howard
Shirley Hoye
Ronald H. Huesman

Lin C. Jensen

John W. Kast
Esther H. Knudson
Ronald M. Krauss

John H. Lawrence
Florence Li
Frank T. Lindgren
John A. Linfoot
Paul Lowinger
John T. Lyman

Marcos F. Maestre
John L. Magee
William McGowan
Howard C. Mel
Robert K. Mortimer

Frank Q. Ngo
Alex V. Nichols

---

*Left Biology and Medicine Division prior to September 30, 1979.
† Retired during fiscal year 1979.

Jerry M. Owens

Suzanne S. T. Pan
*Chin-Tzu Peng
Theodore L. Phillips
*Donald A. Pointer

Julia B. Quint
Jeanne M. Quivey

Michael S. Raybourn
Adrian Rodriquez
Ruth J. Roots
Donald J. Rosenthal

Thornton W. Sargent, III
Walter Schimmerling
John C. Schooley
*Mason M-S Shen
Lon G. Sherman
Helen P. Shu
Alexander T. Shulgin
Jerome R. Singer
Helene S. Smith
Lisa Snow
Charles A. Sondhaus
Martha R. Stampfer
Henry H. Stauffer
Harrison A. Stubbs
Tirunelve S. Subramanian
Pauline Sun

Tom S. Tenforde
Gregory A. Threatte
Cornelius A. Tobias
*Paul W. Todd

*William J. Vaughan

Robert J. Webber
†Graeme P. Welch
Margaret R. White
Eckehart Wiedemann
Tokuko Wiedemann
Priscilla D. Wong

Tracy C. Yang
Yukio Yano
Chi-Kwan Yen

Frank Zisman

DIVISION SUPPORT STAFF

Frederick E. Abrams
Gerald L. Adamson
Kuldip K. Ahluwalia
Steve P. Akeson
Hilda M. Alexander

Cathryne C. Allan
Arlette S. Atwater

Patricia J. Blanche
Carol S. Bohlen
S. Kay Bristol
Philip Brodzinsky
Gerald L. Brooks

John L. Cahoon
Dorothy A. Carpenter
Betsy C. Carr
Emanuela N. Catena
Coleen Caudill
Polly Y. Chang
Larry J. Chevez
*Grace H. Chiang
Huey-Ling C. Chu
*M. Jeanette Cornell
*Karen E. Crabtree
Laurie M. Craise
Freddie L. Crenshaw, Jr.

Randy J. DeGuzman
Stephen J. Dentone
Clardell L. Deuberry
James D. Dixon
*Martha L. Dixon
Virginia K. Docherty
Greta S. Duke
Frank J. Durante

Helen F. Edgar
Peggy A. Eisenbach

Diana E. Fajardo
*Sherry L. Fitzsimmons
Michael B. Fizer
Patricia A. Fobair
Myrtle L. Foster
Roscoe Frazier
Helen M. Friend
Charlie M. Fuller

Patricia A. Garbutt
Christine Giotas
Queen E. Gipson
Catherine R. Gisser
Sally L. Glaser
Bahram Goliaei
Elaine L. Gong
Sara P. Goolsby
*Shelly B. Gordon
*Victoria E. Gorum
Joan M. Graham
Mary R. Graham
William L. Greenberg

Kathleen B. Hall
Kathleen M. Harris
Gloria J. Hathaway
Virginia C. Havens
Lilian E. Hawkins
†Dorothy B. Hedquist
Lynn R. Hlatky
Minghsiu Ho
*Gregory R. Hook
Mildred K. Hughes
James A. Hunter

Jules S. Jaffe
Barbara W. Jansen
Nylan M. Jeung
Nancy Jo
†Muriel B. Johnston
Daniel M. Judd

John M. Kaldor
Heroka Kasai
Jonathan A. Kerner
Barbara R. Komatsu
Natalia Kusubov

Clifford E. Lai
Lennetta G. Lai
*Francine P. Lauderdale
*Helen J. Lawce
Deborah A. Leach
Lynette L. Levy
Judith A. Lowrie
Joan E. Luna
Josephine A. Lundberg
Linda J. Lutgens

Bennett D. McAllister
Beverly G. McCalla
Mara A. McDonald
Tommy J. McKey
Velma B. McNeal
Ian S. Madfes
Lynn J. Mahlmann
Tamara B. Mihailovski
Virginia Modica
Herbert W. Moise, III
Jerome A. Moore
Carol J. Mortensen
Brian R. Moyer

Jeanette S. Nakagawa
Robert W. Nordhausen

Virginia I. Obie
*Oksana Oleszko

Annie C. Y. Pang
Shannon S. Parr
Theresa C. Peters
Elizabeth A. Phalen
Mary C. Pirruccello
Anne K. Poley
Patricia P. Powers-Risius
John C. Prioleau
*Susan E. Proctor

Thomas A. Reed
*John C. Risius
Joanne Rogers
*Zuzana Roos

Thea B. Scott-Garner
Susan W. Shattuck
Andy Shih
Carla J. Simmons
Ester F. Solis
Dorothy S. Sprague
Lore S. Stein
Nancy J. Steinhaus
Jeffrey A. Stephenson
Stephen S. Sylvester

Susan D. Tenforde
Vicki J. Truex
Doris S. Tse
Julia A. Twitchell

Grace V. Walpole
Davie D. Wei
*Jon I. White
Robert D. Wills
Rod A. Wing
*Joachim Wolf-Priessnitz
Wennie H. Wu

Ann S. Yabusaki
Michael J. Yezzi
George Young

*Maria V. Zunzunegui

COMMITTEES

Division Advisory Committee

Edward L. Alpen
Eleanor A. Blakely
James L. Born
Thomas F. Budinger
Joseph F. Garcia
Thomas L. Hayes
Alex V. Nichols
Cornelius A. Tobias
Baird Whaley*

Division Staff Committee

H. John Burki
Stanley B. Curtis, Chair
Shirley N. Ebbe
Trudy M. Forte
John T. Lyman
Thornton W. Sargent III

Equipment Committee

Joseph F. Garcia, Chair
H. John Burki
Aloke Chatterjee
Cornelius T. Gaffey
Jonathan S. Dixon
Herbert Wiener*

Salary Committee

Edward L. Alpen
James L. Born
Thomas F. Budinger
Joseph F. Garcia
Thomas L. Hayes
Cornelius A. Tobias
Baird Whaley*

Donner Library Committee

Robert M. Glaeser, Chair
Edward L. Bennett
Thomas F. Budinger
Gerald M. Connell
Thomas L. Hayes
Frank T. Lindgren
Dorothy E. Denney*
Roy J. Nielsen*

Human Use Committee

James L. Born, Chair
Thomas F. Budinger
Shirley N. Ebbe
William E. Siri
Henry H. Stauffer
Janice C. DeMoor*
Baird Whaley*

Radioactive Drug Research Committee

James L. Born, Chair
Edward L. Alpen
Aloke Chatterjee
Jacob I. Fabrikant
Henry H. Stauffer
Joseph D. Goldstein (consultant)
Janice C. DeMoor*

Animal Welfare Committee

Herman Bonasch
Gerald M. Connell, Chair
Joseph F. Garcia
Joan W. Goodman
John C. Schooley
Robert W. Springsteen*

---

*Ex-officio, nonvoting member.